# HIGH RESOLUTION GAMMA RAY SPECTRAL STUDIES OF THE DECAYS OF $^{117}Te$, $^{119g}Te$, $^{119m}Te$, $^{129g}Te$ AND $^{129m}Te$

By

George J. Uris Berzins

A THESIS

Submitted to
Michigan State University
in partial fulfillment of the requirements
for the degree of

DOCTOR OF PHILOSOPHY

Department of Physics

1967

ABSTRACT

HIGH RESOLUTION GAMMA RAY SPECTRAL STUDIES OF THE DECAYS OF $^{117}Te$, $^{119g}Te$, $^{119m}Te$, $^{129g}Te$ AND $^{129m}Te$

by George J. Berzins

The energy states populated through beta decay have been investigated for the isotopes $^{117}Sb$, $^{119}Sb$, and $^{129}I$ in an effort to obtain information about energy level systematics in this region of the periodic table. Ge(Li) singles and Ge(Li)-NaI(Tl) coincidence spectrometers were used to identify many new gamma transitions which could not be distinguished in previous scintillation studies. Coincidence data, energy sums and relative intensity considerations were used to construct decay schemes for $^{117}Te$, $^{119g}Te$, $^{119m}Te$, $^{129g}Te$ and $^{129m}Te$. In most cases significant changes in previous schemes were necessary to accommodate all of the new transitions and to be consistent with all of the coincidence data.

Excited states accommodating 18 gamma rays have been placed at 719.8, 923.9, 1354.9, 1454.8, 1716.5, 1810.6, 2213, 2285, and 2300.0 keV in $^{117}Sb$. Levels in $^{119}Sb$ at 644.1, 699.6, 1328, 1338.7, 1412.8, 1487, 1749.1 and 1820 keV are populated by the decay of 16h $^{119g}Te$, while the decay of 4.6d $^{119m}Te$ populates levels at 270.3, 1048.1, 1212.6, 1249, 1365.8, 1407, 2129, 2226, 2278, 2283, and

2360 keV. These two sets accommodate 12 and 20 transitions, respectively. The 32 gamma rays observed in the decay of 33d $^{129m}$Te in equilibrium with 70m $^{129g}$Te depopulate excited states at 27.7, 278.5, 487.6, 560, 696.0, 729.6, 769, 830, 844.5, 1049.9, 1111.4, 1261, 1291, and 1402 keV. Of this set, only the 696.0, 729.6, 844.5, 1049.9 and 1402 keV states are populated by direct beta decay of $^{129m}$Te, while the 769 keV state is populated from both isomers.

Unique spin assignments have been made to some levels in these isotopes, while limits on possible spins have been placed on most of the remaining states from log ft values and from the existence of transitions to levels of known spins and parities. Angular correlation experiments were performed with Ge(Li) and NaI(Tl) detectors to obtain bases for some of the unique spin assignments in the decay of $^{119g}$Te.

Comparisons of the low lying energy states in several of the adjoining odd mass antimony and iodine isotopes show systematic behaviors for a number of the low levels. Insofar as is possible, comparisons have been made with the predictions of some of the existing nuclear models.

## ACKNOWLEDGMENTS

I wish to thank Dr. W. H. Kelly for suggesting this region of study. His guidance and patience during the course of these investigations are greatly appreciated.

Dr. C. R. Gruhn spent many hours in realizing a solid state detector laboratory. Without Ge(Li) detectors, most of the experiments performed in this study would not have been possible.

Dr. H. G. Blosser and Dr. W. P. Johnson assisted with the cyclotron irradiations of isotopes for this study.

Dr. R. L. Auble, Dr. L. M. Beyer, Mr. R. C. Etherton, Mr. D. B. Beery, Mr. W. B. Chaffee and Mr. R. Hickey aided greatly with helpful discussions and with data acquisition.

It was a pleasure to collaborate on two joint publications with Dr. W. B. Walters, Dr. G. E. Gordon and Dr. G. Graeffe of MIT.

Mr. L. Kull provided a stimulus for philosophical discussions which were a welcome change of pace from the laboratory. Although it has been proven that the setting for the discussions is conducive to great discoveries, it was our misfortune that the bubble chamber had already been invented.

Miss T. Arnette and Mr. J. O. Kopf made many useful suggestions during my initial bouts with the computer.

Mr. R. L. Dickenson and Mr. A. Kaye were very helpful with the acquisition of equipment and sources for this study.

Dr. H. Griffin of the University of Michigan provided access to the Ford Nuclear Reactor.

Mr. N. R. Mercer and his machine shop crew and Mr. W. Harder and Mr. F. E. Potts of the electronics shop supplied valuable assistance by building much of the physical apparatus for various experiments.

Miss Jean Lowe and Miss Cathy McClure sacrificed much of their time to help with the typing of this thesis. Miss Lowe and Miss Wilma Sanders were helpful in preparing for publication various reports arising from this investigation.

The National Science Foundation provided financial support for most of this investigation.

Finally, I thank my wife Joyce for her patience and her moral and financial support during these past few long and trying years.

TABLE OF CONTENTS


Page

ACKNOWLEDGMENTS . . . . . ii

LIST OF TABLES . . . . . vii

LIST OF FIGURES . . . . . viii

INTRODUCTION . . . . . 1

Chapter

I. NUCLEAR MODELS . . . . . 6

1.1. The Shell Model . . . . . 6
1.2. The Collective Model . . . . . 11
1.3. Particle-Core Coupling Model . . . . 18

1.3.1. Weak Coupling . . . . . 20
1.3.2. Strong Coupling . . . . . 22

1.4. Nucleon Correlations . . . . . 25

II. EXPERIMENTAL APPARATUS AND METHODS AND SOURCE PREPARATION . . . . . 30

2.1. Ge(Li) Singles Spectrometers . . . . 30
2.2. Ge(Li)-NaI(Tl) Coincidence Spectrometers . . . . . 33

2.2.1. Conventional Experiments . . 35
2.2.2. Experiments Utilizing a Split-ring NaI(Tl) Annulus . . . . 37
2.2.3. Angular Correlation Experiments . . . . . 40

2.3. X-ray Intensities . . . . . 43
2.4. Positron Endpoints . . . . . 44
2.5. Data Analysis . . . . . 44

2.5.1. Energy Measurements . . . . 45
2.5.2. Relative Intensity Measurements . . . . . 48
2.5.3. Angular Correlation Measurements . . . . . 49

Chapter Page

III. EXPERIMENTAL RESULTS . . . . . 55

3.1. Summary of Previous Studies of the Activities of the $^{117}Te$, $^{119}Te$ and $^{129}Te$ . . . . . 55

3.2. Results of this Investigation . . . 61

3.2.1. Decay Schemes of $^{129g}Te$ and $^{129m}Te$ . . . . . 61

3.2.1.A. The Gamma Ray Singles Spectra . . . . 61

3.2.1.B. Gamma-Gamma Coincidence Studies . . 67

3.2.1.C. The Proposed Decay Schemes . . . . 75

3.2.2. Decay Schemes of $^{119g}Te$ and $^{119m}Te$ . . . . . 79

3.2.2.A. The Gamma Ray Singles Spectra . . . . 79

3.2.2.B. Gamma-Gamma Coincidence Studies . . 89

3.2.2.C. The Proposed Decay Schemes . . . . 94

3.2.2.D. Angular Correlation . . . . . 101

3.2.3. Decay Scheme of $^{117g}Te$ . . 109

3.2.3.A. The Gamma Ray Singles Spectrum . . . . 109

3.2.3.B. Gamma-Gamma Coincidence Studies . . 113

3.2.3.C. Positron-Gamma Coincidence Studies 115

3.2.3.D. The Decay Scheme 118

3.2.3.E. The Search for $^{117m}Te$ . . . . 122

IV. DISCUSSION OF RESULTS . . . . . 128

4.1. Comparison with Reaction Studies and Identifications of some Corresponding States . . . . . 128

4.2. Comparison with the Core-Coupling Model . . . . . 137

Chapter Page

4.2.1. Levels in $^{119}Sb$ . . . . . 137
4.2.2. Levels in $^{129}I$ . . . . . 142

4.3 Comparison with Pairing and Quadruple Interaction Calculations . . . . . 144

V. CONCLUSIONS . . . . . 148

BIBLIOGRAPHY . . . . . 151

APPENDICES . . . . . 157

LIST OF TABLES


| Table | | Page |
|---|---|---|
| 1. | Typical Calibration Data | 46 |
| 2. | Studies of the Decay of $^{129}Te$ | 56 |
| 3. | Studies of the Levels in $^{119}Sb$ | 57 |
| 4. | Studies of the Levels in $^{117}Sb$ | 58 |
| 5. | Gamma Rays Observed in the Decay of $^{129m+g}Te$ | 66 |
| 6. | Summary of Coincidence Results for $^{129m+g}Te$ | 72 |
| 7. | Energies and Relative Intensities of Gamma Rays Observed in the Decay of $^{119m}Te$ | 86 |
| 8. | Energies and Relative Intensities of Gamma Rays Observed in the Decay of $^{119g}Te$ | 87 |
| 9. | $^{119m}Te$ Gamma-Gamma Coincidence Relationships | 93 |
| 10. | Summary of $^{119}Te$ Gamma-Gamma Angular Correlation Data | 104 |
| 11. | Comparison of Multipolarities Assigned by Various Investigators | 106 |
| 12. | Energies and Relative Intensities of Gamma Rays Observed in the Decay of $^{117}Te$ | 112 |
| 13. | $^{117}Te$ Gamma-Gamma Coincidence Relationships | 115 |
| 14. | Experimentally Observed Energy States in $^{119}Sb$ | 130 |
| 15. | Experimentally Observed Energy States in $^{117}Sb$ | 131 |
| 16. | Properties of Similar States in Odd Mass Antimony Isotopes | 134 |
| 17. | Properties of Similar States in Odd Mass Iodine Isotopes | 136 |

LIST OF FIGURES


| Figure | | Page |
|---|---|---|
| 1. | Examples of rotational and vibrational energy levels which are characteristic of even-even nuclei in the deformed and the spherical regions, respectively, of the periodic table . | 14 |
| 2. | Relative photopeak efficiency curves for three Ge(Li) detectors . . . . . | 32 |
| 3. | Cutaway view of the Ge(Li)-NaI(Tl) annulus coincidence spectrometer (from ref. 26) . . | 34 |
| 4. | A schematic illustration of the Ge(Li)-NaI(Tl) coincidence apparatus . . . . . | 36 |
| 5. | Results of a triple coincidence experiment with the NaI(Tl) annulus and a 7 $cm^3$ Ge(Li) detector . . . . . | 41 |
| 6. | Decay schemes of $^{119}$Te isomers which was constructed from scintillation and conversion electron studies, compared to those constructed from high resolution gamma ray spectral studies . . . . . | 59 |
| 7. | Evolution of the energy level scheme of $^{129}$I as populated by the beta decays of $^{129m+g}$Te . | 60 |
| 8. | Segments of singles spectra of $^{129m+g}$Te and $^{129g}$Te, recorded with a 3 $cm^3$ Ge(Li) detector | 63 |
| 9. | Ge(Li) spectra of $^{129m+g}$Te in coincidence with three regions of the spectrum seen by a 7.6 x 7.6 cm NaI(Tl) detector . . . . . | 69 |
| 10. | A Ge(Li) spectrum of $^{129m+g}$Te in coincidence with pulses corresponding to $\geq$ 150 keV from the NaI(Tl) annulus detector . . . . . | 70 |
| 11. | A spectrum of $^{129m+g}$Te in coincidence with the 28 keV gamma ray . . . . . | 71 |
| 12. | Proposed decay schemes of $^{129m}$Te and $^{129g}$Te . | 76 |

Figure Page

13. Singles spectrum of $^{119m}$Te recorded with a 3 cm$^3$ Ge(Li) detector . . . . . 80

14. Segments of the Ge(Li) spectrum of $^{119m+g}$Te shown on expanded scales . . . . . 81

15. Singles spectrum of $^{121}$Te, recorded with a 3 cm$^3$ Ge(Li) detector after the $^{119}$Te had decayed away . . . . . 88

16. Gamma ray spectra of $^{119m}$Te in coincidence with various segments of the 900-1400 keV region . . . . . 91

17. Gamma ray spectra of $^{119m}$Te in coincidence with the 153 and 270 keV regions . . . . 92

18. Gamma ray spectra in coincidence with the 644-700 keV region in $^{119g}$Te . . . . . 95

19. Proposed decay scheme of $^{119g}$Te . . . . 97

20. Proposed decay scheme of $^{119m}$Te . . . . 98

21. Experimental correlation functions for four gamma ray cascades in $^{119}$Te . . . . . 102

22. Same as Figure 21 for four additional cascades . . . . . 103

23. Singles spectrum of $^{117}$Te below approximately 1800 keV, recorded with a 3 cm$^3$ Ge(Li) detector . . . . . 110

24. High energy portion of a singles spectrum of $^{117}$Te, recorded with a 7 cm$^3$ Ge(Li) detector . . . . . 111

25. Results of a triple coincidence experiment on $^{117}$Te recorded with a 20.3 cm x 20.3 cm NaI(Tl) split annulus and a 7 cm$^3$ Ge(Li) detector . 114

26. Coincidence spectra of $^{117}$Te obtained with a 7 cm$^3$ Ge(Li) counter and a 7.6 x 7.6 cm NaI(Tl) crystal . . . . . 117

27. The proposed decay scheme of $^{117}$Te . . . 119

Figure Page

28. Low lying levels in $_{52}Te_N$ isotopes . . . . 123

29. Low lying levels in $_{51}Sb_N$ isotopes as observed in β-γ decay (9,45) and ($^3$He,d) and (d,d') experiments (54-56) . . . . . 125

30. Comparison of levels in $^{119}$Sb populated by beta decay to those observed in ($^3$He,d) reactions (54-56) . . . . . 132

31. Comparison of $^{117}$Sb levels populated by beta decay to those observed in ($^3$He,d) reactions (54-56) . . . . . 133

32. A comparison of energy levels below 1 MeV in odd mass iodine isotopes . . . . . 143

33. A comparison of the observed low lying energy levels in the odd mass antimony isotopes . . 146

34 A. Typical room temperature diode characteristics of a Ge(Li) detector

B. A schematic illustration of a Ge(Li) drift apparatus . . . . . 170

35. A schematic flow chart of the MIKIMAUS program 179

## LIST OF APPENDICES


| Appendix | | Page |
|---|---|---|
| A. | Beta and Gamma Decay Selection Rules . . . | 158 |
| B. | Manufacture of Ge(Li) Detectors . . . . | 167 |
| C. | Interpretation of Angular Correlation Data . . . . . | 172 |
| D. | Description of the MIKIMAUS Program . . . | 176 |

# INTRODUCTION

In order to test the validity of current nuclear models, it is necessary to obtain a set of experimental measurements that is as complete as possible. The models themselves, although usually abounding with empirical parameters, are a measure of our understanding of nuclear structure. Advances in this understanding can be expected to be reflected by improved agreement between experimental results and theoretical calculations. Moreover, while experiment is a necessary test for theory, it can also serve as a motivation for new concepts.

The region chosen for this study, just beyond a major closed shell at Z = 50, has two main features of potential value. First, because of the existence of a large number of stable tin and tellurium isotopes, many nuclei are readily accessible through proton or neutron bombardments. Hence, one can hope to obtain information for a large number of similar nuclei. In particular, a comparison can be made of the low-lying energy levels in successive odd-mass isotopes in an effort to obtain information about the effects of the addition of neutron pairs.

Second, one of the current nuclear models, the core-coupling model, is best applicable near closed major shells. This model considers a nucleus as composed of an even-even core plus an extra-core nucleon(s) (1-5). The description of properties of even-even nuclei in terms of collective oscillations has been rather successful. Hence, it is of interest to extend this treatment to odd-mass nuclei by coupling the motion of the extra particle to that of the even-even core. This description should be applicable to antimony isotopes (N even, Z = 50 + 1) and, to a lesser extent, to the isotopes of iodine (N even, Z = 50 + 3). A second type of calculation, based on pairing and quadrupole forces, has also been applied with a fair degree of success to this region of the periodic table (1,6). This latter treatment is somewhat more general in that it considers interactions among all particles outside closed shells. This, and the core-coupling model, are similar in that both recognize properties characteristic of collective motions of the whole nucleus, and both attempt to treat nucleons outside of closed shells via "residual interactions." These residual interactions are small compared to the shell model potential. The primary difference lies in the fact that the pairing plus quadrupole calculation deals with more particles, and hence is more general

and can be applied to a larger region of the periodic table, while the core-coupling treatment, at least in its present form, is limited to regions where all but only a few nucleons can be considered to make up a tightly bound core.

The experimental methods employed in this study were those of gamma ray spectroscopy. This approach has become significantly more valuable recently as a result of the development of high resolution Ge(Li) detectors. Although all of the decay schemes studied here had been investigated previously with scintillation counters, a wealth of new information was obtained from experiments utilizing Ge(Li) detectors. In most cases, existing decay schemes had to be modified considerably to accommodate all of the new transitions and to be consistent with high resolution coincidence data.

Beta and gamma decay selection rules, which are discussed in Appendix A, limit the number of levels which can be populated in beta and subsequent gamma decay. A further restriction is imposed by the available beta disintegration energy. These disadvantages are partially circumvented by the existence of nuclear isomerism in the region which was studied. Hence, a much richer decay spectrum could be obtained, with access to both low and high spin levels.

An additional limitation on the nature of the experiments is imposed by the halflife of the parent. Studies in this investigation were made, with reasonable success, of activities as short as 1 hour.

The parent isotopes chosen for this study were $^{117}$Te, $^{119}$Te, and $^{129}$Te. The first two of these decay to the corresponding isotopes of antimony, while the third populates levels in $^{129}$I. The $^{119}$Te and $^{129}$Te both have longer lived isomeric states which were shown to decay to sets of states different from those populated by the ground state activity. No isometric state was found in $^{117}$Te.

The particular choice of isotopes was made to be compatible with an overall effort in this laboratory to obtain systematic information about the energy level structure for a large number of odd proton-even neutron isotopes in this region of the periodic table. Levels in $^{125}$Sb, $^{123}$Sb and $^{121}$Sb have recently been investigated (7-9), making $^{119}$Sb and $^{117}$Sb logical choices for continuation of the study. Of those iodine isotopes which are accessible via beta decay, $^{127}$I had also been recently studied (10), while $^{131}$I was investigated concurrently (11) with the $^{129}$I reported here.

As mentioned previously, the information which can be obtained in this type of investigation is limited by beta decay endpoints, by beta and gamma

decay selection rules and by limitations on experimental equipment. Hence, to present a fair test to theoretical predictions, these data should be supplemented with results of other types of experiments, such as stripping and pickup reactions and Coulomb excitations. These experiments can be expected to populate some additional states which may be inaccessible to beta decay. Moreover, comparisons of relative population rates in the various types of experiments could conceivably present a key to the particular mechanisms of formation of some excited states.

# CHAPTER I

# NUCLEAR MODELS

Since one primary objective of this investigation is to compare experimental results with predictions of current nuclear models, brief discussions of these models are presented in the following sections. These are not intended to be exhaustive theoretical treatments, but merely summaries of the main ideas involved, with the hope of putting the subject of nuclear models into proper perspective for comparison with experimental results.

## 1.1. The Shell Model

Among the earliest motivations for a shell model (12) was the occurence of the so-called "magic numbers." Nuclei with either Z or N = 2, 8, 20, 28, 50, 82 or 126 exhibit several characteristic properties. First, there is a greater than normal abundance of stable nuclei of this type. For example, Z = 50 has ten stable isotopes, compared to only two each for Z = 49 and 51, eight each for Z = 48 and 52, and two and one, respectively, for Z = 47 and 53. Similar trends can be seen in regions of other magic numbers. The tendency of nuclei which are two nucleons removed from a magic number to be more stable than those with one or three nucleons removed, should be noted.

Second, magic number nuclei are especially tightly bound, deviating significantly in experimental binding energies from values predicted by most semi-empirical mass formulas.

Another characteristic, which indicates the reluctance of magic number nuclei to change their configurations is a sharp drop in thermal neutron capture crossections. For nuclei with N = 50, 82 or 126, this crossection is smaller by factors of 10 to 100 than for neighboring nuclei.

These properties led Mayer (13) and Haxel, Jensen and Suess (14) to postulate the existence of a shell structure analagous to that for atomic electrons. An immediate problem arose from the fact that, while the Coulomb interaction for electrons is well understood and can be treated even for departures from point charges, the nuclear interaction is comparatively only slightly understood.

The assumption has been made that each nucleon moves in an average, spherically symmetric potential V(r) which is due to all of the other nucleons (12). Two restrictions are imposed on V(r) by the short range of nuclear forces and by a presumed approximately uniform nucleon distribution throughout the nucleus. The first of these requires that V(r) go to zero rapidly for $r > R$ ($R = 1.4A^{1/3} \times 10^{-14}$ cm = nuclear radius), while the second prevents singularities at $r = 0$.

Two common potentials yielding energy level sequences which would result in magic numbers are those of the infinite square well and isotropic harmonic oscillator. However, these potentials, or a more realistic potential obtained from combining the two, give sets of magic numbers which include only 2, 8, and 20, and are each in error for the higher values.

A reconciliation can be obtained if an $\underline{\ell}\cdot\underline{s}$ term is added to the potential. Evidence for such a spin-orbit force is suggested by polarized proton beams resulting from scattering by light nuclei. Whereas the energy eigenvalues of the isotropic oscillator are degenerate in orbital angular momentum, deformation of this potential toward a square well removes this $\ell$ - degeneracy. Next, the addition of an $\underline{\ell}\cdot\underline{s}$ term to the new, deformed oscillator potential makes the energy also dependent upon the total angular momentum j. Expanding $\underline{\ell}\cdot\underline{s}$ gives:

$$2\ \underline{\ell}\cdot\underline{s} = \underline{j}\cdot\underline{j} - \underline{\ell}\cdot\underline{\ell} - \underline{s}\cdot\underline{s}$$

which reduces to:

$$2\ \underline{\ell}\cdot\underline{s} = \begin{cases} \ell & \text{for } j = \ell + 1/2 \\ -(\ell + 1) & \text{for } j = \ell - 1/2 \end{cases}$$

where $\ell$, s, and j are the orbital, spin, and total angular momenta, respectively. Hence, for a given $\ell$, the $j = \ell \pm 1/2$ levels are expected to be split by an amount proportional to $2\ell + 1$. This now leads to a set

of levels which can be made to account for all of the magic numbers. A schematic diagram of this set is shown in reference 12 and many other texts.

If one now begins to fill such a set of states and simultaneously inspects existing data, a number of features become evident: (1, 12).

1. To be consistent with the exclusion principle, filled shells and subshells should have the total angular momentum $J = 0$. Such is the case experimentally.

2. Empirical evidence suggests a tendency for nucleons in an unfilled sub-shell to pair off to zero resultant angular momentum, leaving the unpaired particle to determine J of the whole nucleus.

3. Because of a neutron excess for all except the light nuclei, neutrons and protons fill different sub-shells essentially independently. Because of this and number 2 above, all even-even nuclei have ground state $J = 0$.

4. As a consequence of angular momentum coupling rules, an $\ell$-sub shell which is more than half filled can be treated as containing "holes" (equal to the number of missing particles), which behave as particles.

5. In a few cases where two different subshells are close in energy, the pairing tendency favors a pair in the shell with the higher $\ell$ value at the expense of an unpaired particle in the lower shell.

6. In nuclei where both proton and neutron numbers are odd, the odd proton and neutron couple to give the resultant J. The coupling, in general, follows what are often referred to as Nordheim's rules: Let $j_p$, $\ell_n$, and $j_p$, $\ell_n$, denote the total and orbital angular momenta of the proton and neutron, respectively. Define Nordheim's number N as:

$$N = (j_p - \ell_p) + (j_n - \ell_n)$$

then, for a given nucleus,

$$\text{if } N = 0 \longrightarrow J = |j_p - j_n|$$

and

$$\text{if } N = \pm \longrightarrow J = \begin{matrix} |j_p - j_n| \\ j_p + j_n \end{matrix} \text{ or}$$

These are sometimes referred to as the strong rule and the weak rule, respectively.

Among the phenomena which can be accounted for, at least qualitatively, by a shell model are nuclear isomerism, beta decay transition rates, and magnetic moments. In some cases, it is possible to have closely lying levels of opposite parites having J values that differ by 3 or more units of $\hbar$ within the same major shell. Hence, if there are no intermediate levels between these, electromagnetic transition lifetimes may be long enough for the higher level to be classified as

metastable. One such "island of isomerism" occurs in the region where N(or Z) is odd and between 39 and 49, and Z(or N) is even. This island is caused by the proximity of the $p_{1/2}$ and $g_{9/2}$ subshells. A similar island, due to the $h_{11/2}$ vs. the $d_{3/2}$ and $s_{1/2}$ subshells occurs where Z or N is between 64 and 82. A third island is present for $101 \leq N_{odd} \leq 125$.

Beta decay transition probabilities between shell model levels can be classified according to the order of forbiddenness and are, in general, consistent with experimental results. Magnetic moments, $\mu$ in a strict shell model framework, should be due essentially to the unpaired nucleons. Experimental evidence generally shows that the values of $\mu$ fall into two groups, according to whether $j = \ell + 1/2$ or $\ell - 1/2$. However, marked deviations from calculated values for magnetic moments, and even more for quadrupole moments, suggest a limit on the interpretation of independent motion of nucleons in an average potential. Hence, for a more comprehensive picture, interactions among the nucleons in an unfilled shell, or even collective motion of the nucleus as a whole, should be considered.

## 1.2. The Collective Model

Experimental evidence for the existence of collective motion of nucleons is obtained from nuclei in the spherical and the deformed regions of the periodic

table. First, as is suggested by the names, nuclei in the spherical and deformed regions have very small and very large quadrupole moments, respectively. Second, E2 transition probabilities are greatly enhanced in the deformed region. Third, even-even nuclei in both regions exhibit similar low energy level structures, characteristic of the particular region. The characteristic features of the collective model are summarized here in a manner which follows the more detailed treatment presented by Preston (1), with additions or exceptions as noted.

For any nucleus, the electromagnetic transition probability between initial and final states can be expressed as,

$$T = \frac{8\pi\,(L+1)}{L[(2L+1)!!]^2}\,\frac{k^{(2L+1)}}{\hbar}\,B(\sigma L)$$

where L is the angular momentum carried off by the photon with energy $\hbar ck$.

The quantity $B(\sigma L)$, often referred to as the reduced transition probability, contains the dependence upon the nuclear wave function, and is given by

$$B(\sigma L) = \frac{1}{2J_i + 1} \sum_{m_f} \sum_{m_t} \left| \langle f \left| \sum_p \mathcal{M}_L^{\sigma}(p) \right| i \rangle \right|^2$$

where $\mathcal{M}_L^{\sigma}$ is the electric ($\sigma = E$) or magnetic ($\sigma = M$)

multipole operator of order L, and $J_i$ is the spin of the initial state. In regions of deformed nuclei (where both Z and N are far from closed shells), B(E2) values are typically 10-100 times greater than expected from calculations for single particle transitions.

In the spherical region (i.e. near closed shells) even-even nuclei show (15) an energy level structure similar to that shown in Figure 1. The salient features are the spins and ratios of the energies of the excited states. The ground and first excited states have spin parity $0^+$ and $2^+$ respectively. A closely spaced triplet with $J = 0^+$, $2^+$ and $4^+$, though not necessarily in that order, has sometimes been found to exist at approximately twice the energy of the first excited state. A $3^-$ level and other negative parity states are often also found near the $0^+$, $2^+$, $4^+$ triplet.

The low energy level structure in the deformed region (far from closed shells) is also illustrated (15) in Figure 1. The energy ratios are typically $E_4/E_2 \approx 3.3$, $E_6/E_2 \approx 7$, and $E_8/E_2 \approx 12$.

To explain these features, Bohr and Mottleson (16, 17) proposed a hydrodynamic model based on the motion of surface shapes of an incompressible fluid. The equation

$$R(\theta,\phi) = Ro\,[1 + \sum_{\lambda\mu} \alpha_{\lambda\mu}\, Y_\lambda^\mu\,(\theta,\phi)]$$

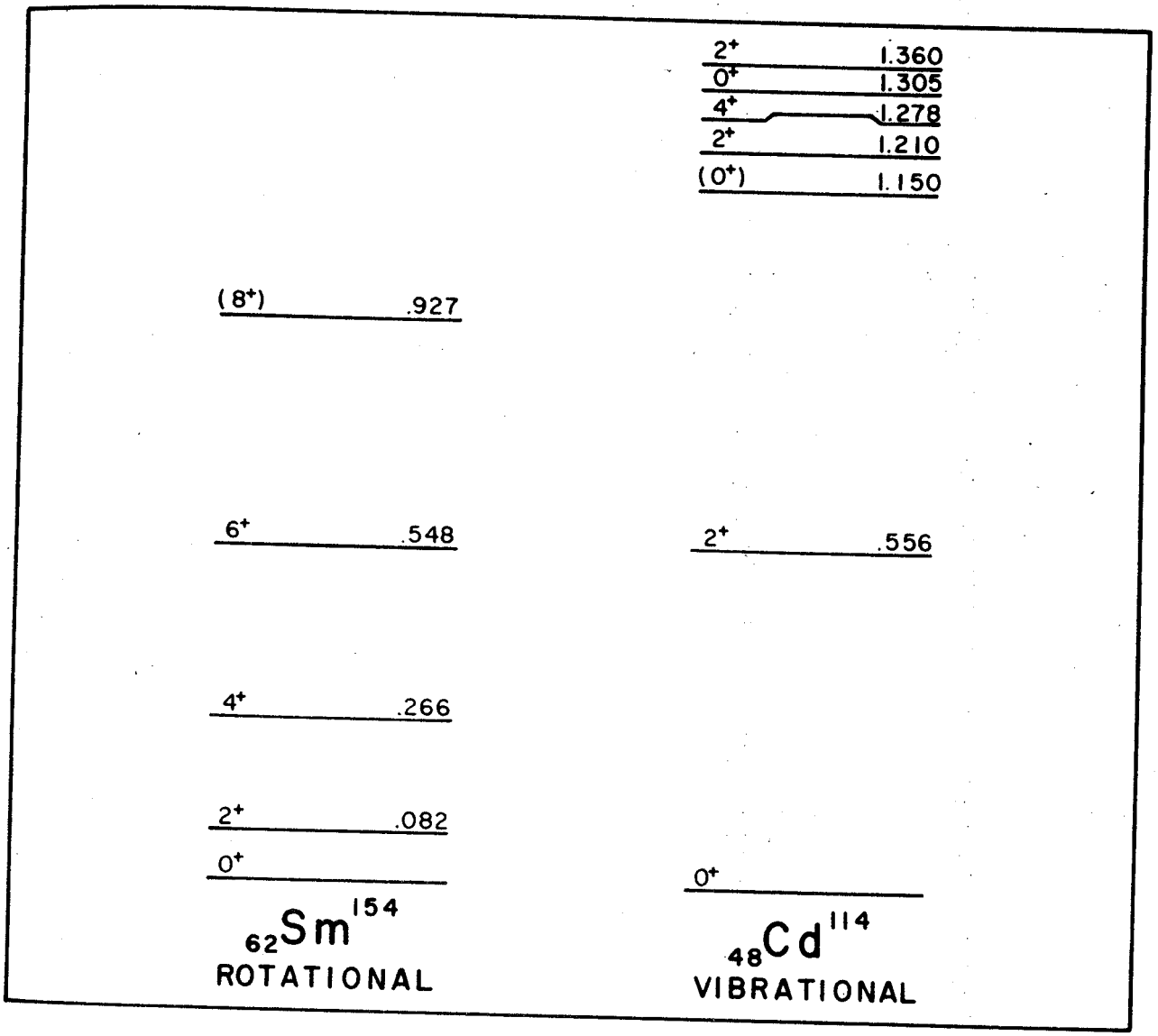


Fig. 1 Examples of rotational and vibrational energy levels which are characteristic of even-even nuclei in the deformed and the spherical regions, respectively, of the periodic table.

locates a point on a surface of general shape. The time dependence of this point is contained in the coefficients

$$\alpha_{\lambda\mu} = \alpha_{\lambda\mu}(t)$$

$R_o$ is a constant, and $Y_\lambda^\mu(\theta,\phi)$ are the spherical harmonies. The Hamiltonian for such a surface can be written as

$$H = T + V = 1/2 \sum_{\lambda\mu} [B_\lambda |\dot{\alpha}_{\lambda\mu}|^2 + C_\lambda |\alpha_{\lambda\mu}|^2]$$

This is in the form of a harmonic oscillator Hamiltonian with the coefficients $B_\lambda$ and $C_\lambda$ corresponding to inertial and surface tension parameters, respectively. Terms of order $\lambda = 0$ are ignored since they correspond to density changes of the nucleus as a whole. This can occur, but only a very high energies. Similarly, $\lambda = 1$ terms are dropped since they correspond to the motion of the center of mass.

Solution of the oscillator equation gives excitation energies of the nuclear states as $\sum_\lambda n_\lambda \hbar\omega_\lambda$, where $\omega_\lambda = \sqrt{C_\lambda/B_\lambda}$ is the frequency of oscillation. Hence the energy of the nucleus can be interpreted as due to $n_\lambda$ phonons, each having energy $\hbar\omega_\lambda$. Furthermore, it can be shown that each phonon carries angular momentum with z component $\mu$ and parity $(-)^\lambda$.

As $\lambda = 0, 1$ terms have been ruled out, the lowest phonon states are of quadrupole ($\lambda = 2$) nature and would

be expected to have energy $E = \hbar\omega_2$ and $J^\pi = 2^+$. The addition of a second $\lambda = 2$ phonon would give rise to a state at $E = 2\ h\omega_2$ and $J\pi = 0^+$, $2^+$, or $4^+$, which is in good agreement with experimental evidence in the spherical region if one realizes that the degeneracy of the two-phonon states can be removed by secondary interactions which are outside a strict oscillator framework.

Moreover, a semi-classical treatment of $B_\lambda$ and $C_\lambda$ indicates that $\omega_3 \simeq 2\omega_2$ and $\omega_4 \simeq 3\omega_2$. This is in agreement with experimental evidence for negative parity states near the two $\lambda = 2$ phonon triplet.

To describe the deformed shapes, one can specify the orientation of a nucleus by the Euler angles of the principal set of axes of the nucleus with respect to a set of space-fixed axes. Then other parameters can be introduced to specify the nucleus with respect to its principal axes. The surface equation for quadrupole shapes can be rewritten with respect to the principal axes as

$$R = Ro\ [1 + \sum_\mu a_{2\mu}\ Y_2^\mu\ (\theta', \phi')]$$

where the $a_{2\mu}$ are related to the $\alpha_{2\mu}$ through the angular momentum D-matrices. Because principal axes are used, only the $a_{20}$ and $a_{22} = a_{2-2}$ coefficients are non-zero. New parameters, $\beta$ and $\gamma$, can be defined as $a_{20} = \beta \cos\gamma$ and $a_{22} = \sqrt{1/2}\ \beta \sin\gamma$.

Interpretations of $\beta$ and $\gamma$ as parameters for the total deformation and for the shape, respectively, is illustrated if one writes increments of length of the principal axes,

$$\delta R_k = \sqrt{\frac{5}{4\pi}}\ Ro\ \beta\ \cos(\gamma - k\ \frac{2\pi}{3})$$

The terms of the Hamiltonian for the system become, after transformation of coordinates,

$$T = 1/2\ B\ (\dot{\beta}^2 + \beta^2\ \dot{\gamma}^2) + 1/2 \sum_{r=1}^{3} \mathcal{J} \delta_k\ \omega_k^2$$

$$\text{and } V = 1/2\ C\ \beta^2$$

where in the rotational type term, $\mathcal{J}_k$ are effective moments of inertia and the $\underline{\omega}$ is the angular velocity of the space fixed axes with respect to the body fixed axes. If an axis of symmetry exists, then $\mathcal{J}_3 = 0$ and $\mathcal{J}_1 = \mathcal{J}_2 = \mathcal{J} = 3\beta B^2$. Thus, the Hamiltonian can finally be written as

$$H = H_\beta + H_\gamma + H_{rot} + V$$

The first and second terms of the Hamiltonian to $\beta$ and $\gamma$ vibrations, respectively. The third term can be rewritten as $H_{rot} = \sum_{k=1}^{3} \frac{L_k^2}{2\mathcal{J}_k}$ where the $L_k$ are angular momentum components with respect to the moving axes. If the 3-axis is a symmetry axis, then $L_3 = K$ is a constant of motion along with the total rotational angular momentum $L^2 = J(J+1)$ and its projection on the

z axis, $L_z = M$. The energy eigenvalues for this term are $E_{rot} = \frac{\hbar^2}{2\mathcal{J}} J(J+1)$. It can be shown that if K = 0 the wave functions vanish for odd values of J. Hence, nuclei with an axis of symmetry are expected to exhibit the $2^+$, $4^+$, $6^+$, $8^+$ structure shown in Figure 1. This structure is best observed in highly deformed even-even nuclei. The high deformation, $\beta$, is necessary to make $\mathcal{J} \approx 3\beta B$ large, making $E_J$ in turn small compared to other types of excitations, while the even-even condition insures that Jintrinsic = 0. Furthermore, the energy ratios of the rotational levels are seen from the expression for $E_{rot}$ to be $E_4/E_2 = 3.33$ $E_6/E_2 = 7$, $E_8/E_2 = 12$, etc., in good agreement with observed values.

## 1.3. Particle-Core Coupling Model

Since the collective model works so well for even-even nuclei in many regions of the periodic table, it is natural to attempt to extend it to odd-mass nuclei in these same regions. If the properties of the even-mass isotopes are well explained by collective motions of all the particles, one would expect that the addition of an extra particle should lead to a behavior resembling that of the even-mass core but modified by the presense of the extra particle. For the most part, the summary of the core-particle coupling treatment follows the more detailed presentation of Preston (1).

The Hamiltonian for such a system should then be expressed as

$$H = H_c + H_p$$

where the subscripts c and p refer to core and particle, respectively. Questions which arise are concerned with how one describes the core-particle interactions, and, for cases where several particles are outside closed shells, what constitutes a core. In the simplest approximation, the second of these questions can be disposed of by assuming the core to be made up of all paired particles. More ambitious schemes would consider the core to be made up of closed major shells and subshells only, necessitating treatments of one or more extra-core particles (or holes). The introduction of small residual interactions among particles outside closed shells is sometimes referred to as the "intermediate coupling" scheme. The particle states obtained in this manner are then used as the particle states in particle-core coupling calculations.

The other question, that of the particle-core interaction, can be discussed in two extremes, the "strong" and "weak" couplings, with a poorly defined boundary or overlap between the two. A coupling is considered "strong" if a permanent deformation exists, significantly changing the "average shell model potential" experienced by the particles. In the other extreme, near closed shells, the coupling generally leads to only very small deformations

from sphericity. Hence, in the spherical regions, perturbation methods should be applicable.

1.3.1. Weak Coupling

In the weak coupling approximation the interaction is added as a perturbing term

$$H = H_c + H_p^o + H_{int}$$

The term $H_p^o$ is taken to be the spherical single particle Hamiltonian and $H_{int}$ is expressed in terms of the deformation parameters $\alpha_{\lambda\mu}$ and the spherical harmonies as

$$H_{int} = -\sum_i^n k(r_i) \sum_\mu \alpha_{2\mu} Y_2^\mu \quad (\theta_i, \phi_i)$$

for "n" particles outside the core. In most calculations, the coupling parameter $k(r_i)$ is treated as a constant for a given nucleus, with allowances for variations with mass number.

The states of such a system with angular momentum J are formed by vector addition of the single particle state $|jm\rangle$, with angular momentum j, and the collective state $|NR\rangle$, with N phonons and angular momentum R. Diagonalization of H then yields the new set of states with the new set of energy levels. Several semi-quantitative generalizations can be made from the application of perturbation methods in the quadrupole approximation:

1. For perturbation techniques to be applicable, it is necessary that

$$\left(\frac{5}{16\pi}\right)^{1/2} \frac{k}{(\hbar\omega C)} 1/2 \qquad << 1$$

where $\hbar\omega$ is the phonon energy and C is the oscillator potential constant. This, as has been mentioned previously, can be expected to hold in the spherical regions.

2. Because of the second order spherical harmonic $Y_2^{\mu}$, only those single particle states which have the same parity and a spin difference $\leq 2$ will mix.

3. For appreciable mixing to take place, the states must be close in energy.

4. Vibrational levels may be built upon the ground state or upon single particle excitations. Thus, each phonon - particle coupling will yield a set of the smaller of (2j + 1) or (2R + 1) states. The degeneracy of these is removed by the admixture of other particle or phonon states.

5. The center of gravity of a multiplet of core-particle states in an odd-mass nucleus should occur at the same energy as the corresponding collective state in the neighboring even-even nucleus. A general form of this center-of-gravity theorem was first presented by Lawson and Uretsky (18).

6. Since $\alpha_{2\mu}$ has been shown to have non-zero matrix elements only between states which differ by

exactly one phonon, deexcitations of two-phonon coupled states should occur via cascades involving at least two transitions.

One of the first calculations of the core-coupling type was performed by deShalit (2), in which he considered the coupling of $j = 1/2$ particle states to $2^+$ and $0^+$ phonon levels for a number of isotopes in various regions of the periodic table. In the same paper deShalit derived general expressions for first order shifts of the coupling multiplets and expressions for transition probabilities.

More recently calculations have been performed on several odd-mass iodine isotopes by Banerjee and Gupta (3), by O'Dwyer and Choudhury (4), and by Silverberg (19). Those dealing with $^{129}I$ will be discussed in more detail in Chapter IV.

## 1.3.2. Strong Coupling

When large permanent deformations are present, the interaction term can no longer be obtained from a first order expansion of the potential about its equilibrium value in terms of the deformation parameters, as was possible for weak coupling. In this case the deformation parameters are embedded in the expression for the potential well, yielding a set of generalized shell model single particle states. Values for the parameters

$\beta$ and $\alpha$ are obtained by minimizing the total particle energy, giving rise to a self-consistency problem for the potential.

If one assumes that the nuclear orientation changes much more rapidly than does the shape, then $\beta$ and $\gamma$ can be treated as approximately constant in the particle potential, and a rotational term can be separated from the particle Hamiltonian

$$H = T_{rot} + \sum_p H_p$$

$$T_{rot} = \sum_{k=1}^{3} \frac{R_k^2}{2\mathcal{I}_k}$$

The angular momenta to be considered are J, R, and j for the whole nucleus, the core, and the extra-core particle(s), respectively, and are related through $\underline{J} = \underline{R} + \underline{j}$.

In general, the treatment for the strong coupling case becomes considerably more complicated than for weak coupling. One simplification is obtained for the case of axial symmetry. The energy levels of the axially symmetric system are characterized by a single particle energy and a set of rotational levels built upon the single particle state. The expression has been shown to be

$$E_{JK} = \varepsilon_K + \left(\frac{\hbar}{2\mathcal{I}}\right)^2 [J(J+1) - 2K^2 + \delta_{K,1/2}\, a\, (-)^{J+1/2} (J+1/2)]$$

The quantum numbers J and K represent the total angular momentum and its projection on the symmetry axis. The parameter "a" is called the decoupling parameter and consists of a combination of admixture coefficients from the wave function. The Kronecker delta arises from expansion of $\underline{R}^2 = (\underline{J} - \underline{j}) \cdot (\underline{J} - \underline{j})$ and corresponds to terms which include raising and lowering operators $J^{\pm} j^{\mp}$. The properly symmetrized wave functions include both $\pm K$ components, hence only K = 1/2 states will yield non-zero expectation values for operators involving $J^{\pm} j^{\mp}$. Physically, this term corresponds to a Coriolis type interaction.

Single particle states in distorted nuclei were first studied by Nilsson (20) for the axially symmetric nuclei and later by Newton (21) for the general case. Nilsson's treatment consists of a number of approximations and transformations, leading eventually to a wave equation for an anisotropic oscillator plus correction terms. The oscillator solutions can be obtained in either Cartesian or pseudospherical coordinates. The states are characterized by quantum numbers $|n_1\ n_2\ n_3\rangle$ and $|N,\ell,\Lambda,\Sigma\rangle$ for the Cartesian and pseudospherical case, respectively. The numbers $n_1$, $n_2$, $n_3$ correspond to the numbers of excitations along the three axes, while $N = n_1 + n_2 + n_3$. The number $\ell$ is the eigenvalue of a pseudo angular momentum operator $\lambda$, defined in terms of the transformed

position and gradient operators. The eigenvalue of $\lambda_3$ is $\Lambda$, and $\Sigma = \pm 1/2$ is the value of the spin component $S_3$.

The correction terms in the Nilsson Hamiltonian are $C\underline{\lambda} \cdot \underline{s}$ and $D\lambda^2$. The first of these corresponds to the spin-orbit term of the spherical shell model potential. The second term was found necessary to lower the energies of oscillator states of high angular momentum.

Numerical solutions for this system have been published by Mottelson and Nilsson (20). The parameters C and D were chosen so as to give the shell model results for spherical nuclei. Then the splitting of the various shell model levels was plotted as a function of the nuclear deformation.

A number of calculations have been performed for deformed nuclei and the strong coupling. Among the best known of the more general treatments probably are those of Davydov (22). Pashkevich and Sardaryan (23) have applied the treatment for non-axial nuclei to $^{119}Sb$, among others, which is one of the nuclei studied in this thesis.

## 1.4. Nucleon Correlations

While the simple shell model provides good qualitative explanations of many pheneomena, quantitative discrepancies generally exist when one considers excited state energies, transition probabilities, moments, etc.

This should not be surprising, since only particles in average potential wells have been considered, with no provision for interactions among particles in unfilled shells. What is, in fact, surprising, is that in spite of a known very strong nucleon-nucleon force, the interaction between these nucleons is no larger than it is. Hence, it is possible to write the Hamiltonian as the sum of two parts--a part containing all of the ingredients contributing to the average (shell model) potential well and a "residual interaction" term.

One fairly successful treatment considers the residual interaction as made up of a short range pairing force and a long range quadrupole interaction (1). That a pairing force of some kind exists is suggested by empirical evidence. The pair is assumed to have identical quantum numbers except for opposite spin projections. Then the pair is assumed to move in a correlated manner, along with other pairs, over several available single particle levels. Hence, the wave function of the pair may contain admixtures of many single particle states. The excitation of a pair will result in a different admixture of states in the wave function of the pair, and, because of the exclusion principle, will also cause a change in the wave-functions of other pairs.

The long range part of the residual interaction is taken to be dependent upon the quadrupole operator $r^2 Y_2^{\mu}$.

This "quadrupole interaction" is largely responsible for collective motions of the whole nucleus.

The solution to the system is obtained by first solving for the pairing force and then treating the quadrupole interaction by perturbation methods. The wave function is written as a combination of single particle states $|jm\rangle$, weighted by the probability amplitudes $U_j$ ($V_j$) that the state is unoccupied (occupied). One condition on $U_j$ and $V_j$ is that $U_j^2 + V_j^2 = 1$. The quantities $U_j$ and $V_j$ are also defined in terms of other parameters as

$$U_j^2 = 1/2 \left[1 + \frac{\varepsilon_j - \lambda}{\sqrt{(\varepsilon_j - \lambda)^2 + \Delta^2}}\right]$$

$$V_j^2 = 1/2 \left[1 - \frac{\varepsilon_j - \lambda}{\sqrt{(\varepsilon_j - \lambda)^2 + \Delta^2}}\right]$$

where $\Sigma_j$ is the single particle energy arising from the shell model well. The other parameters, $\lambda$ and $\Delta$, can be interpreted as an average Fermi energy and a measure of the thickness of the Fermi energy surface, respectively. These can be obtained from N, the number of particles outside the closed shell, and G, the coupling parameters of the pairing interaction, where

$$N = \sum_j (2j + 1)\ V_j^2$$

and

$$\Delta = G \sum_j (j + 1/2)\ U_j\ V_j$$

The mathematical manipulations are best handled after a canonical transformation to a "quasi-particle" formalism. A quasi-particle can be interpreted as a mixture of a nucleon in the state $|j,m\rangle$ and a hole in $|j, -m\rangle$, with appropriate weights $U_j$ and $V_j$ in the wave function. This transformation results in a set of quasi-particle wave functions in which the shell model plus pairing Hamiltonian is diagonal. Then, with this set as a basis, the quadrupole interaction can be treated by perturbation methods. The quasi-particle energy in a state j (neglecting the quadrupole interaction) is given by

$$E_j = [(\varepsilon_j - \lambda) + \Delta^2]^{1/2}$$

Since the quasi-particles are non-interacting, the energy spectrum of the system is obtained from the sum of the individual quasi-particle energies $E_{j_1}$, $E_{j_1} + E_{j_2}$, $E_{j_1} + E_{j_2} + E_{j_3}$, etc.

A calculation based on pairing and quadrupole forces has been performed by Kisslinger and Sorensen (6) for nuclei from nickel to lead. In this work the single particle energies were chosen once for all nuclei in a large region of the isotope table. But allowance had to be made for smooth variations in these levels with A in order to obtain reasonable agreement with experiment. Furthermore, different level spacings had to be used for neutrons and for protons. Since neutrons and protons fill

separate shell model levels, only pairing between protons and neutrons separately was considered. However, neutron-proton quadrupole interactions could not be excluded. The coupling parameters G were taken to be equal for protons and for neutrons, i.e. $G_p = G_n = G$, as were the quadrupole force strength constants X, i.e. $X_p = X_n = X_{np} = X$. Allowances for a mass dependence in both G and X were made.

# CHAPTER II

# EXPERIMENTAL APPARATUS AND METHODS AND SOURCE PREPARATION

While many standard experimental techniques were employed in this investigation, several new methods were developed. The first few of the following sections give brief descriptions of the experimental apparatus. The next sections summarize the data handling techniques which were employed to facilitate a more rapid and accurate analysis than was possible previously without computers and without the high resolution data recording apparatus. Finally, the last section of this chapter deals with the production and chemical separation of the various tellurium isotopes whose decay schemes were studied.

## 2.1. Ge(Li) Singles Spectrometers

The development of lithium drifted germanium, Ge(Li), detectors in the last two to three years has made possible the observation of many new gamma rays in complex spectra. An improvement of a factor of about 10 in the resolution of the Ge(Li) detectors over that of NaI(Tl) scintillation counters has resulted in the identification of many low intensity gamma rays which are buried by strong neighboring transitions in

spectra recorded with the NaI(Tl) detectors. However, major drawbacks in the Ge(Li) detector are a very low photopeak efficiency, and a very high ratio of Compton to photo electric events. The latter of these is especially bothersome in spectra containing intense high energy gamma rays whose Compton distributions can easily obscure less intense lower energy transitions. Both of these disadvantages are presently being reduced by large volume detectors ($\approx$10 - 30 $cm^3$ as compared to $\approx$1$cm^3$ for the original counters).

The larger volumes increases not only the probability of a photoelectric interaction in the detector, but also the probability of secondary events, i.e. interaction of Compton scattered photons before they escape from the crystal, as well. The effect of larger volume on the full energy peak can be seen in Figure 2, which shows relative efficiency curves obtained for three detectors of different volumes.

The manufacture and principles of operation of Ge(Li) counters have been extensively discussed in the literature, which includes at least two detailed reports (24, 25). A brief summary of the methods employed in this laboratory is given in Appendix B.

In order to derive the maximum benefit from solid state counters, it is necessary for the associated electronics to have very low noise characteristics and high stability. The best resolution obtained so far in

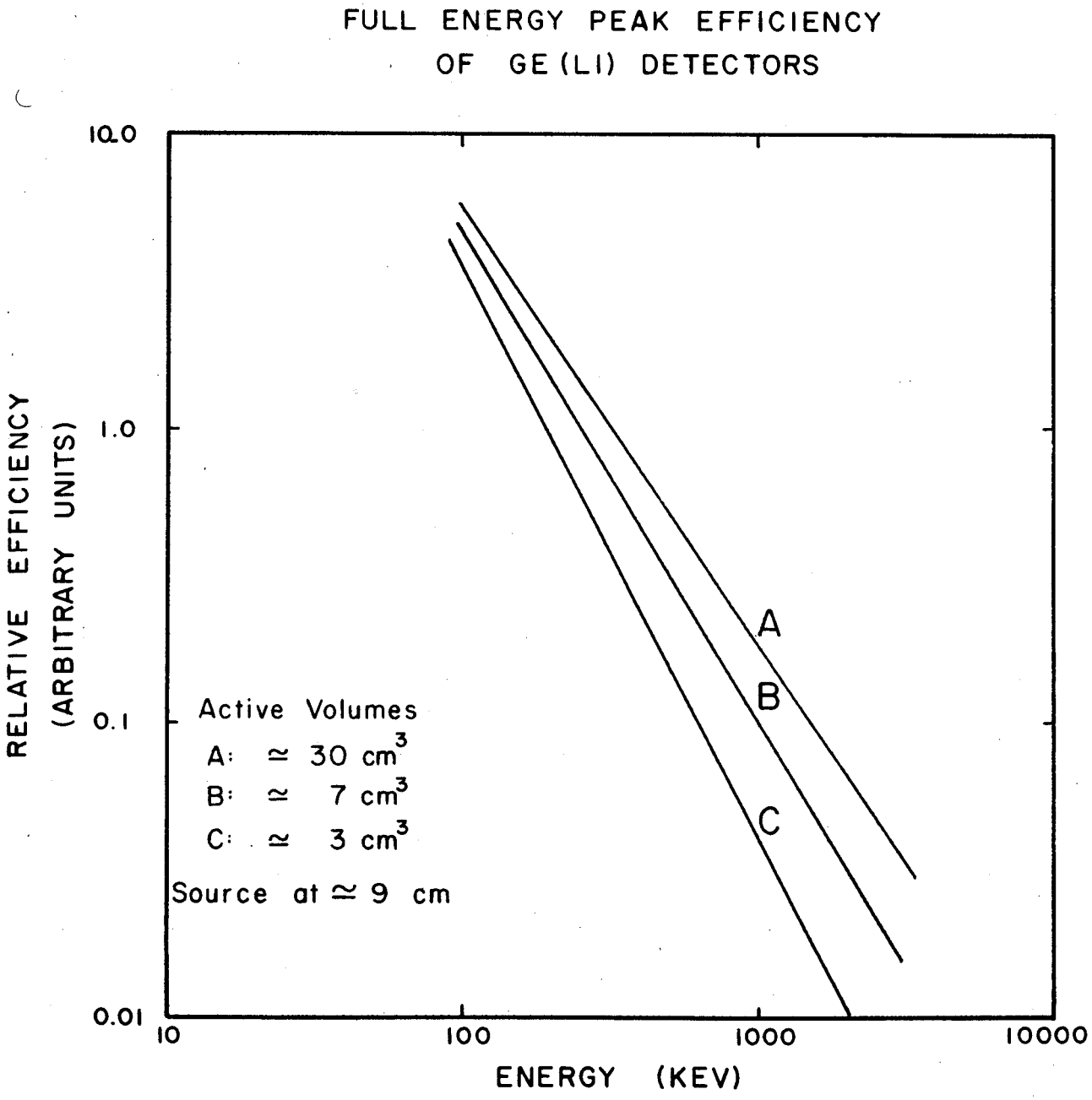


Fig. 2 Relative photopeak efficiency curves for three Ge(Li) detectors. Data for curves A and B were recorded with sources approximately 9 cm from the nearest face of the detector. Data for curve C were recorded at a different time, and the reference point for this curve has been adjusted so that the results approximately correspond to the counting conditions for curves A and B.

this laboratory has been with a 0.8 $cm^3$ detector of approximately 10 pf capacitance, used with an ORTEC 118 room temperature FET preamplifier, a Tennelec TC-200 amplifier, and a Nuclear Data 1024 channel analyser. The full width at half maximum (FWHM) for the 662 keV line emitted by $^{137}Cs$, was approximately 2.8 keV. Typically, resolutions have been approximately 4-5 keV FWHM for $^{137}Cs$.

Various mounting systems have been employed in the laboratory, the most popular being a "dip-stick" arrangement. It can be seen as part of the multiple coincidence spectrometer in Figure 3.

## 2.2. Ge(Li)--NaI(Tl) Coincidence Spectrometers

Lifetimes of nuclear states deexcited by gamma decay are short, typically within a few orders of magnitude of a nano-second. Thus, gamma rays emitted in the deexcitations of successive levels can be effectively considered to be emitted simultaneously. It is therefore possible to use two detectors to record coincident gamma rays, suggesting gamma ray cascades. By considering energy sums, relative intensities, and coincidence relationships among the various gamma rays present in the beta decay of an isotope, it is usually possible to construct a unique scheme of the energy levels populated in that decay.

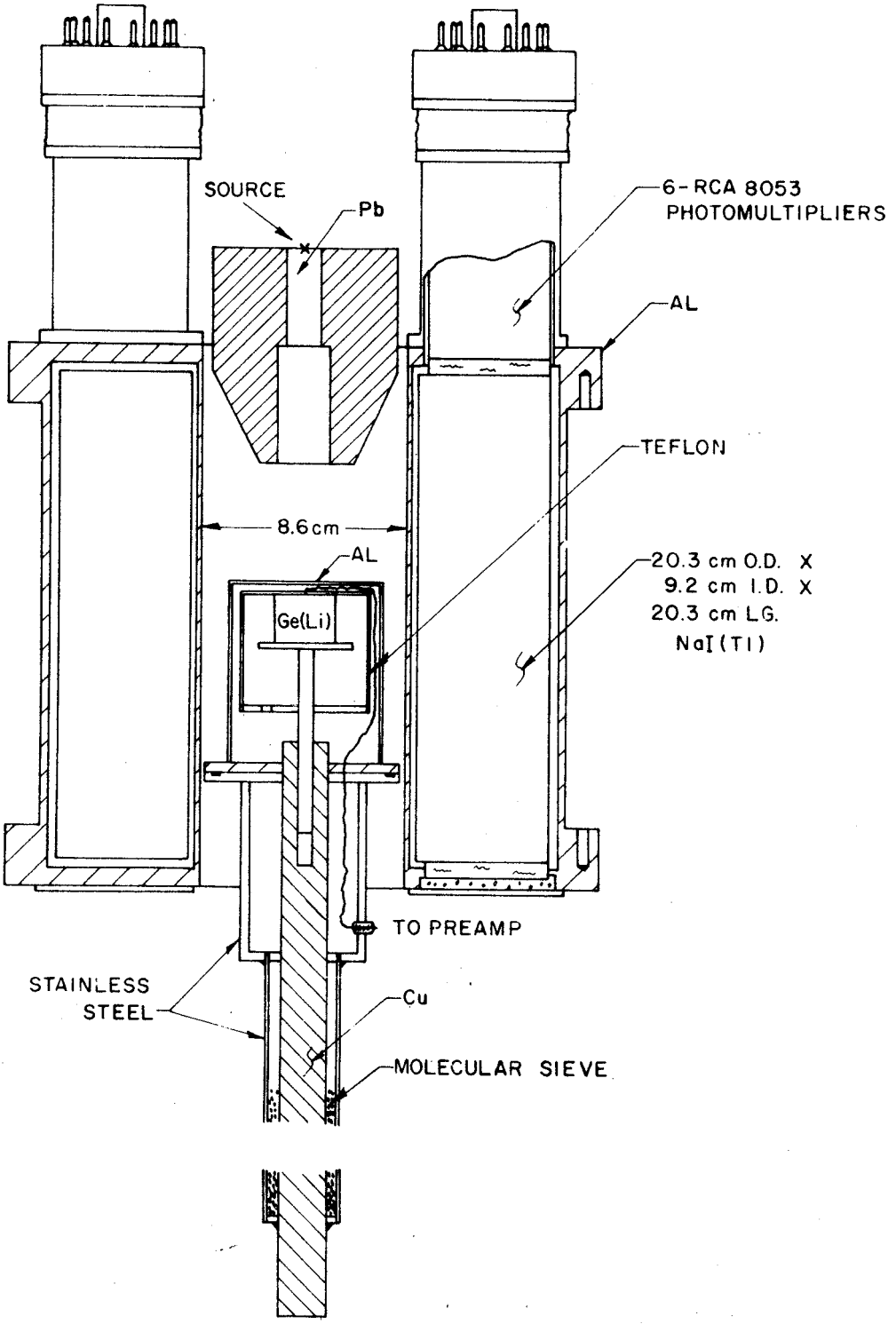


Fig. 3 Cutaway view of the Ge(Li) - NaI(Tl) annulus coincidence spectrometer (from ref. 26). Only two of the six photomultiplier tubes are represented. The lead collimator is used primarily in recording anti-compton and double-escape spectra.

The advantage of excellent resolution in Ge(Li) counters can be carried over to coincidence experiments, but only at a considerable sacrifice in counting efficiency. However, as is evidenced by some of the complex spectra discussed in section 3.2, the Ge(Li)--NaI(Tl) coincidence combination is essential if most of the ambiguities of the proper relationship of the gamma rays in the decay of a nucleus are to be resolved.

### 2.2.1. Conventional Coincidence Experiments

The experimental coincidence counting arrangement is schematically illustrated in Figure 4. In general, only a narrow segment of the spectrum seen by the NaI(Tl) detector was selected by the single channel analyser. Then those events in the Ge(Li) detector, which were in coincidence with this region of the NaI(Tl) spectrum, were recorded in the analyser.

To avoid gain drifts during the long counting times involved, it was often found desirable to enclose a large share of the apparatus in a styrofoam box, in which the temperature was controlled to within $\pm 0.5$ C°. Because of the large amount of Compton scattering out of the Ge(Li) crystal, either shielding and/or careful geometric orientation of the crystals was necessary.

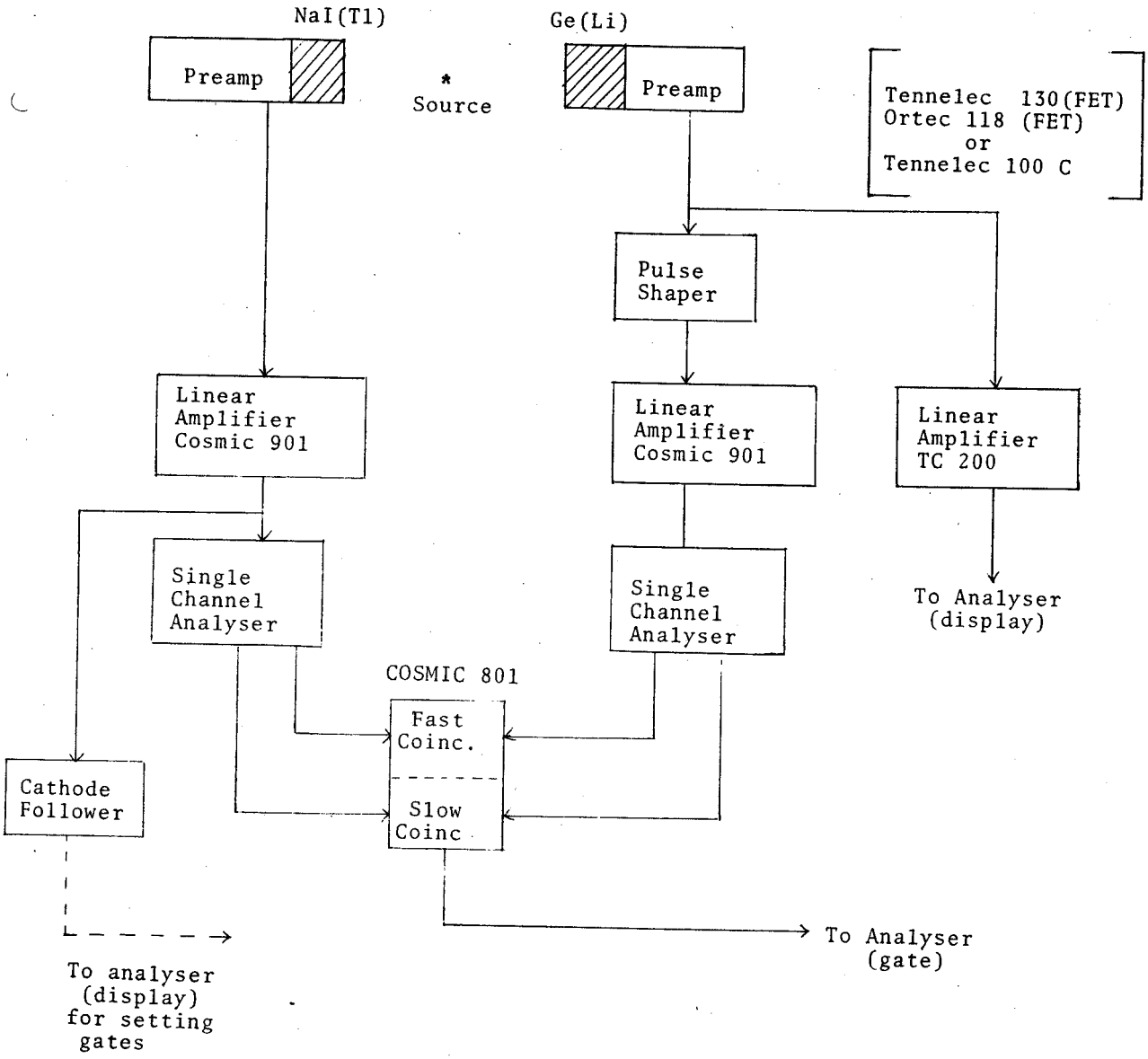


Fig. 4. A schematic illustration of the Ge(Li)-NaI(Tl) coincidence apparatus.

## 2.2.2. Experiments Utilizing a Split-ring NaI(Tl) Annulus

A Ge(Li)--NaI(Tl) coincidence system employing a 20.3 cm x 20.3 cm split ring NaI(Tl) annulus was used for some experiments. Since this system is discussed in some detail elsewhere (26), only a brief description will be presented here.

The detector arrangement is illustrated in Figure 3. If the gamma rays are collimated into the Ge(Li) counter as shown, the system can be used either as an anti-Compton or as a double escape spectrometer. In the former case, because of the shielding from the collimator, the majority of the pulses which arise from the NaI(Tl) crystal are those due to Compton scattering from the Ge(Li) crystal (and its mount) into the NaI(Tl). Hence, by closing the analyser gate whenever simultaneous pulses are detected in the solid state counter and in the annulus, most of the Compton events occuring in the Ge(Li) counter are rejected from the spectrum. One serious drawback to the arrangement, as shown, is that the Compton crossection favors scattering back toward the source. Hence pulses corresponding to Compton knees are less likely to be rejected. In fact, if the Ge(Li) counter is lowered further, decreasing the solid angle through which scattered photons may escape from the annulus, the Compton knee takes on a peak-like appearance, and can cause some confusion in complex spectra. So far, attempts

to insert low Z material above the Ge(Li) counter for the purpose of directing some of the backscattered photons to the annulus through secondary scattering, have not yielded significantly improved results. An improvement can be obtained if a 7.6 cm x 7.6 cm NaI(Tl) crystal is inserted in the top portion of the hole and is used together with the annulus. However, in this case the source must be placed inside the annulus and a loss of counts due to coincident gamma rays will result.

The application of this system as a double escape spectrometer is probably the most impressive. Because of the split crystal, it is possible to require simultaneous signals from both halves of the annulus and from the Ge(Li) counter (i.e. triple coincidence experiments). If the window for each half is set to include only signals corresponding to 511 keV, then the only events, in principle, which are counted by the spectrometer are those in which a gamma ray interacts with the Ge(Li) counter by pair production, with one of the subsequent annihilation quanta being detected by each half of the annulus. If an uncollimated positron emitting source is placed inside the annulus, gamma rays which are in coincidence with annihilation radiation following $\beta+$ decay are also recorded in the Ge(Li) spectrum. That events due to multiple scattering and to chance coincidences are practically eliminated can be seen in some of the figures presented in the next chapters.

Other useful applications include triple coincidence, any-coincidence, and anti-coincidence experiments. For all of these, the collimator is removed and the source placed close to the Ge(Li) counter. The usefulness of triple coincidence experiments for identification of cascades should be obvious. The any-coincidence and anti-coincidence are, in a sense, complementary experiments, but represent a tool with a subtle power which is not fully appreciated in general. Since integral gates with low discriminator settings are generally used, the Compton as well as photo events in the gating NaI(Tl) annulus detector can trigger a coincidence signal, increasing the overall coincidence efficiency. Thus, a comparison of relative intensities in these spectra to relative intensities in singles serves to immediately establish any levels which are populated by beta decay only and de-excite directly to ground. In addition, these relative intensity measurements can suggest cascades and can indicate which transitions originate from heavily gamma fed levels.

Extra caution must sometimes be exercized when interpreting coincidence spectra recorded with very large detectors such as the annulus. Because of the large solid angle subtended by the NaI(Tl) detector, more than one gamma ray of a given cascade may be detected by this crystal, giving rise to a pulse corresponding to the sum of the energy of the two gamma rays. Because of this

summing, coincidence events may be lost from the Ge(Li) spectrum since the NaI(Tl) pulse will no longer fall inside the gate region selected by the coincidence circuitry. A major advantage of this summing is a "clean up" effect on Compton backgrounds. The Compton scattered gamma ray from the Ge(Li) counter may also be picked up by the annulus detector. Since the resulting pulse from the annulus will no longer satisfy the gate requirements, that Compton event will not be recorded in the Ge(Li) spectrum. A striking example of this effect can be seen in Figure 5, which shows triple coincidence spectra from the decay of $^{119m}$Te (This activity is discussed in considerable detail in Chapter 3). Because of summing in the gate the Compton distribution of the 912 keV gamma ray in spectrum B of Figure 5 is essentially absent.

### 2.2.3. Angular Correlation Experiments

One can obtain information about energy level spins and transition multipolarities by measuring the relative angular distribution of gamma rays emitted in cascade. The direction of one gamma ray is chosen as the z-axis, and the coincidence counting rate is recorded at various angles with respect to that axis. A more detailed description of angular correlation experiments and their interpretations is given in Appendix C.

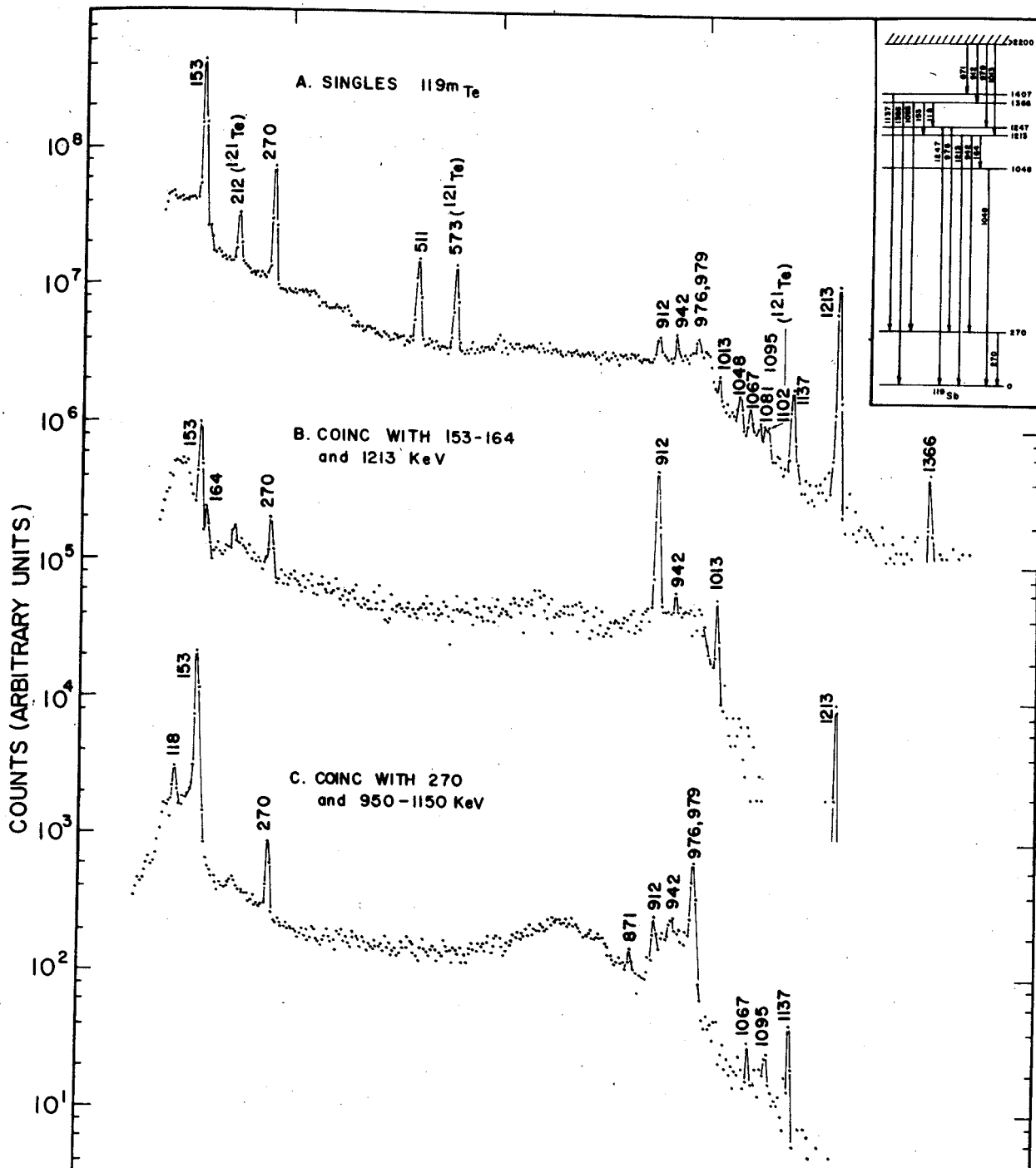


Fig. 5 Results of a triple coincidence experiment with the NaI(Tl) annulus and a 7 $cm^3$ Ge(Li) detector. The pertinent part of the decay scheme being investigated is shown in the upper right-hand corner of the figure. A singles spectrum is shown for easier identification of coincident photopeaks. Note the absence of the Compton distribution of the 912 keV gamma ray in spectrum B.

The angular correlation apparatus can also be schematically illustrated as in Figure 4. In this case the NaI(Tl) detector was mounted on a movable arm which enabled the detector to be rotated from 90° to 270° with respect to a line defined by the center of the fixed Ge(Li) crystal and the source. The NaI(Tl) crystals employed were of two sizes--7.6 cm x 7.6 cm and 5.08 x 5.08 cm. During the course of the experiments, two different Ge(Li) detectors were used. Both of these were of the 5 sided wrap-around type and had active volumes of approximately 20 $cm^3$ and 30 $cm^3$. The best resolution obtained for these detectors was ≈ 4.5 keV FWHM for the 662 keV line in $^{137}Cs$. However, since a different preamplifier was used for the correlation experiments and pulse shaping requirements for the coincidence circuitry had to be met, typical resolutions were ≈ 8 to 9 keV FWHM. The larger of these counters was mounted with the p-type core in a vertical position, while the core of the smaller crystal was in a horizontal position with the open face farthest from the source. Both detectors were mounted in elbow-type cryostats with a liquid air reservoir placed above the coldfinger.

To minimize gain drifts in the electronics, the temperature surrounding most the apparatus was kept constant to within $\pm$ 0.5 C°. In order to compensate for any small drifts which might occur, spectra were recorded at

each angle for short periods (typically 40 minutes) only. The final spectra for each angle were summations over a number of such individual spectra, and included spectra recorded at 360° minus that angle. In this manner first order corrections were also made for small misalignments in the source position and for source decay.

A multiple coincidence unit with a variable resolving time was employed, and spectra were simultaneously recorded in the two halves of a 1024 channel analyser. Typical resolving times were $\lesssim$ 80 nanosec.

Source strengths were of the order of a few microcuries. Typically $10^3$ pulses/sec from the NaI(Tl) detector satisfied the gate requirements. Approximately 0.5% of these were in coincidence with pulses from the Ge(Li) detector.

## 2.3. X-ray Intensities

A 2.5 cm x 3.8 cm NaI(Tl) crystal with a 0.013 cm thick Be window was used for x-ray measurements. The relative efficiency of the detector was checked with $^{137}$Cs and $^{113}$Sn sources, both of which have x-rays of well-known intensity relative to a gamma ray (15). The energies of these x-rays fell on both sides of the region of interest. No significant absorption by the Be window was observed for x-rays in the 25-30 keV range. The intensity of the x-ray in the "unknown" spectrum was

then determined relative to that of a prominent gamma ray or group of gamma rays.

## 2.4. Positron Endpoints

Positron endpoints of $^{117}$Te were measured with a 0.64 cm thick plastic scintillator mounted on a phototube. Aluminized mylar of 0.0013 cm thickness was used as the window.

Energy calibrations were made from conversion lines of $^{113}$Sn and $^{207}$Bi. The centroids and weighted energies of the composite K and L lines were used. The spectra were recorded with a source distance of several millimeters. After a carbon absorber was inserted between the source and the detector, counts were subtracted from the spectrum in the analyser to correct for Compton events of gamma rays.

Positron spectra were recorded in coincidence with annihilation radiation and in coincidence with the strongest gamma rays de-exciting suspected positron fed levels. Because of source thickness, attenuation in the window and in air, and poor resolution of the plastic, no conclusive evidence in regard to spectral shapes could be obtained.

## 2.5. Data Analysis

In order to take full advantage of the high resolution and accuracy afforded by the Ge(Li) spectrometers, and to facilitate handling large amounts of data rapidly, much

of the analysis were carried out on the MSU CDC-3600 and the MSU Cyclotron Labratory's SDS SIGMA-7 computers. Most of the data were plotted with the CDC-3600 system using modifications of the GRAPH program originally written by T. Rice (27).

Energy and relative intensity determinations are discussed in more detail below.

### 2.5.1. Energy Measurements

The energies of the prominent lines in "unknown" spectra were determined by counting the unknown source simultaneously with several standard sources which emit gamma rays of well-known energy. To correct for non-linearities in the system, both first and second order least squares calibration equations were constructed. The peak positions were taken to be the centroids, which were determined after an appropriate subtraction of the background under the peaks. All of these computations were performed by the MIKIMAUS program, which is described in more detail in Appendix D.

The errors quoted on the gamma ray energies are based on deviations from mean values obtained from several measurements. The individual runs were weighted by the reproducibility of the standard energies from the calibration curves. A set of typical calibration data with both linear and quadratic fits, is shown in Table 1 . The non-linearity of the system is readily apparent. It can

Table 1.--Typical Calibration Data

Linear Calibration: Energy = 9.855 + 1.514 x (Channel)
Quadratic Calibration: Energy = 14.404 + 1.490 x (Channel) + 0.0000 23 x $(\text{Channel})^2$

| Energy | Channel | Linear Fit | Deviation | Quadratic Fit | Deviation |
|---|---|---|---|---|---|
| 284.307[a] | 180.63 | 283.357 | 0.950 | 284.296 | 0.011 |
| 364.467[a] | 234.09 | 364.296 | 0.171 | 364.454 | 0.013 |
| 661.595[b] | 431.53 | 663.248 | -1.653 | 661.654 | -0.059 |
| 1173.226[c] | 768.58 | 1173.582 | -0.356 | 1173.126 | 0.100 |
| 1132.483[c] | 872.94 | 1331.595 | 0.888 | 1332.547 | -0.064 |

[a]Present in the decay of $^{131}I$; energy value from Reference 15.

[b]Present in the decay of $^{137}Cs$; energy value from Reference 25.

[c]Present in the decay of $^{60}Co$; energy value from Reference 25.

also be seen that the standards typically reproduced to within ± 0.1 keV from the accepted value. Errors quoted on standard energies (such as 1173.226 ± 0.040 and 1332.483 ± 0.046 keV (25) for the gamma rays in $^{60}Co$) were usually ignored since they are approximately only 10% of the other errors.

Once the prominent lines were accurately measured (usually to less than ± 0.5 keV), they were used as internal calibration points for measuring the weaker lines in subsequent spectra. In these cases the uncertainties of the calibration points were taken into account when assigning errors to the weaker lines.

It should be pointed out that the accuracy in the energy measurements can be significantly increased if one uses larger analysers such as 4096 channel system. The uncertainty in the energy of a peak is dependent upon the error in the position of the centroid of the peak. Hence spreading out the same spectrum over four times as many channels reduces this contribution to the energy error by a factor of four. Namely, an uncertainty of 0.1 channels in the position of the centroid corresponds to 0.2 keV if an analyser calibration of 2.0 keV/channel is used as opposed to only 0.05 keV if the calibration can be increased to 0.5 keV/channel. A further advantage of a larger system arises from the fact that at a lower keV/channel calibration, the peak will be composed of more points, which will result in a better approximation of a

smooth curve. It has been pointed out by Heath et al. in a comprehensive study of energy measurement accuracy (28) that a minimum of 5 channels per peak is necessary to make contributions to the error from finite channel widths negligible. With some of the present detectors (FWHM 3.0 keV) and a 1024 channel system this requirement is satisfied only for energies up to approximately 1 MeV. As counting systems with better resolution become available, a larger analyser will become even more necessary in order to obtain a high degree of accuracy without a sacrifice in resolution.

### 2.5.2. Relative Intensity Measurements

Relative photopeak efficiency curves were obtained in two ways. First, a set of standard gamma ray sources whose absolute intensities were measured with NaI(Tl) detectors were used. However, because of uncertainties in geometry and in NaI(Tl) efficiency tables (29), errors of $\pm$10% were assigned to the individual intensities.

Second, a set of points was obtained from sources emitting several gamma rays whose relative intensities were obtained from existing decay schemes. An example of an especially good source for this is the decay of 5.6 day $^{120}$Sb into $^{120}$Sn. All of the beta feeding is to an excited state in $^{120}$Sn which de-excites only by a four step cascade, with no crossovers (30). Hence, all of the transitions at 89, 196, 1022, and 1171 keV are of

equal intensity. From the known multipolarities, only the 89 keV transition has a significant correction for internal conversion.

In general, efficiency curves obtained for a detector by each of the above methods were in very good agreement.

Relative intensities of at least the prominent lines in "unknown" spectra were determined with calibrated detectors and in geometry closely matching that used in the calibration. These strong lines then served as internal detector efficiency calibration points in later spectra, making relative intensity determinations of other gamma rays in the spectra approximately absorption and geometry independent.

### 2.5.3. Angular Correlation Measurements

A more detailed discussion of the interpretation of angular correlation measurements is given in Appendix C and in section 2.2.D of Chapter III. This section is primarily concerned with difficulties encountered in measuring the angular correlation coefficients accurately.

The correlation coefficients obtained were approximately corrected for the diminutive effects of the finite solid angles subtended by the detectors. The correction for the NaI(Tl) detector was obtained from calculated tables (31). Because of the irregular geometry, calculations become

very difficult for Ge(Li) detectors. It was assumed that an approximate correction could be made from tables for NaI(Tl) detectors of comparable size. That this assumption was not grossly in error was demonstrated by performing the angular correlation measurements on well known cascades (15) present in the decays of $^{60}Co$ and $^{152}Eu$. Results of experiments on the well known correlations in these two isotopes suggest that the finite size detector correction is approximately 5% for gamma ray energies in the 1 MeV region, and increases to possibly 10% near 100 keV. All measurements were performed with the same source to detector distance, 5.2 cm.

Peak areas were generally determined as discussed in section 2.5.2. First order corrections for coincidences with Compton events in the gate were made from spectra recorded in coincidence with regions adjacent to the peak. Wherever possible, gates were simultaneously set on the photo-peak and on regions on both sides of the peak. The two Compton gates were of approximately equal width, which, in turn, was approximately one-half the width of the photopeak gate. The outputs of the two Compton coincidence circuits were combined and the resulting Compton coincident spectrum was recorded in that half of the analyser memory which was not used to store counts in coincidence with the photopeak region.

Corrections for random coincidence events were made in one of two ways. First, a chance coincidence spectrum was recorded by delaying the signal from either detector by a time greater than twice the resolving time of the coincidence unit. After any counting time and/or decay corrections, the appropriate number of counts could be subtracted from the true plus random coincidence spectra. A second method was sometimes used if a given line in the spectrum was known definitely to be not in true coincidence with any events of any type in the gate. Normalization of a singles spectrum to this line then yielded an appropriate correction.

In general, the gate was set on the higher energy member of a given cascace. The advantages in this case are threefold. First, the greater efficiency of NaI(Tl) relative to Ge(Li) for high energy gamma rays increases the coincidence count rate. Second, in the higher energy regions of the spectrum there are fewer gamma rays whose Compton distributions will fall in the gate. Hence Compton corrections will usually be smaller, and in some cases can be eliminated. Third, because of a decrease in the total number of counts (photo plus underlying Compton) in the gate, the chance rate due to the unwanted gating counts will also be reduced.

The errors assigned in the correlation measurements are based primarily on the reproducibility of the correlation function over several measurements, and on the uncertainty in the solid angle corrections. It was found that typically the values reproduced to an average value ± approximately 10 to 20%. The primary difficulty was suggested to be due to poor statistics resulting from the very low count rates. This, combined with an estimated 5 to 10% uncertainity in solid angle corrections, implies the results to be good to approximately ± 20%.

## 2.6. Source Preparation

The $^{129}$Te parent was produced by neutron bombardments of tellurium metal, enriched to 99 per cent in $^{128}$Te. The $^{129m+g}$Te activity was obtained by irradiating 20 mg samples in a thermal neutron flux of $\approx 2 \times 10^{14}$ n cm$^{-2}$sec$^{-1}$ for periods of seven days in the ORR reactor at the Oak Ridge National Laboratory. Besides $^{131}$Te and its daughter $^{131}$I, other activities were made in minor quantities. The most significant difficulty was caused by $^{110}$Ag which was present in some aged sources. The 70 minute $^{129g}$Te activity was produced by repeated short (7 to 60 min) irradiations of 10 mg samples of enriched $^{128}$Te in a flux of $4 \times 10^{12}$ n · cm$^{-2}$sec$^{-1}$ in the Ford Nuclear Reactor at the University of Michigan.

Proton bombardments of natural antimony metal, or of $SbCl_3$, were used to obtain the $^{119}Te$ and $^{117}Te$ activities from the $^{121,123}Sb$ (p,xn) reaction. Various proton energies from 26 to 52 MeV were used. The primary activities produced were $^{117}Te$, $^{118}Te$, $^{119}Te$, $^{121}Te$, $^{120}Sb$, and $^{122}Sb$. the optimum proton energy for producing $^{119}Te$ was found to be approximately 34 MeV. Above 39 MeV, the $^{118}Te$ contaminant was also produced in significant quantities, while at lower energies the ratio of $^{121}Te$ to $^{119}Te$ increased. While sufficient amounts of $^{117}Te$ could be produced at 48 MeV, the relative yield of $^{117}Te$ to $^{119}Te$ approximately doubled when the proton energy was raised to 52 MeV. The proton beams were produced with the MSU cyclotron.

The tellurium activities were chemically extracted from the target material by precipitation with $SO_2$ gas. The metal target was dissolved in aqua regia and converted to the chloride form by boiling the solution to dryness to remove any nitrates. The residue was dissolved in 3N HCl, and hydroxylamine hydrochloride was added. The solution was placed in a warm water bath, and $SO_2$ gas was bubbled through it to precipitate tellurium metal (32).

In cases where the target material was $SbCl_3$, the chloride form was obtained directly by dissolving the target in HCl. Because of the more rapid chemical separation, the $SbCl_3$ targets were used to obtain the 1.1 hour $^{117}Te$

activity from short (a few minutes) bombardments. For longer bombardments this form of target was unsatisfactory because of its low melting point and deliquescence.

The $^{129m+g}Te$ activity was allowed to stand until traces of the $^{131}I$ had disappeared, eliminating the need for confining the iodine vapors. No chemistry was attempted on the $^{129g}Te$ activity. In the case of $^{119}Te$ and $^{117}Te$, it was necessary to add tellurium carrier in order to remove the microscopic amount of tellurium from the many milligrams of antimony.

# CHAPTER III

## EXPERIMENTAL RESULTS

### 3.1. Summary of Previous Studies on the Activities of $^{117}Te$, $^{119}Te$ and $^{129}Te$

Prior to the development of high resolution Ge(Li) detector systems, the decay schemes of $^{117}Te$, $^{119}Te$ and $^{129}Te$ had been studied by several investigators (32-43). During the study performed in this laboratory, results of several other investigations of $^{119}Te$ and $^{129}Te$ were published (44-49). Although most of these latter studies utilized Ge(Li) detectors, there were many points of disagreement among the individual decay schemes. Hence it was felt that a continuation of the present study was justified.

Brief summaries of the results obtained by various groups are presented in Tables 2, 3, and 4. For brevity, while several similar reports are available from different investigators, only one or two of these, representative of a given technique or type of experiment, are listed. Major steps in the evolution of the energy level schemes of $^{119}Sb$ and $^{129}I$ are shown in Figures 6 and 7, respectively.

Table 2.--Past studies of the decay of $^{129}$Te.

| Investigators | Techniques Used | Quantities Measured | Levels (keV) or other Principal Results |
|---|---|---|---|
| 1. Graves, Mitchell (41) | magnetic lens spectrometer, scintillation detectors | $E_\gamma$, $I_\gamma$, $\gamma\gamma$-coinc $\beta$ -coinc | 27, 502, 720, 1150 |
| 2. Ramayya, Yoshizawa, Mitchell (42) | scintillation detectors | $E_\gamma$, $I_\gamma$, $\gamma\gamma$-coinc $\beta\gamma$-coinc | 27, 280, 492, 570 710, 840, 1045, 1127 1255, 1400 |
| 3. Devare, Devare (43) | scintillation detectors, $\beta$-spectrometer | $E_\gamma$, $I_\gamma$, $\gamma\gamma$-,$\beta\gamma$-coinc $\beta$-shapes $\delta_T$ of $\gamma_{28keV}$ | 27, 275, (350 or 755), 482, 550, 695, 810, 830, 1105, 1235, 1385 1415 |
| Present Investigations Begin | | | |
| 4. Bornemeier, Potnis, Ellsworth, Mandeville (46) | Ge(Li) detector, scintillation detectors | $E_\gamma$, $I_\gamma$, $\gamma\gamma$-coinc[a] | 27, 277, 482, 550, 750, 497, 837, 1065, 1112, 1222, 1385; Identify several new transitions |
| 5. Gupta, Saha (47) | scintillation detectors | $E_\gamma$, $\gamma\gamma$-coinc $\gamma\gamma$ ($\theta$)[a] | b |
| 6. Hurley, Mathiesen (48) | Ge(Li) counter, scintillation counters | $E_\gamma$, $I_\gamma$, $\gamma\gamma$-coinc[a] | 27, 278, 343, 487, 557, 697, 730, 831, 846, 1022, 1077, 1083, 1112, 1262, 1378, 1404, 1427 |
| 7. Bemis, Fransson (49) | Iron core double focussing electron spectrometer | $E_{ce}$, $x_\alpha$, $\delta^2$ of 28 keV transition | c |
| 8. Walters, Gordon (50) | Ge(Li) detector, scintillation counter | $E_\gamma$, $I_\gamma$, coinc[d,e] | 28, 278, 487, 560, 696, 730, 769, 830, 845, 1050, 1111, 1260, 1291, 1402 |
| 9. Eastwood, Witzke, Walker (52) | Ge(Li) detector | $E_\gamma$, $I_\gamma$[e] | f |

[a] Coincidence counting performed with NaI(Tl) detectors only.

[b] Interpretation of angular correlation data based on decay scheme proposed by Devare and Devare, reference 43.

[c] Measurements confined to properties of 28 keV state.

[d] Coincidence counting performed with Ge(Li)-NaI(Tl) detector combination.

[e] Results in very good agreement with our investigation.

[f] Did not publish a decay scheme.

Table 3.--Studies of the Levels in $^{119}Sb$.

| | Investigators | Techniques and Apparatus | Quantities Measured | Energy Levels (keV) or Other Principal Result |
|---|---|---|---|---|
| 1. | Fink, Andersson, Kantele (32) | magnetic spectrometers, scintillation counters | $E_\gamma$, $I_\gamma$, $\gamma\gamma$-coinc, $T_{1/2}$ | 270, 648, 1220, 1370 1390, 1760, 2360 |
| 2. | Gupta, Pramilla, Raghavan (36) | scintillation counters | $E_\gamma$, $I_\gamma$ $\gamma\gamma$-coinc | 270, 645, 1220, 1370 1760, (2150), 2220, 2290, 2370 |
| 3. | Kantele, Fink (37) | scintillation counters | $E_\gamma$, | 271, 645, 702, 1054 1221, 1374, 1755, (2130), 2205, 2291, 23 |
| 4. | Svedberg, Andersson (38) | magnetic spectrometer, scintillation counters | $E_\gamma$, $E_{ce}$, $\alpha_{total}$, $\alpha_K$ | a |
| | | Present Investigations Begin | | |
| 5. | Ramayya (39) | scintillation counters | $\gamma\gamma$ ($\theta$) | b |
| 6. | Singru, Devare, Devare (44) | Ge(Li) and scintillation $\pi$ $\sqrt{2}$ double focussing spectrometer | $E_\gamma$, $I_\gamma$, $E_{ce}$, $I_{ce}$, $\gamma\gamma$ ($\theta$), $\gamma\gamma$-delay $\alpha_K$, $\alpha_L$[c] | 270, 1048, 1212, 1365 2281, 2292, 2349, 2365 |
| 7. | Graeffe, Hoffman, Sarantites (45) | Ge(Li), Si(Li) and scintillations counters | $E_\gamma$, $I_\gamma$, $\gamma\gamma$-coinc, $\gamma\gamma$ ($\theta$)[d] $\alpha_K$, $\alpha_{L+M}$ | 270, 644, 700, 1048 1213, 1250, 1338, 1366 1407, 1413, 1387, 1750 1822, 2129, 2226, 2278 2284, 2360[e] |
| 8. | Bassani et al. (54) | $^{118}Sn$ ($^3He$,d) reactions | Q-values | 268, 604, 668, 1315, 1370, 1808, 2118, 2264 2346, 2702, 2776 |
| 9. | Ishimatsu et al. (55) | $^{118}Sn$ ($^3He$,d) reactions | Q-values | 270, 660, 710, 1370, 1490 |
| 10. | Barnes et al. (56) | $^{118}Sn$ ($^3He$,d) reactions | Q-values | 261, (385), 635, 695, 1335, 1460, 1640, 1830 1950, 2075, 2215, 2280 2355, 2545 |

[a]Assign spins to some levels in decay scheme proposed by Kantele and Fink, Reference 37.

[b]Report includes study of angular correlations only.

[c]Coincidence counting performed with scintillation detectors only.

[d]Coincidence counting performed with Ge(Li)-NaI(Tl) detector combination.

[e]Decay scheme in very good agreement with that proposed in our investigation.

Table 4.--Studies of the levels in $^{117}Sb$.

| Investigators | Techniques Used | Quantities Measured | Levels (keV) or Other Principal Results |
|---|---|---|---|
| 1. Vartanov, et al. (33) | twin lens electron spectometer, scintillation counters | $E_\gamma$, $I_\gamma$, $T_{1/2}$, $E_{\beta+}$ $\gamma_k$ | a |
| 2. Fink, Andersson, Kantele (32) | magnetic spectrometer, scintillation counters | $E_\gamma$, $I_\gamma$, $E_{\beta+}$ | 718, 1290, 1720, 2240, 2800 |
| | Present Investigations Begin | | |
| 3. Butement Qaim (34) | scintillation counters | $E_{\beta+}$, $T_{1/2}$ | suggest $^{117m}Te$ |
| 4. Bassani et al. (54) | $^{116}Sn$ ($^3He$,d) reactions | Q-values | 530, 700, 915, 1328 1778, 1840, 2172, 2244 |
| 5. Ishimatsu et al. (55) | $^{116}Sn$ ($^3He$,d) reactions | Q-values | 520, 720, 920, 1320, 1380, 1470, 1790, 1990, 2140, 2210, 2280, 2410, 2520, 2610, 2880, 2980, |
| 6. Barnes et al. (56) | $^{116}Sn$ ($^3He$,d) reactions | Q-values | 530, 725, 941, 1337, 1389, 1570, 1681, 2240, 2320, 2443, 2502, 2562 2629 |

[a]Preliminary publication; decay scheme not available.

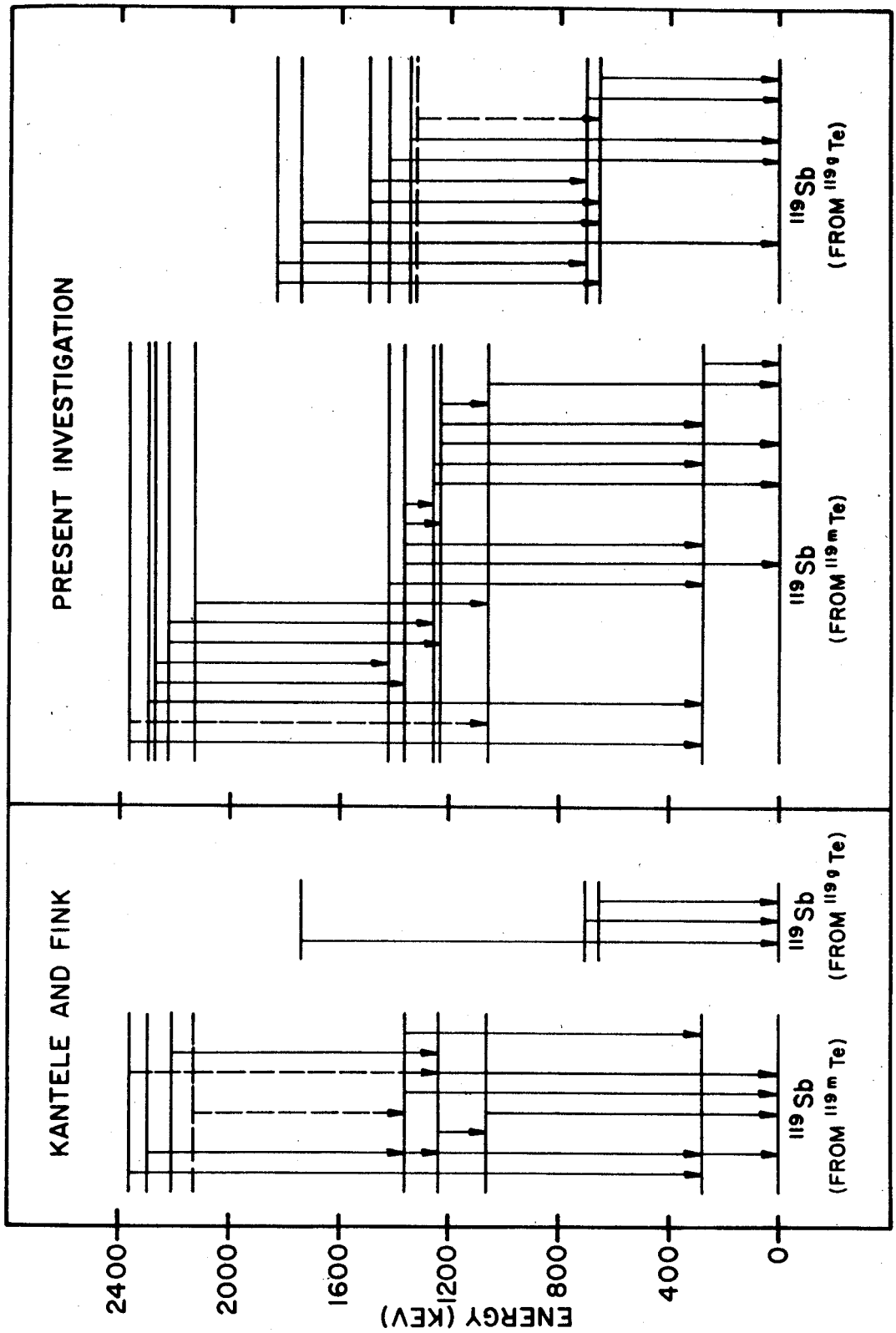


Fig. 6 Decay schemes of $^{119}$Te isomers which were constructed from scintillation and conversion electron studies, compared to those constructed from high resolution

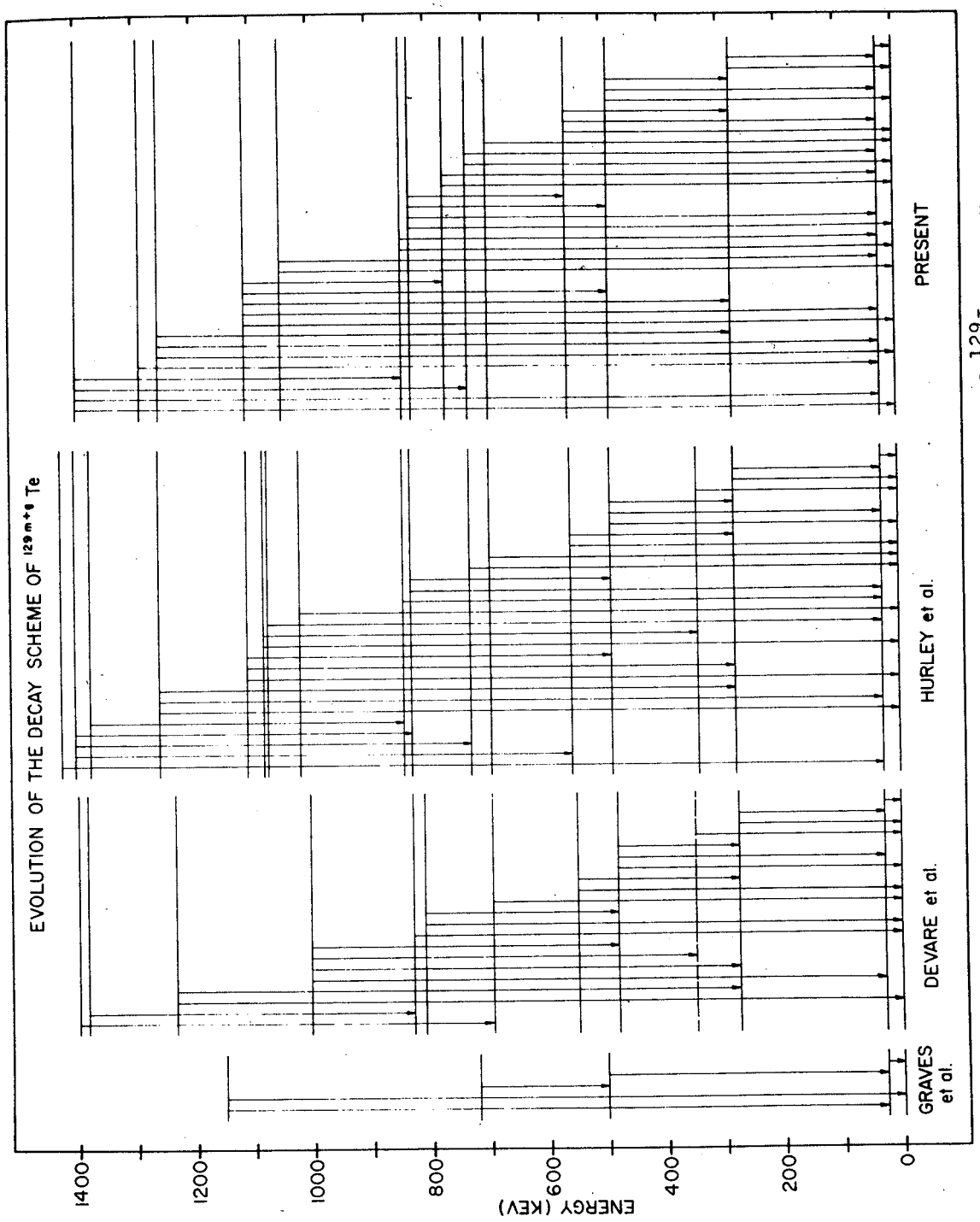


Fig. 7 Evolution of the energy level scheme of $^{129}$I as populated by the beta decays of $^{129m+g}$Te. Further comparisons are made in table 2.

Near the end of our study of $^{129}$Te, a preliminary publication showed our results to be in excellent agreement with those obtained by investigators at Massachusetts Institute of Technology (MIT) (50). Becase of the good agreement, it was decided to present a joint publication of the results obtained at MIT and here (51). These results were also confirmed by an independent third group of investigators at Chalk River (52).

In the case of $^{119}$Te, our results were again in excellent agreement with those obtained by another group at MIT (45). However, no joint publication was attempted since our manuscript was already prepared before either group was aware of the others' results.

Another joint MSU-MIT publication is being prepared at present for the case of $^{117}$Te (53). Again, it should be stressed that the investigations were performed independently. Additional strength is given to this publication because different methods were used to produce the $^{117}$Te activity. The MIT group used the $^{116}$Sn ($\alpha$, 3n) reaction while the MSU group obtained sources from the (p, 5n) reaction on $^{121}$Sb.

## 3.2. Results of this Investigation

### 3.2.1. Decay Schemes of $^{129g}$Te and $^{129m}$Te.

3.2.1.A.--The gamma ray singles spectra--Singles spectra of 70 min. $^{129g}$Te and 33 day $^{129m}$Te in

equilibrium with $^{129g}$Te are shown in Figure 8. These spectra were recorded with a 3 cm Ge(Li) detector. The suggested presence of gamma rays at 769 and 1374 keV in these figures was confirmed in later spectra with better statistics. The energies and relative intensities of the gamma rays are given in Table 5. These are in good agreement with results obtained independently at about the same time by Walters et al. (50) of M.I.T., Eastwood et al. (52) of Chalk River and Hurley et al. (48) of NRDL. The results from these different investigations are compared in Table 5.

The relative intensities of the 279 and 343 keV given in Table 5 were determined from coincidence experiments, since the gamma rays involved in each pair were too close in energy to be resolved by our detectors. The identification of these two doublets is discussed in a later section. In the case of the first pair, the spectra in coincidence with the 833 keV gamma ray were compared to singles and the missing intensity of the 279, relative to the 250 keV line, was assigned to the 281 keV gamma ray. In the latter case, the intensities were determined by comparing the intensities of the 624 and 343 keV lines in singles and in coincidence with the 459 keV gamma ray.

The energy of the 28-keV transition was measured with a proportional counter and its intensity with a

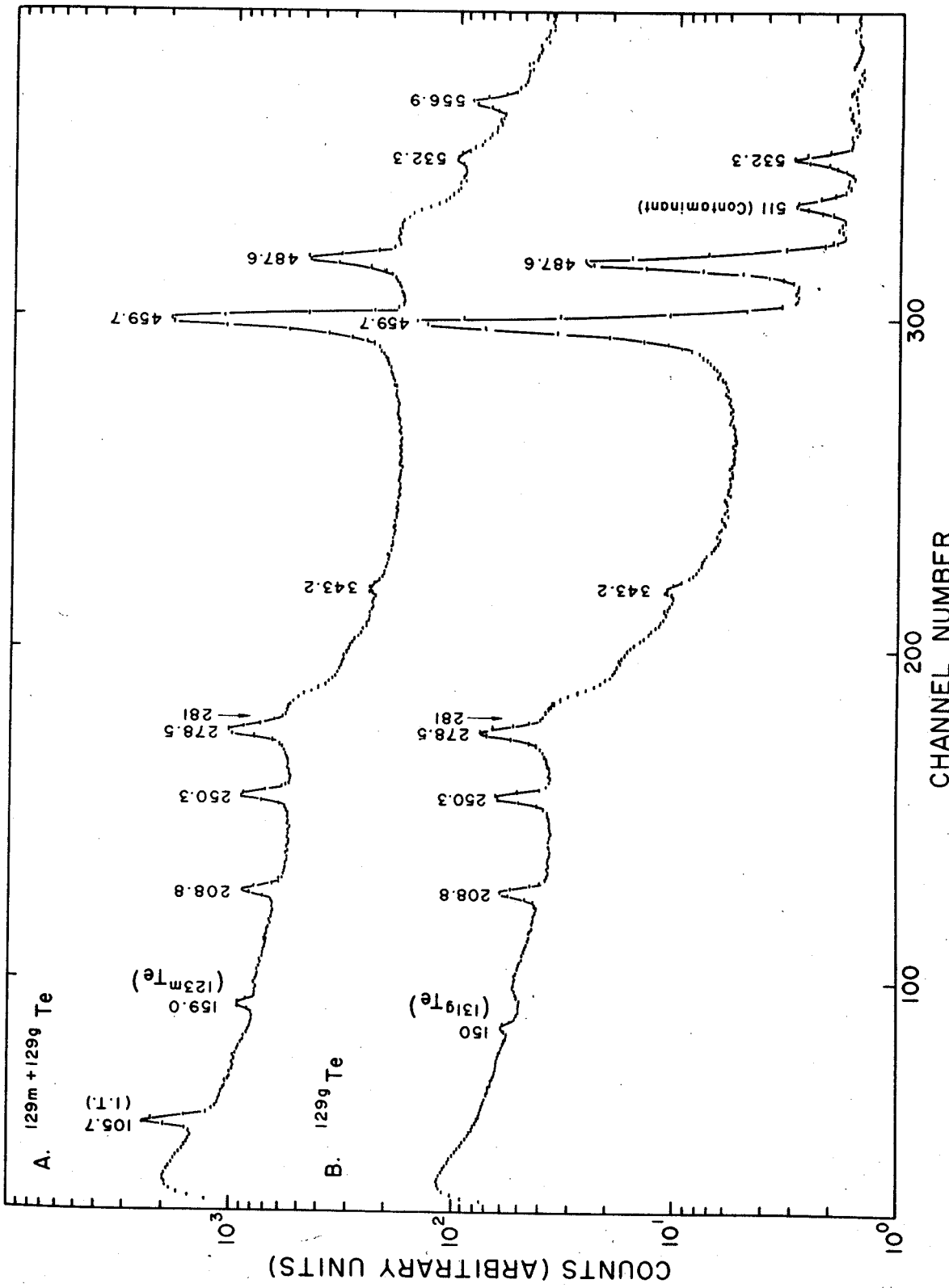


Fig. 8 Segments of singles spectra of $^{129m+g}Te$ and $^{129g}Te$, recorded with a 3 $cm^3$ Ge(Li) detector.
A and B: 50 to 600 keV
C and D: 600 to 950 keV
E and F: 950 to 1420 keV

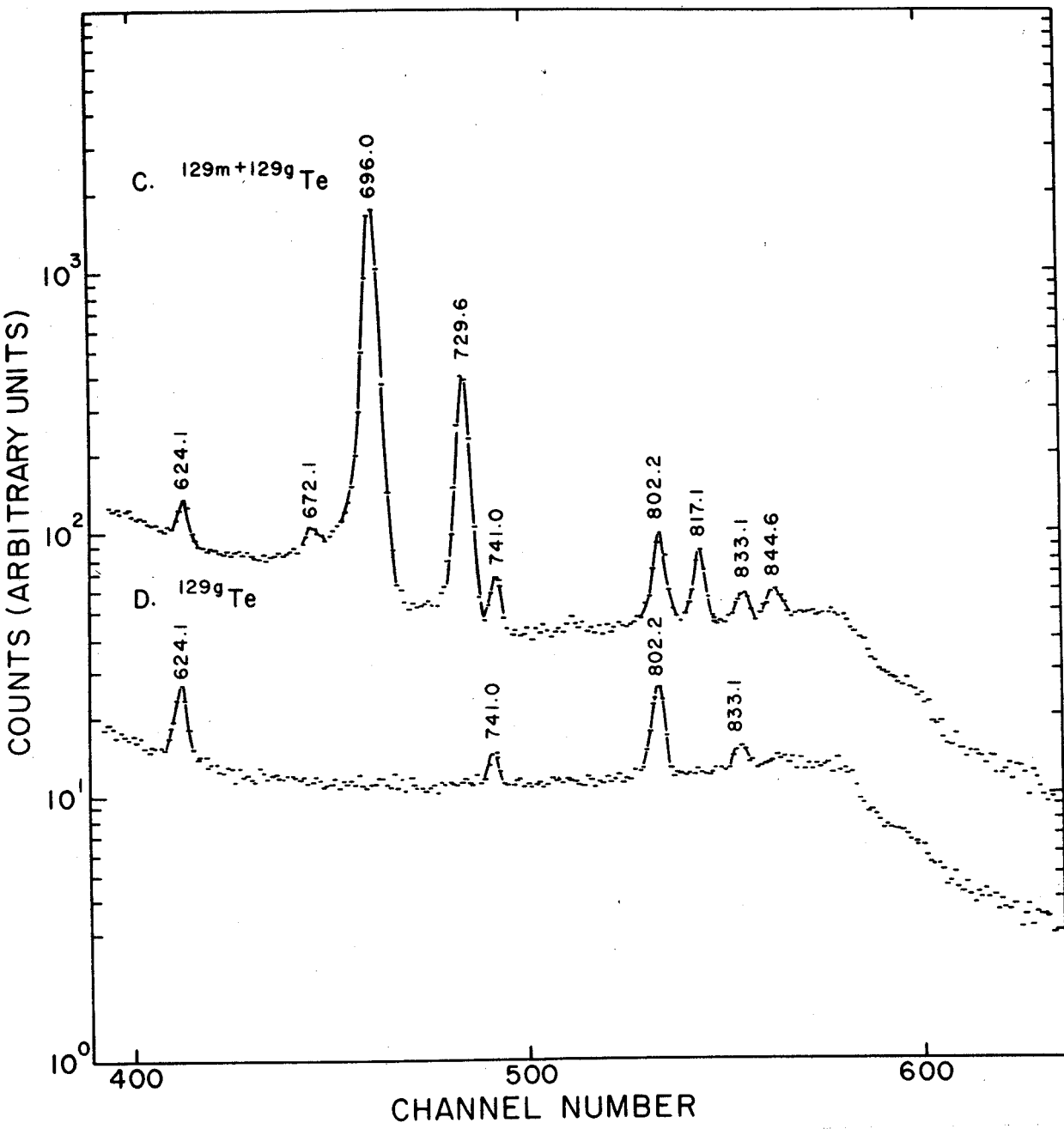


Fig. 8 (continued)

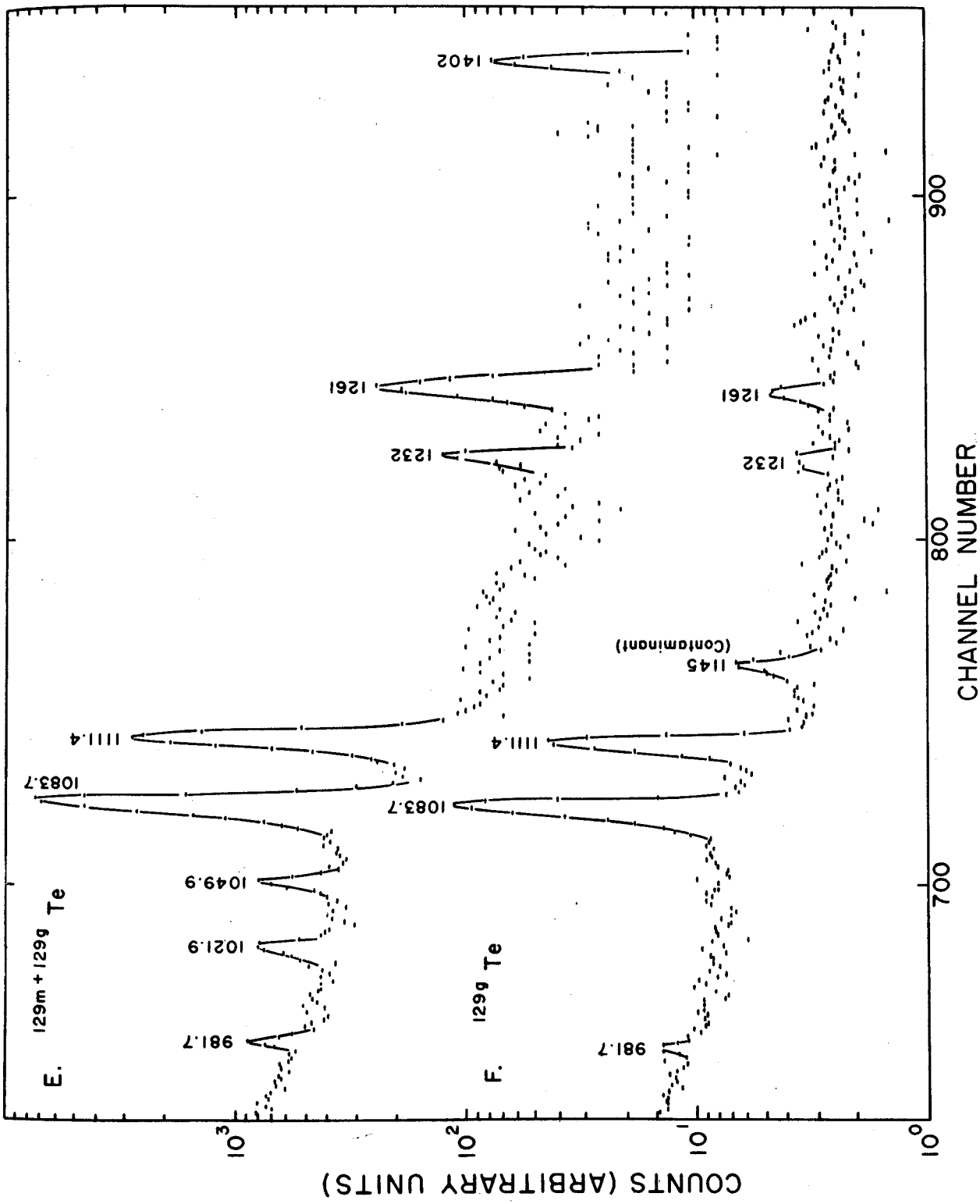


Fig. 8 (continued)

Table 5.--Gamma Rays Observed in the Decay of $^{129m+g}Te$.

| Present | | Walters et al.[a] | | Eastwood et al.[b] | | Hurley et al[c] | | Bornemeier et al.[d] | |
|---|---|---|---|---|---|---|---|---|---|
| Energy[e] | Relative Intensity[f] | Energy | Relative Intensity | Energy | Relative Intensity | Energy | Relative Intensity | Energy | Relative Intensity |
| 27.7 | 183 | | | | | 27 | | | |
| 105.7[g] | 2.2 | | | | | | | | |
| 208.8 | 3.0 | 209.2 | 2.8 | 208.5 | 2.5 | 208 | 2.9 | 205 | 1.53 |
| 250.3 | 6.2 | 250.8 | 5.5 | 250.7 | 4.9 | 250 | 4.8 | 250 | 0.48 |
| | | 271 | 0.13 | | | 278 | 8.7 | 277 | 12.10 |
| 278.5 | 9.8 | 278.7 | 9.1 | 278.4 | 9.6 | 280 | 1.0 | | |
| 281 | 2.1 | 281.7 | 1.8 | | | 343 | 0.3 | 340 | 0.74 |
| 343.2[h] | 0.5 | 343.5 | 0.7 | 342.9 | 0.9 | 345 | 0.1 | | |
| 459.7 | 100 | 459.5 | 100 | 459.8 | 100 | 460 | 100.0 | 455 | 100.00 |
| 487.6 | 19 | 487.3 | 17.8 | 487.8 | 19.9 | 487 | 19.0 | 482 | 22.20 |
| 532.3 | 1.0 | 531.8 | 0.9 | 531.7 | 1.9 | 532 | 2.3 | 523 | 2.65 |
| 556.9 | 2.4 | 556.2 | 2.1 | 556.5 | 2.7 | 557 | 2.1 | 550 | 2.61 |
| | | 560 | 0.5 | | | 573 | 0.6 | | |
| 624.1 | 1.1 | 624.8 | 1.2 | 624.6 | 1.2 | 624 | 1.0 | 630 | 1.01 |
| 672.1 | 0.5 | 672.1 | 0.6 | 673.3 | 0.54 | 673 | 0.5 | 660 | 0.60 |
| 696.0 | 62 | 696.1 | 63.5 | 696.0 | 69.5 | 697 | 73.0 | 698 | 83.60 |
| | | 702.0 | 0.5 | | | | | | |
| 729.6 | 15 | 730.0 | 15.6 | 729.4 | 16 | 730 | 15.8 | 725 | 19.80 |
| 741.0 | 1.0 | 741.1 | 1.1 | 741.0 | 0.76 | 742 | 0.8 | | |
| 769 | 0.1 | 769 | 0.1 | | | | | 770 | 3.53 |
| 802.2 | 2.6 | 802.0 | 2.7 | 804.7 | 3.0 | 804 | 2.8 | 797 | 2.72 |
| 817.1 | 1.6 | 816.9 | 1.7 | 817.1 | 1.9 | 819 | 1.8 | 810 | 1.53 |
| | | 829.8 | 0.1 | | | | | | |
| 833.1 | 0.6 | 833.5 | 0.6 | 835.7 | 0.68 | 837 | 0.7 | 835 | 1.44 |
| 844.6 | 0.6 | 844.7 | 0.7 | 847.6 | 0.77 | 848 | 0.8 | | |
| 981.7 | 0.2 | 982.0 | 0.3 | 983.7 | 0.37 | 982 | 0.3 | 945 | 0.62 |
| 1021.9 | 0.4 | 1022.8 | 0.4 | 1021.3 | 0.70 | 1022 | 0.5 | | |
| 1049.9 | 0.4 | 1050.2 | 0.4 | 1050.4 | 0.60 | 1050 | 0.5 | | |
| 1083.7 | 7.8 | 1084.4 | 8.5 | 1083.2 | 12.5 | 1083 | 10.0 | 1085 | 9.86 |
| 1111.4 | 3.0 | 1112.0 | 3.3 | 1111.3 | 4.0 | 1112 | 3.5 | 1112 | 3.03 |
| 1231.9 | 0.1 | 1232.1 | 0.1 | 1231.1 | 0.19 | 1233 | 0.3 | 1222 | 0.60 |
| 1260.9[h] | 0.3 | 1259.8 | 0.2 | 1260.0 | 0.52 | 1262 | 0.7 | | |
| | | 1263.3 | 0.1 | | | | | | |
| 1374 | 0.02 | | | | | | | | |
| 1402 | 0.1 | | | 1398.3 | 0.18 | 1400 | 0.3 | | |

[a]Reference 50. [b]Reference 52. [c]Reference 48. [d]Reference 44.

[e]Uncertainties in energy values are typically $\leq$ 0.5 Kev, for gamma rays of relative intensity $\geq$ 1.0, and are $\leq$ 1.0 keV for the weaker lines.

[f]Uncertainties in relative intensities are estimated as $\pm$ 10%, except for the very weak lines.

[g]Isomeric transition.

[h]Doublet.

NaI(Tl) detector. Contributions from I x-rays from conversion of the 150 keV line in $^{131}I$ were much reduced by the time lapse of at least two half lives of $^{131g}Te$ prior to measurements. Calibration points were obtained from x-rays present in the decay of $^{137}Cs$, $^{109}Cd$, and $^{113}Sn$. The energy obtained was 27.7 $\pm$ 0.2 keV, in good agreement with the value 27.78 $\pm$ 0.05 keV obtained in recent conversion-electron studies (49). With the intensities of the 662 keV gamma ray and 32-keV x-ray of $^{137m}Ba$ as reference points, and using $\alpha_K$ of 0.089 for the 662 keV transition (57), and correcting for fluorescent yield, a $\gamma$-ray intensity of about 185, relative to 100 for the 460-keV line, was obtained. Using 5.23 for the total conversion coefficient (49), a value of approximately 1150 was obtained for the total relative transition intensity of the 27.7 keV transition.

3.2.1.B.--Gamma-gamma Coincidence Studies--Initial coincidence counting was done with a source taped directly to the Ge(Li) detector package which was immersed in liquid nitrogen. A 7.6 cm X 7.6 cm NaI(Tl) crystal was positioned outside the dewar and was used as the gating detector. Because of the small size ($\approx$1 $cm^3$) of the Ge(Li) crystal, count rates were very low and experiments often had to be continued for several days.

Some results of the coincidence experiments are shown in Figures 9 through 11. A summary of all the coincidence data is given in Table 6. It should be noted that gamma rays of 279 and 343 keV were shown to be doublets by coincidence experiments.

Pulses from the Ge(Li) detector that were in coincidence with the desired pulses in the NaI(Tl) detector were stored in the memory of the analyzer. The good resolution of the response of the Ge(Li) detector makes this technique valuable in spite of the low efficiency of the Ge(Li) counter. The utility of such studies is well illustrate in the study of coincidences between gamma rays in the 500- and in the 800-keV regions. Reference to Figure 8 will show two $\gamma$ rays in the 500-keV region, 532 and 557 keV, and four $\gamma$ rays in the 800-keV region, 802, 817, 833, and 845 keV. Earlier studies had indicated coincidences between these two regions (42-48) where it was not possible to determine exactly which $\gamma$ rays were in coincidence. In Figure 9, spectrum C where the Ge(Li) spectrum in coincidence with the 800-keV region is shown, major coincident $\gamma$ rays are clearly seen at 251, 278, and 557 keV. This indicates that the 557- (but not the 532-keV) $\gamma$ ray is in coincidence with one or more $\gamma$ rays in the 800-keV region. In Figure 9, spectrum B where the Ge(Li) spectrum obtained in coincidence with the 500-keV region is shown, the two peaks at 817 and 845 keV stand out as major coincidences. Thus, the two

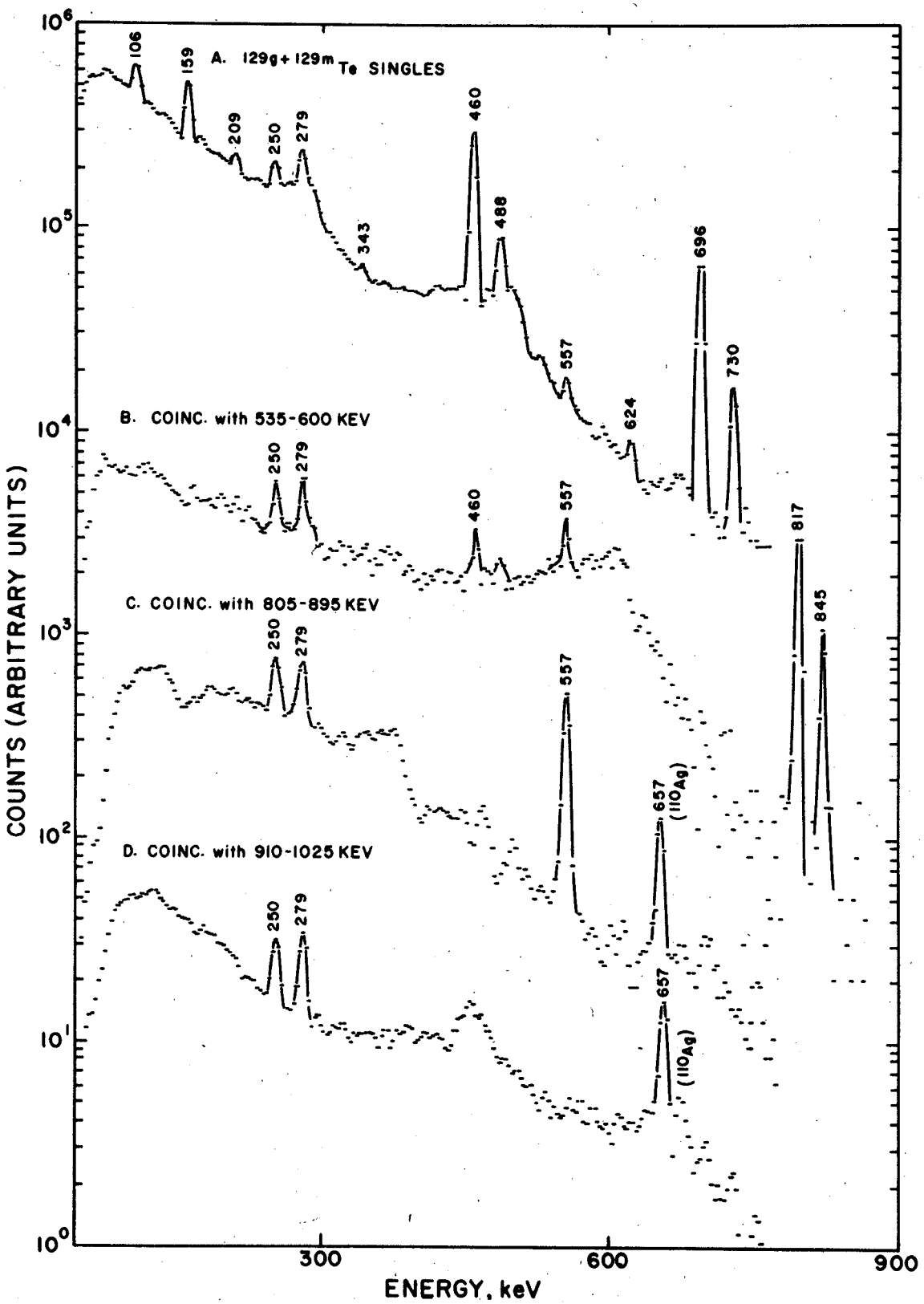


Fig. 9 Ge(Li) spectra of $^{129m+g}$Te in coincidence with three regions of the spectrum seen by a 7.6 x 7.6 cm NaI(Tl) detector. A 1 cm$^3$ Ge(Li) detector was used. A singles spectrum is shown for reference. The coincident spectra have been gain shifted by the computer to allow an easier comparison.

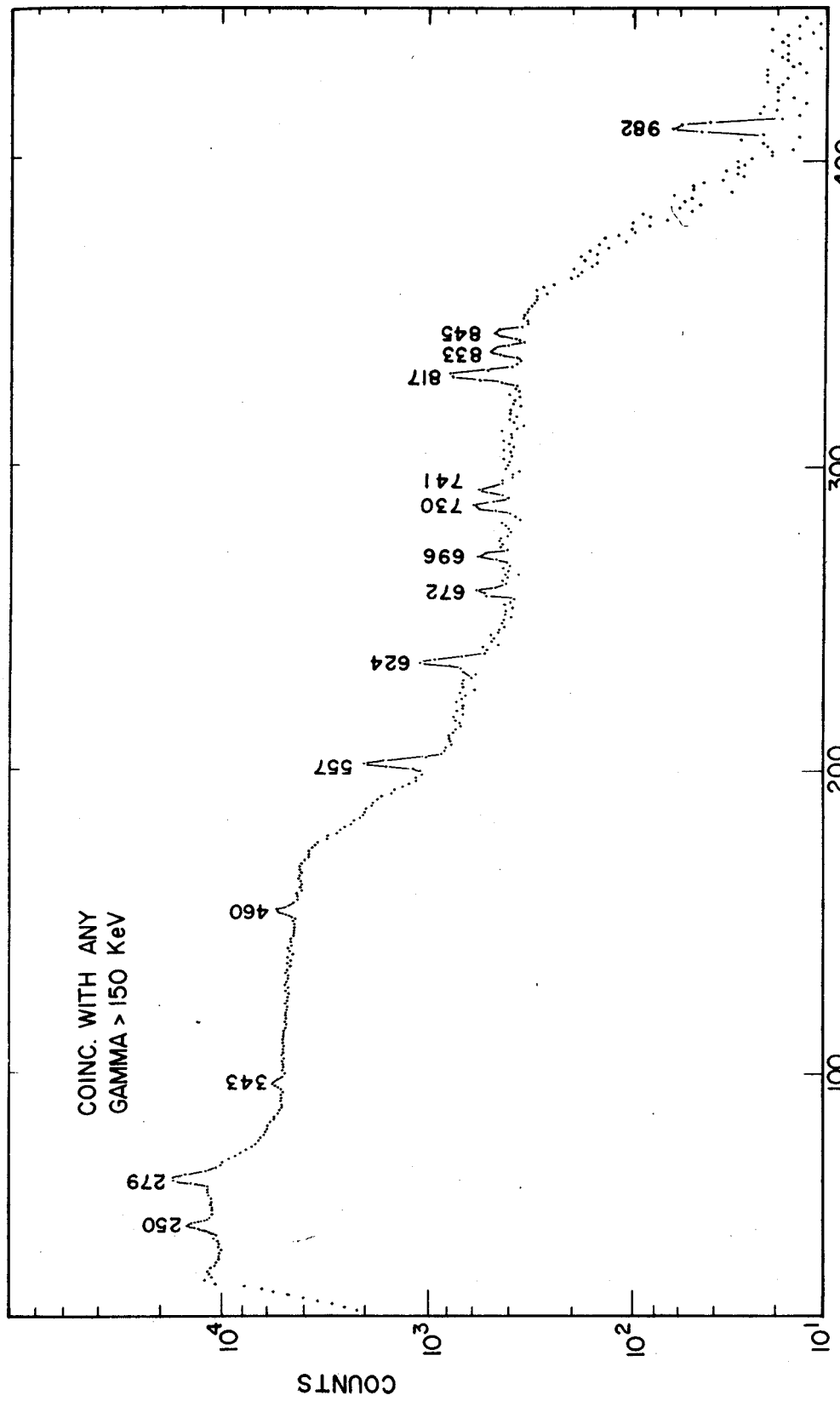


Fig. 10 A Ge(Li) spectrum of $^{129m+g}$Te in coincidence with pulses corresponding to ≥150 keV from the NaI(Tl) annulus detector.

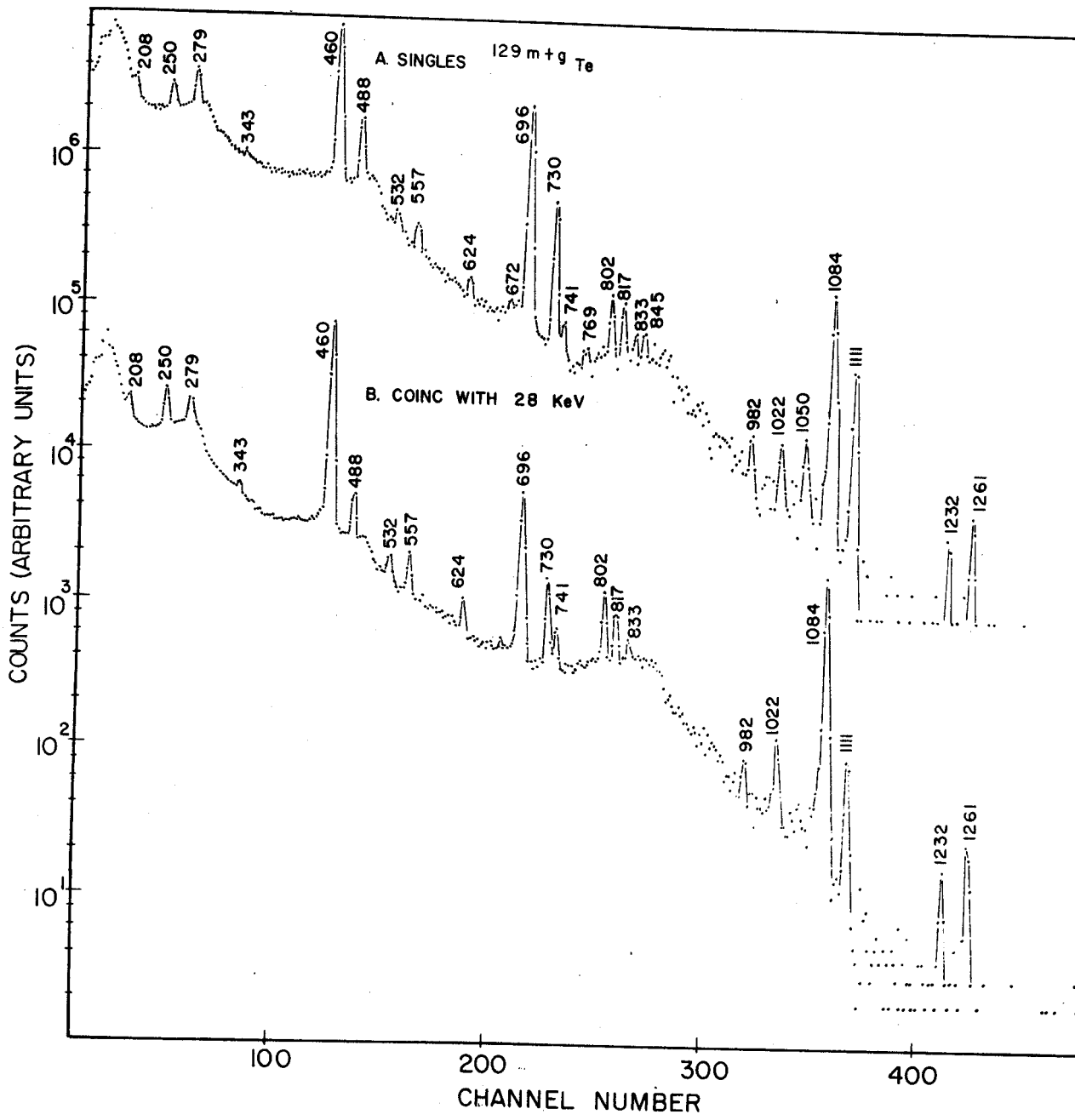


Fig. 11 A spectrum of $^{129m+g}$Te in coincidence with the 28 keV gamma ray. Because only about 5% of the counts in the gate (corresponding to the 28 keV gamma ray and to x-rays) are in coincidence with other transitions, a large contribution to the spectrum arises from chance coincidences. The coincidence peaks can be identified by comparing their relative heights in the coincidence and singles spectra. A 7 cm$^3$ Ge(Li) detector and a 2.5 x 3.8 cm NaI(Tl) crystal with a thin Be window were used.

Table 6.--Summary of Coincidence Results for $^{129m+g}Te$.

A. Differential gates

| Energy Interval in Gate (keV) | Photopeaks in gate[a] (keV) | Coincident with peaks in gate | Coincident with Comptons & Contaminants in Gate |
|---|---|---|---|
| 910-1025 | 981, 1022 | 250, 279 | 657[b] |
| 805-895 | 802, 817 833, 845 | 250, 279, 557 | 657[b] |
| 650-730[c] | 624, 672, 696 730, 741 | 343, 460, 672 729 | 250, 279, 557 |
| 535-600 | 532, 557, 624 | 460, 817, 845 | 250, 279, 557 |
| 420-500[c] | 460, 488 | 343, 624 | 557, 460 |
| 260-280[c] | 250, 279, 281 | 135[d], 209, 250 279, 281 | 557, 624 |
| 28[e] | 208, 250, 281, 343[f], 460, 532[f], 557[f], 741, 802, 817, 833[f], 982, 1022, 1084, 1232, 1261 | | |

B. Integral gates

| Energy in Gate (keV) | Coincident Gamma Rays |
|---|---|
| 150 | 250, 279, 281, 343, 460, 557, 624, 657[b], 672, 730, 741, 817, 833, 845, 982 |
| 300[c] | 208, 250, 279, 343, 460, 488, 557, 624, 657[b] 672, 730, 741, 817, 845, 885[b], 937[b] |
| 770[c] | 250, 279, 657[b], 885[b], 937[b] |

[a]Including photopeaks only partially inside gate.

[b]Due to $^{110m}Ag$ contaminant.

[c]Spectra not shown.

[d]Presumably backscatter of 279 keV doublet.

[e]Includes 28 keV gamma ray and x-rays.

[f]Weak evidence due to poor statistics.

experiments, taken together, serve to establish the 557-keV γ ray as being coincident with the γ rays at 817 and 845 keV. It is possible, therefore, to overcome the inability to resolve closely lying peaks in the gating detector and to determine exactly which peak or peaks are causing coincidences to be observed using the above approach to the analysis of the data.

In most of the coincidence spectra shown there are a number of additional peaks resulting from chance coincidences and from real coincidences with Compton background events. The latter can be treated quantitatively by a knowledge of the width and position of the gate and of the γ rays coincident with the higher energy γ rays whose Compton events fall in the gate. A good example of this is seen in Figure 9, spectrum B, where the 557-keV peak appears in coincident with 535- to 600-keV area. Three explanations of this observation are possible: (a) the 557-keV γ ray may be in true coincidence with the 532-keV line; (b) the 557-keV photopeak may arise solely from random coincidences; and (c) it may be in true coincidence with the 817- and 845-keV transitions both of which contribute to the Compton events falling in the gate. The first possibility is eliminated as a 532-557 cascade, as it would require that the 532-keV γ ray be present with at least as great an intensity as the 557-keV γ ray. Case (b) is ruled out

as the ratio of peak areas 557/696 would have to be the same as in the singles spectrum; the peak at 696-keV, which is essentially absent in Figure 9, arises entirely from random events as the 696-keV transition has not been observed in any coincidence spectra. Thus, we are left with case (c), that the photopeak at 557-keV arises from true coincidences with Compton events from the 817- and 845-keV $\gamma$ rays.

In Figure 10 is shown the "any-coincidence" Ge(Li) spectrum which is the spectrum that is coincident with any events that deposit more than 150 keV in the NaI(Tl) detector. This spectrum serves two important functions. First, it indicates which $\gamma$ rays are involved in cascades and, thus, must be properly placed in the decay scheme to obtain correct intensity balance. Second, and perhaps more important, it shows which $\gamma$ rays are not involved in cascades. Those $\gamma$ rays whose peaks do not occur here, or in Figure 11 which shows coincidences with the 28-keV $\gamma$, almost certainly lead to the ground state. Furthermore, those whose peaks appear in Figure 11 but not in the any-coincidence spectrum must terminate at the 28-keV level. Notable absences from the any-coincidence spectrum are $\gamma$ rays of energies 532, 696, 802, 1022, 1050, 1084, 1111, 1232, 1261 and 1402 keV.

3.2.1.C.--The proposed decay schemes--Transitions at 271, 560, and 702 keV were observed at M.I.T. by Walters et al. (50,51). using a higher resolution system. In our spectra, the 702 keV line could not be resolved from the very intense 696 keV gamma ray. The other two lines, if real, are present in the decay of $^{129g}$Te, and were masked in our spectra by the presence of $^{129m}$Te. The 271, 560, and 702 keV lines are placed in our decay schemes (shown here) as a part of a joint publication on the decay of $^{129}$Te with the M.I.T. group, (51). It should be emphasized that the paper was a joint report on independent investigations, with collaborations only on the final interpretations of the final results.

The proposed decay schemes of the $^{129}$Te isomers are shown in Figure 12. It is well known that the ground state of $^{129}$I has a spin and parity 7/2+ and the first excited state, at 28 keV, has $J\pi$ = 5/2+ (15). The observation of several pairs of $\gamma$ rays separated in energy by about 28 keV suggests that each pair results from the decay of an excited state to these lowest two levels. For all such pairs, except the 1374- and 1402-keV pair, coincidence data are available (See Figure 11) that confirm the existence of a level at an energy equal to that of the high energy member of the pair. Namely, for levels at 278, 487, 560, 730, 769, 830, 845, 1050, 1111, and 1260 keV, $\gamma$ rays of energies 251, 460,

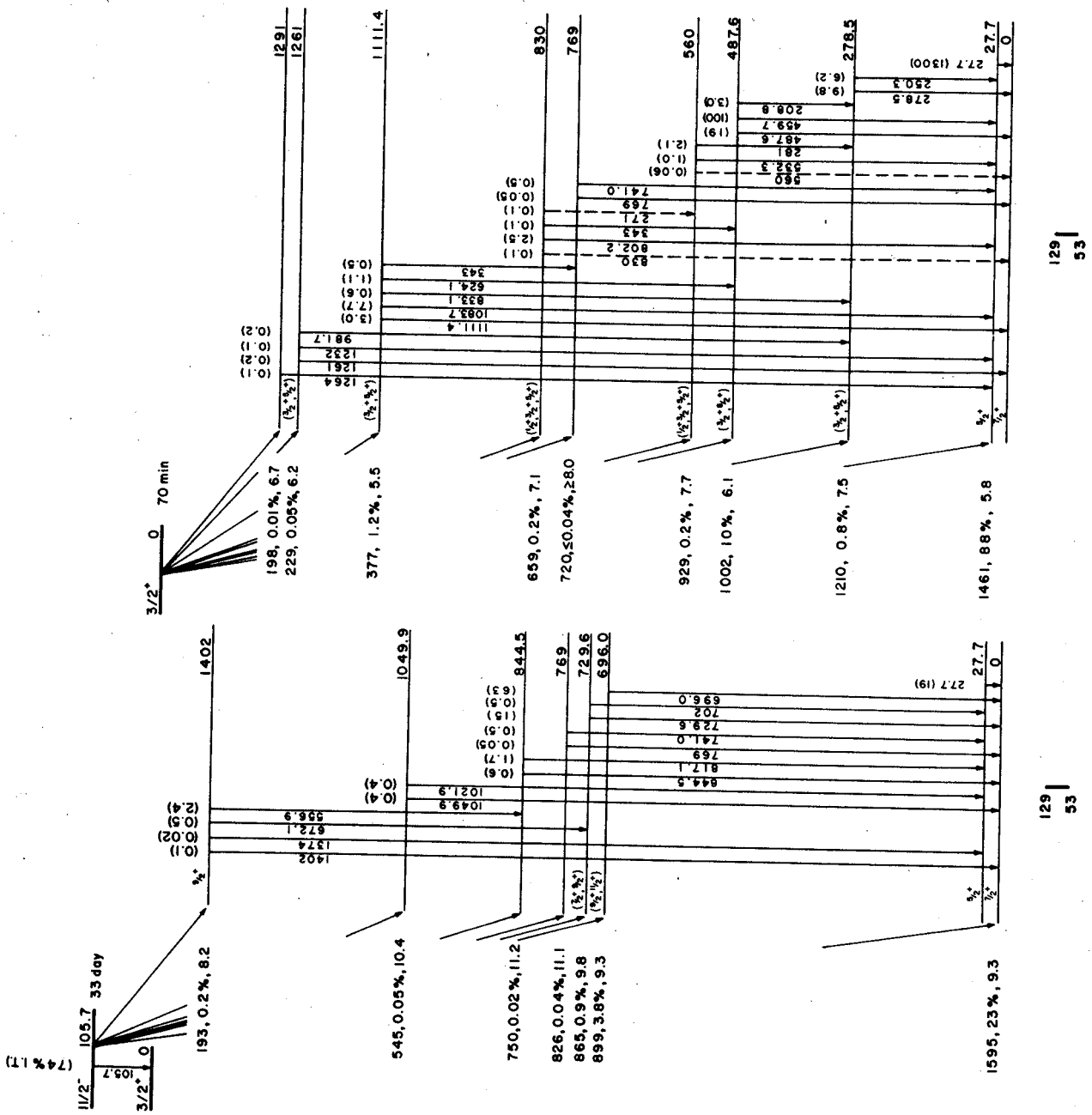


Fig. 12 Proposed decay schemes of $^{129m}Te$ and $^{129g}Te$. The dashed lines represent transitions which were observed at MIT (refs. 50 and 51) but could not be reliably identified in our investigation. They are included because of a joint MSU-MIT publication.

532, 702, 741, 802, 817, 1022, 1084, and 1232 keV, respectively, have been observed in coincidence with the 28-keV γ ray. Furthermore, transitions depopulating the levels at 278, 487, 730, 769, and 845 keV have been observed to be in coincidence with the 833- and 982-, 343- and 624-, 672-, 343-, and 557-keV transitions, respectively, giving further support for the placement of levels at 830, 1111, 1260, and 1402 keV. The relatively high intensity of the 1261-keV doublet in the spectrum in coincidence with the 28-keV transition suggests a level at 1292 keV. The low intensity of the 1374- and 1402-keV transitions makes coincidence experiments with these transitions impractical at present and so both of these gamma rays are placed as depopulating the 1402- keV level on the basis of energy sums and the above mentioned cascades that have been observed.

The large intensity of the 696-keV γ ray in the $^{129m+g}$Te singles spectrum, in conjunction with its absence from all coincidence spectra, indicates the existence of a level at 696 keV.

The placement of a level at 769 keV has been made on the basis of intensity data and the presence of a very weak γ ray at 769 keV. There is little doubt that the 741- and 343-keV γ rays are in coincidence and represent a cascade from the 1111- keV level to the

28-keV level. In the decay of $^{129m}$Te, the intensity of the 741-keV line is greater than that of the 343-keV γ ray by an amount sufficient to indicate independent beta decay to a level at 769 keV. The presence of a weak 769-keV γ ray serves to confirm this assignment. In the decay of $^{129g}$Te, the intensities of the 741- and 343-keV γ rays are equal within the limits of the experimental error. If we make the reasonable assumtion that there is only one 741-keV γ ray, then there is little doubt about the order of emission of the 343- and 741-keV γ rays in the decay of the 1111-keV level. For a level to exist at 371 keV, the existence of two 741-keV γ rays, whose energy separation is less than 1 keV, must be postulated. No significant shift in the centroid of the 741 keV peak was observed in spectra obtained from $^{129g}$Te from those obtained from $^{129m+g}$Te.

The Q values for the β groups shown in Figure 12 were derived from the endpoint energy for the transition from $^{129m}$Te to the $^{129}$I ground state, 1595 keV, measured by Devare and Devare (43) and the γ-ray energies of this work. The intensities of the β groups and the I.T. (isomeric transition) branching fractions for $^{129m}$Te were determined from the net flow of γ-ray intensities out of each level and the ratio of intensities of the 1595-keV β group as determined by Devare and Devare (43). The resulting value for the fraction of $^{129m}$Te decay by I.T.,

72%, is in reasonable agreement with previous values of 64% (43) and 68% (58). Log ft values were determined from the partial half lives and endpoint energies of the various beta groups by use of Moszkowski's nomogram (59).

### 3.2.2. Decay Schemes of $^{119g}$Te and $^{119m}$Te

3.2.2.A.--Gamma Ray Singles Spectra--In order that activities decaying with different half lives could be properly identified, singles spectra were recorded periodically as the sources aged. Gamma rays were assigned to the decay of $^{119g}$Te or 4.7 day $^{119m}$Te from measurements of their intensities, relative to the 644 and 1213 keV lines, in successive singles runs. A total of twelve transitions are tentatively assigned to $^{119g}$Te and twenty to $^{119m}$Te. The singles spectrum and expanded segments of singles spectra are shown in Figures 13 and 14a through 14e. Lists of the gamma rays and relative intensities measured in this and other investigations are given in Tables 7 and 8.

Because of the longer halflives (17 day and 154 day), identification of transitions belonging to the $^{121}$Te isomeric impurities presented relatively little difficulty. A spectrum of $^{121}$Te, recorded after many halflives of $^{119m}$Te, is displayed in Figure 15. The energies and relative intensities of the gamma rays present, including the very weak 910 and 988 keV lines, are in very good agreement with

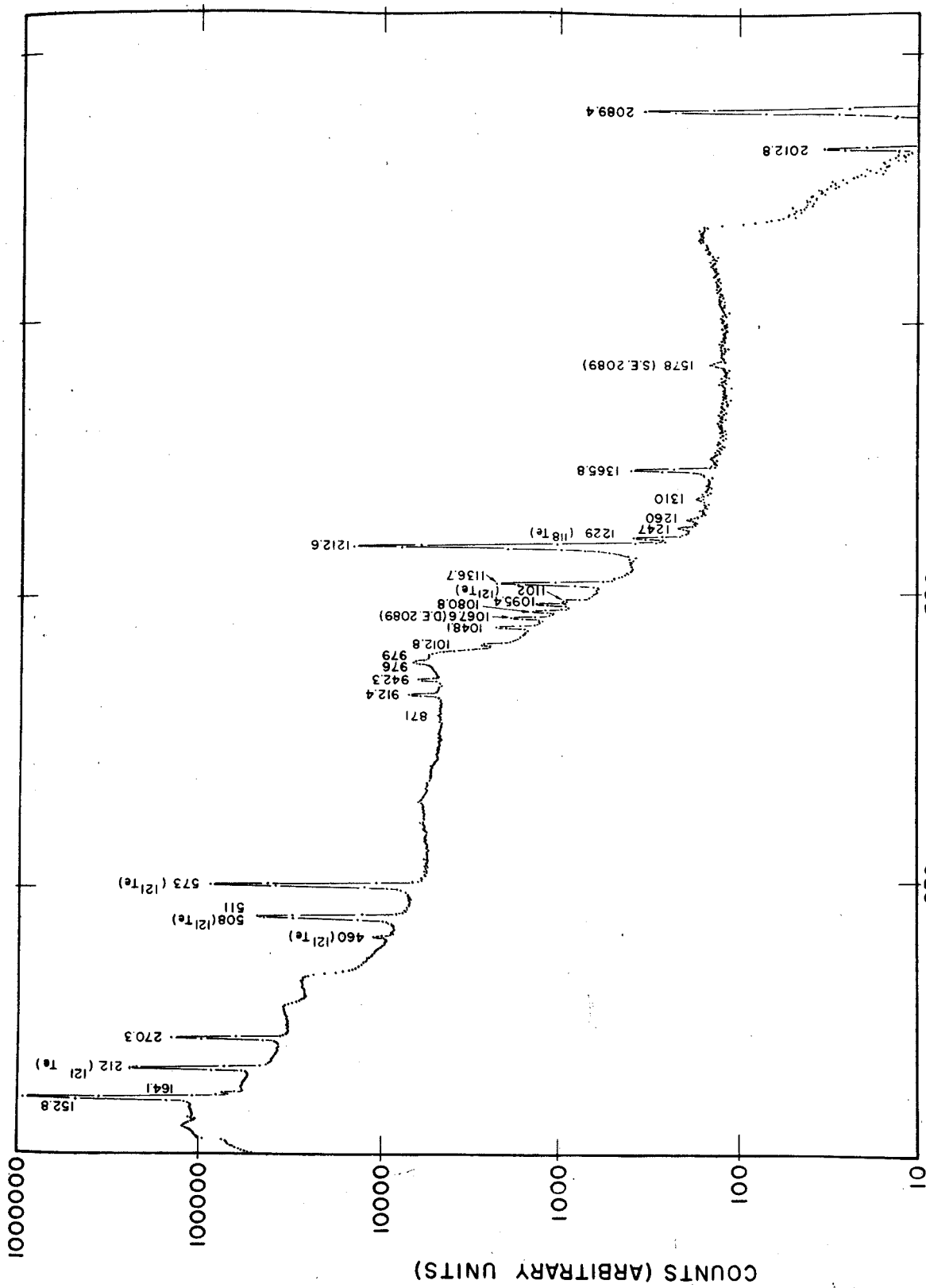


Fig. 13 Singles spectrum of $^{119m}$Te recorded with a 3 cm$^3$ Ge(Li) detector.

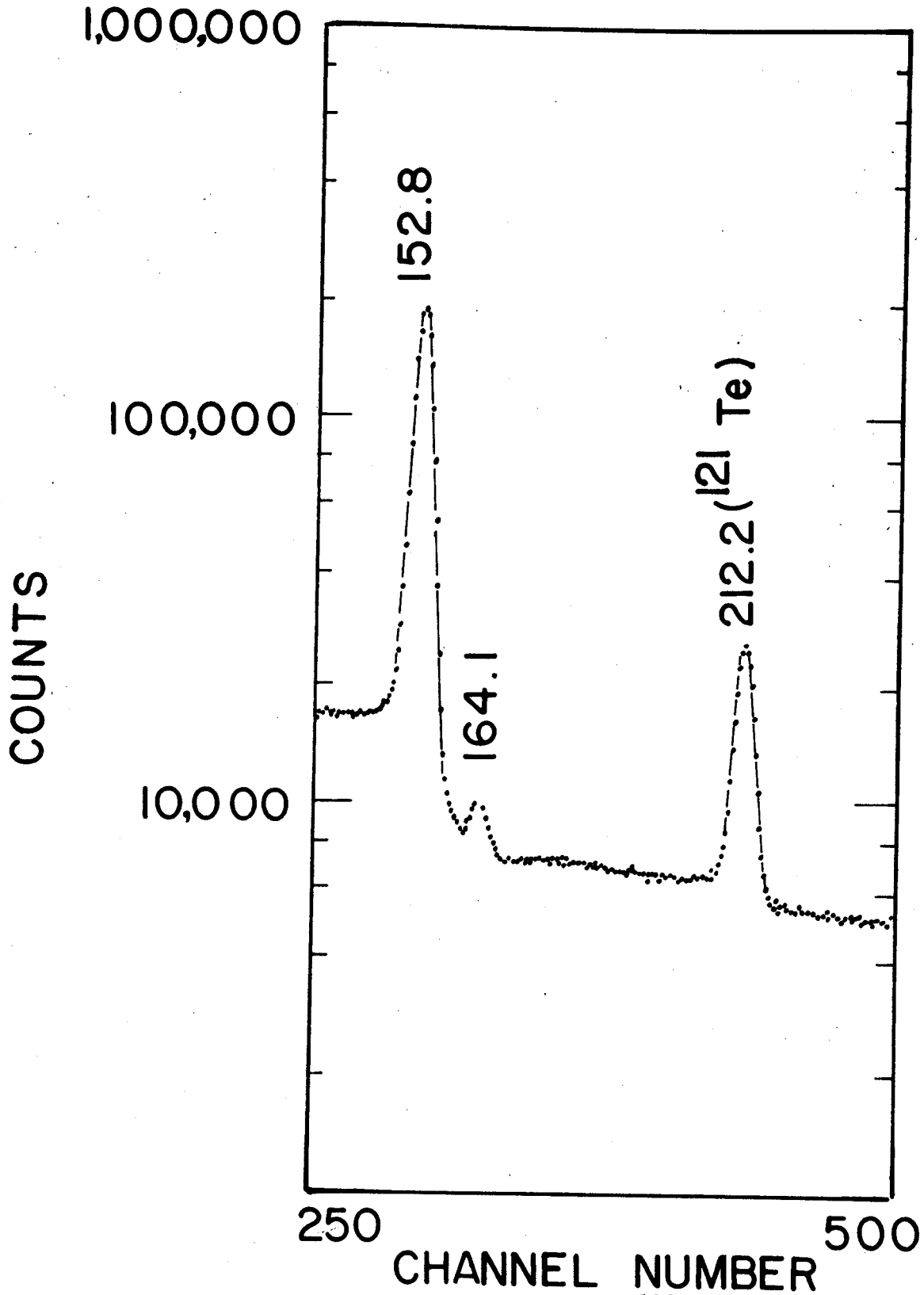


Fig. 14 Segments of the Ge(Li) spectrum of $^{119m+g}$Te shown on expanded scales. Transitions belonging to $^{119g}$Te are indicated by an asterisk (*). a) 120 to 250 keV region, b) 500 to 800 keV region, c) 900 keV region, d) 900 to 1800 keV region, e) high energy region.

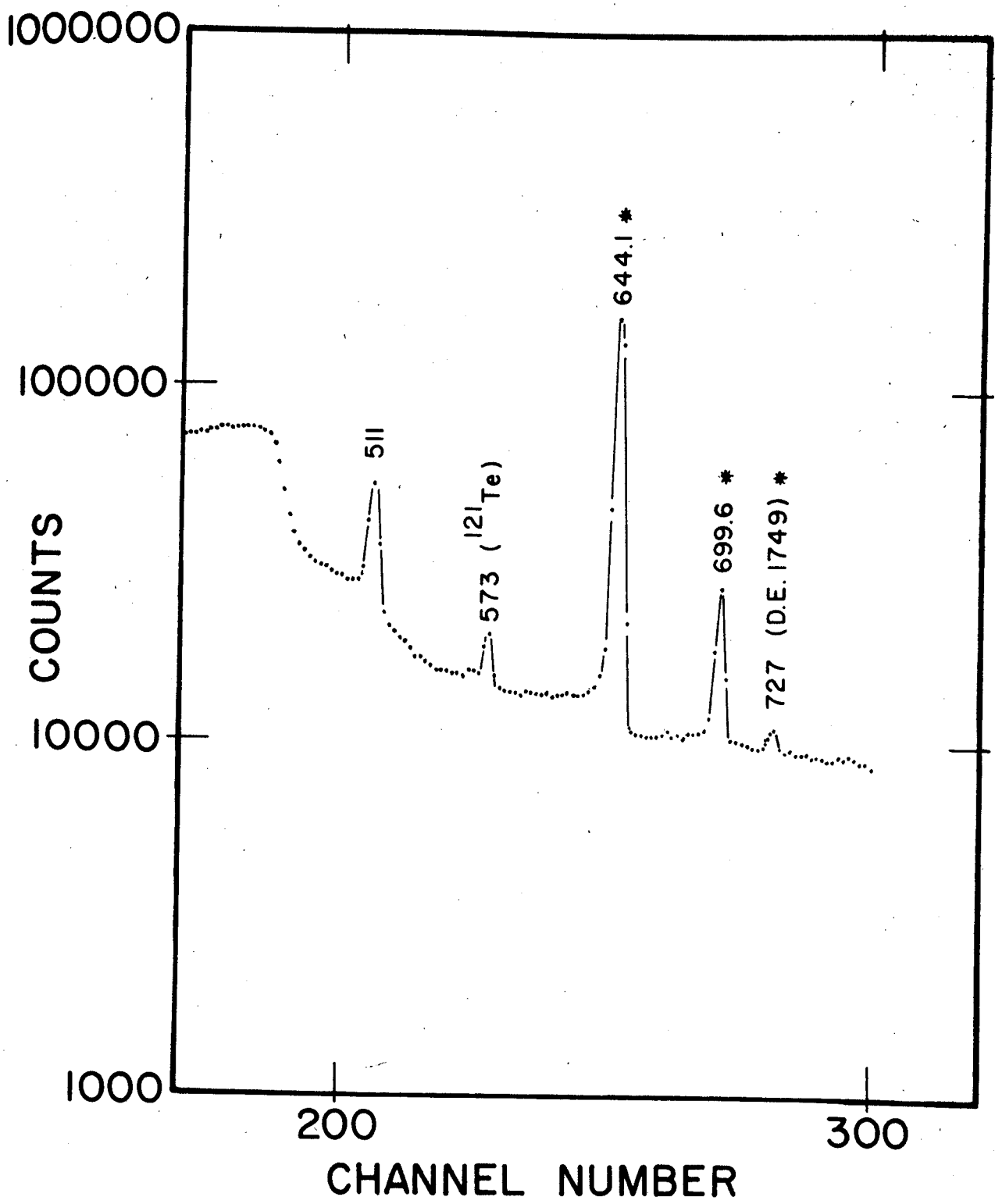
1000000
100000
10000
1000
COUNTS
511
573 ($^{121}$Te)
644.1 *
699.6 *
727 (D.E. 1749) *
200
300
CHANNEL NUMBER

Fig. 14b

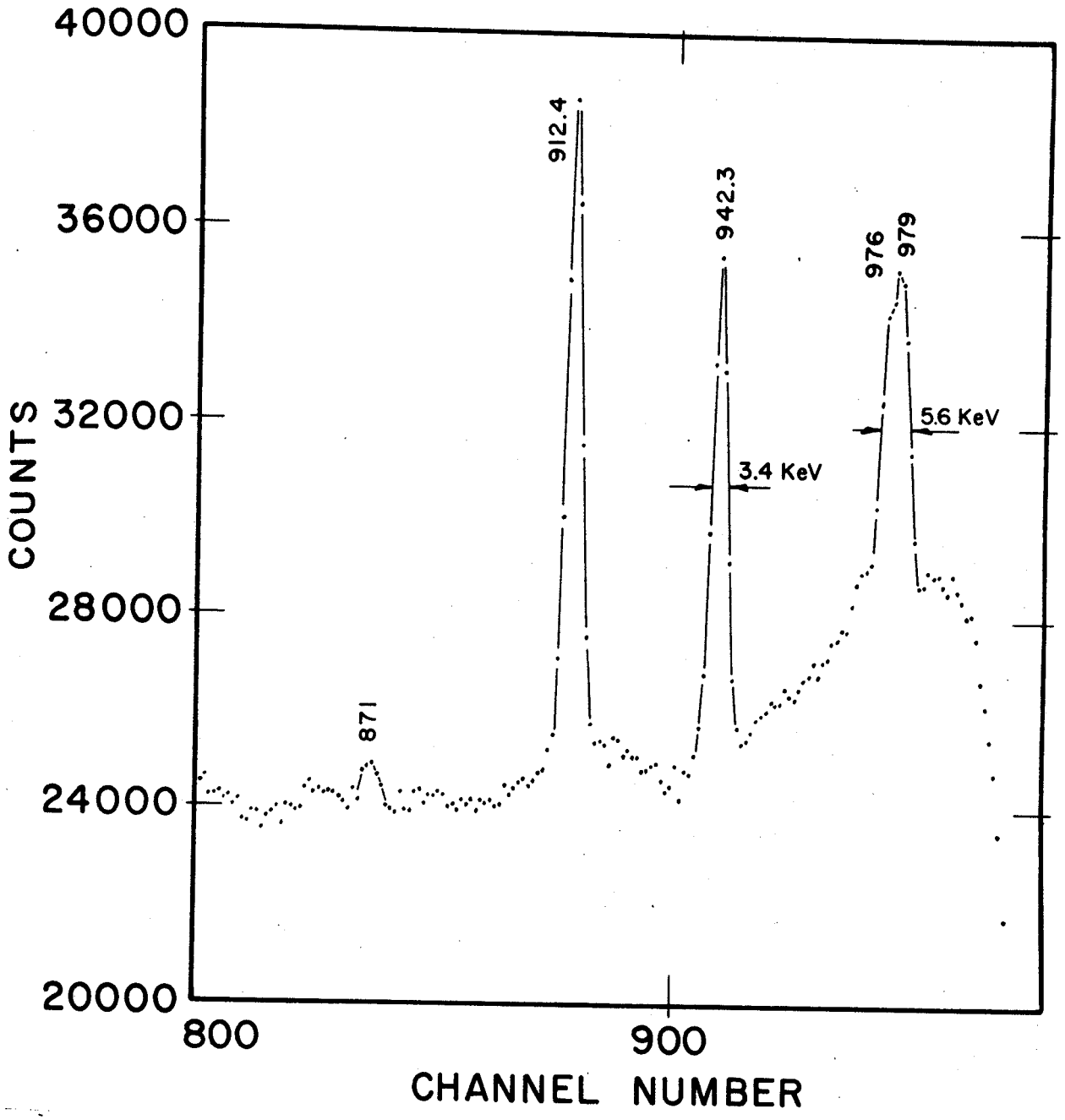
40000
36000
32000
28000
24000
20000
COUNTS
800
900
CHANNEL NUMBER
871
912.4
942.3
976
979
3.4 KeV
5.6 KeV

Fig. 14c

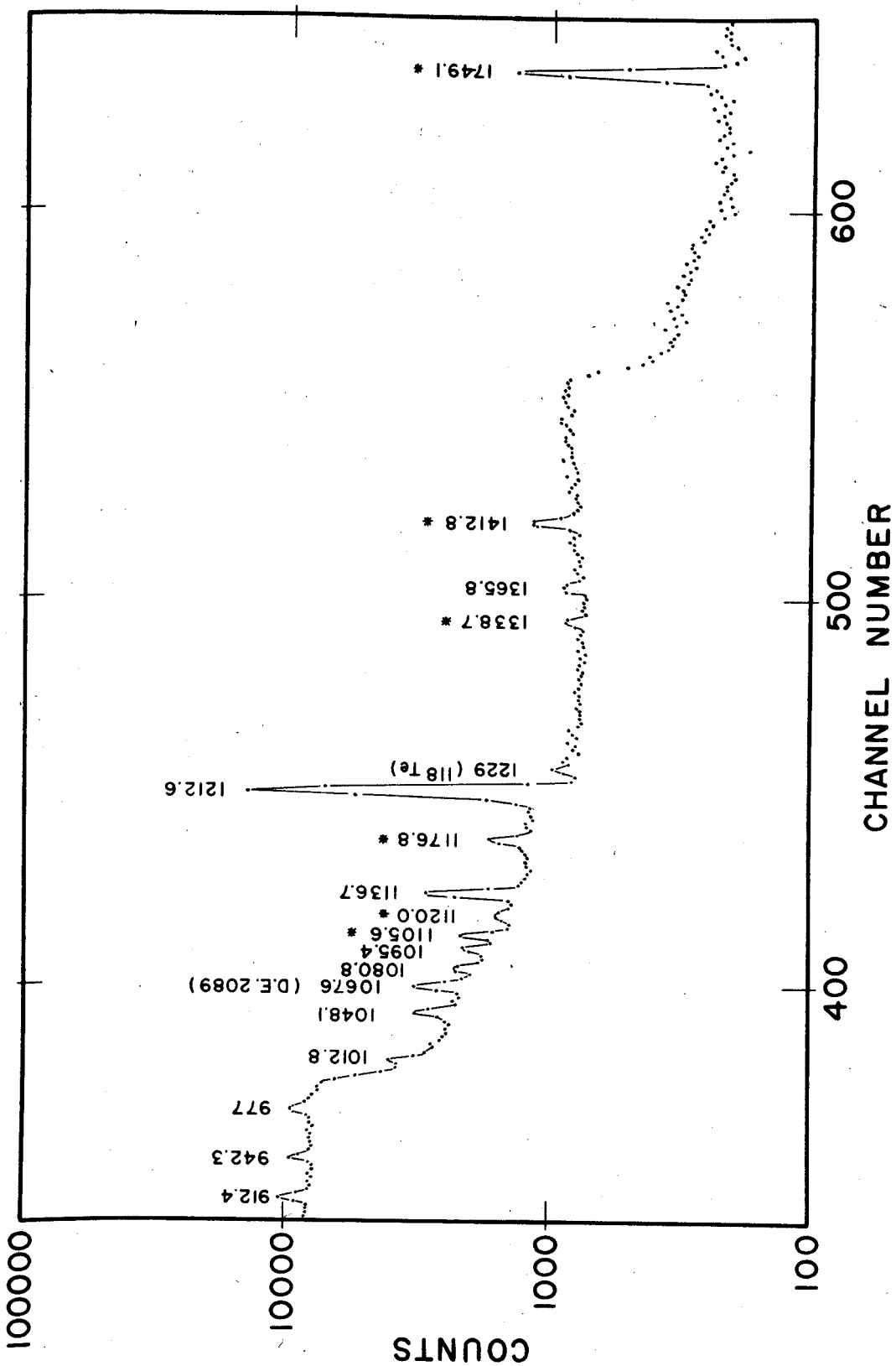
COUNTS
100000
10000
1000
100
CHANNEL NUMBER
400
500
600
912.4
942.3
977
1012.8
1048.1
1067.6 (D.E. 2089)
1080.8
1095.4
1105.6 *
1120.0 *
1136.7
1176.8 *
1212.6
1229 (118 Te)
1338.7 *
1365.8
1412.8 *
1749.1 *

Fig. 14d

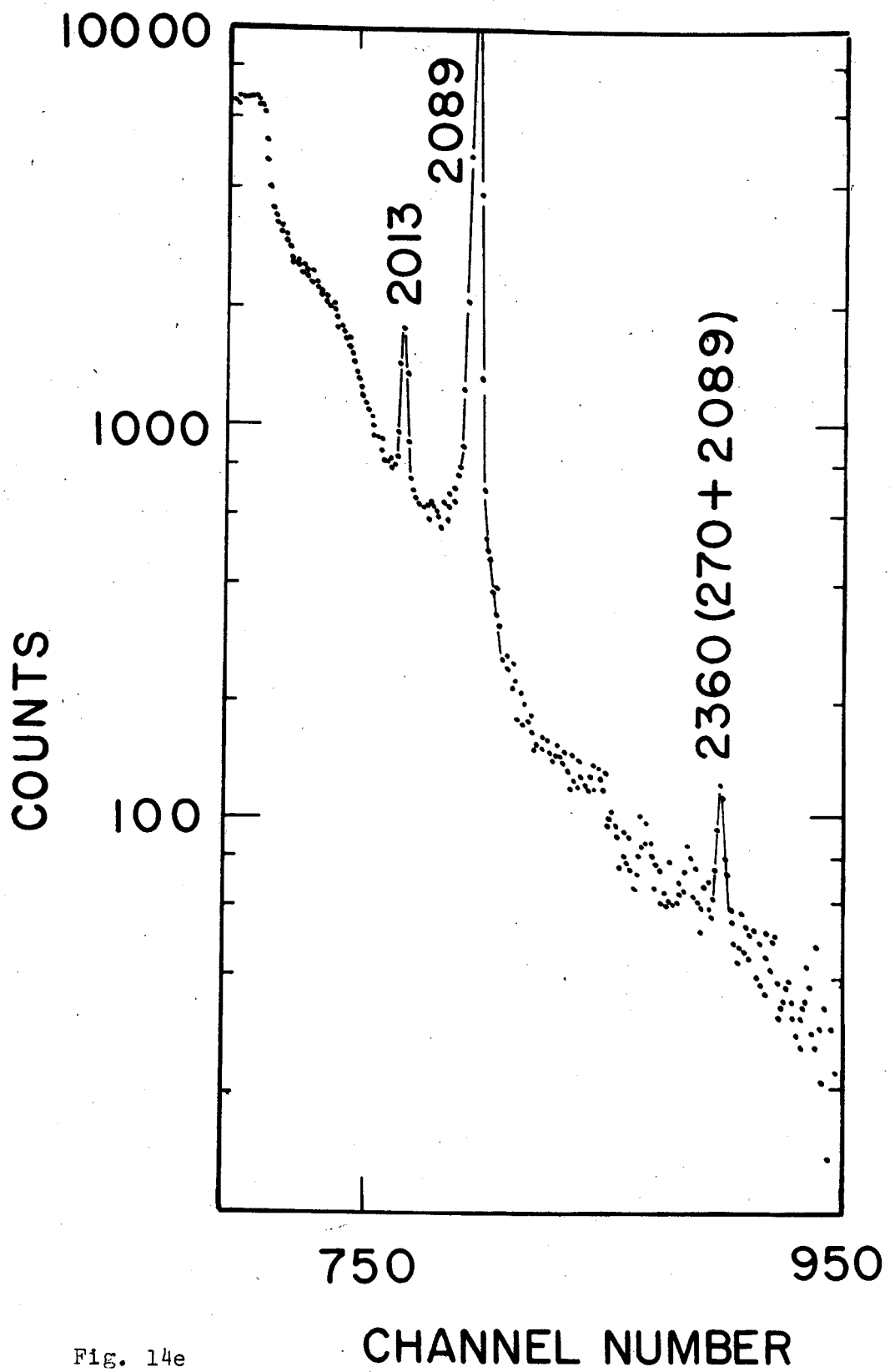
10000
1000
100
COUNTS
2013
2089
2360(270+2089)
750
950
CHANNEL NUMBER

Fig. 14e

Table 7.--Energies and Relative Intensities of Gamma Rays Observed in the Decay of $^{119m}$Te.

| Present Work | | | Kantele and Fink[c] | | Graeffe et al.[d] | |
|---|---|---|---|---|---|---|
| Energy | Uncertainty[a] | Rel. Int.[b] | Energy | Rel. Int. | Energy | Rel. Int. |
| 117 | 2.0 | <0.5 | | | 115.5 | 0.7 |
| 152.8 | 0.5 | 100 | 153.0 | 94 | 153.0 | 99 |
| 164.1 | 1.0 | 1.7 | 163.9 | 6 | 163.9 | 1.7 |
| 270.3 | 0.3 | 42 | 270.6 | 38 | 270.6 | 39 |
| | | | 400 | | | |
| | | | 760-780 | | | |
| 871 | 1.0 | ≤0.6 | 800 | | 872.0 | 0.4 |
| 912.4 | 0.6 | 9.7 | 917 | 6 | 912.4 | 10.2 |
| 942.3 | 0.6 | 6.3 | 946 | 9.5 | 942.1 | 5.9 |
| 976 | 1.5 | 4.5 | | | 976.4 | 3.9 |
| 979 | 1.5 | 4.5 | 984 | 12 | 979.0 | 4.5 |
| 1012.8 | 1.0 | 2.7 | | | 1012.9 | 3.9 |
| 1048.1 | 0.7 | 4.7 | 1054 | 8 | 1048.3 | 4.7 |
| 1080.8 | 0.9 | 2.8 | | | 1081.0 | 2.3 |
| 1095.4 | 0.5 | 3.0 | 1099 | 7 | 1096.0 | 3.4 |
| 1136.7 | 0.9 | 11.5 | 1140 | 10 | 1136.0 | 11.7 |
| 1212.6 | 0.5 | 100 | 1221 | 100 | 1212.7 | 100 |
| 1249 | 2.0 | 0.3 | | | 1249.6 | 0.2 |
| 1311 | 2.0 | ≤0.3 | | | 1311.0 | 0.2 |
| 1365.8 | 0.7 | 1.7 | 1374 | 2.2 | 1365.8 | 2.0 |
| | | | 1500 | <0.4 | | |
| | | | 1760-1780 | <0.4 | | |
| | | | 1900 | <0.4 | | |
| 2012.5 | 0.7 | 0.4 | | | 2013.0 | 0.5 |
| 2089.4 | 0.7 | 7.3 | 2094 | 7.3 | 2089.7 | 6.2 |
| | | | 2350 | <0.05 | | |
| | | | 2570 | <0.03 | | |

[a]Uncertainties in energies are rms deviations from the mean values obtained from many measurements.

[b]Gamma intensities only. The uncertainties are estimated to be ±10% for the prominent lines.

[c]Reference 37. [d]Reference 45.

Table 8.--Energies and Relative Intensities of Gamma Rays Observed in the Decay of $^{119g}$Te.

| Present Work | | | Kantele and Fink[e] | | Graeffe et al.[d] | |
|---|---|---|---|---|---|---|
| Energy (keV) | Uncertainty[a] (keV) | Rel. Int.[b] | Energy | Rel. Int. | Energy (keV) | Rel. Int. |
| | | | | | 270.6 | 0.2 |
| | | | | | 373.7 | 0.2 |
| 644.1 | 0.3 | 100 | 645 | 100 | 644.3 | 100 |
| 699.6 | 0.5 | 12 | 702 | 13 | 700.0 | 11.5 |
| 684[e] | 1.5 | 0.1 | | | | |
| 768[e] | 1.5 | 0.1 | | | | |
| 788[e] | 1.5 | 0.2 | | | 787.3 | 0.2 |
| 843[e] | 1.5 | 0.3 | | | 843.2 | 0.3 |
| 1105.6 | 0.7 | 1.0 | | | 1105.5 | 0.8 |
| 1120.0 | 0.6 | 0.6 | | | 1120.9 | 0.2 |
| 1177.8 | 1.1 | 1.0 | | | 1177.2 | 1.0 |
| 1338.7 | 0.7 | 0.3 | | | 1338.5 | 0.2 |
| 1412.8 | 0.4 | 1.2 | | | 1413.2 | 1.1 |
| 1749.1 | 0.5 | 4.8 | 1755 | 4.2 | 1749.3 | 4.4 |

[a]Uncertainties in energies are based on rms deviations from mean value.

[b]Gamma intensities only. Uncertainties in relative intensities are estimated to be ±10% for the prominent lines.

[c]Reference 37.

[d]Reference 45.

[e]Energy and relative intensity obtained from coincidence data.

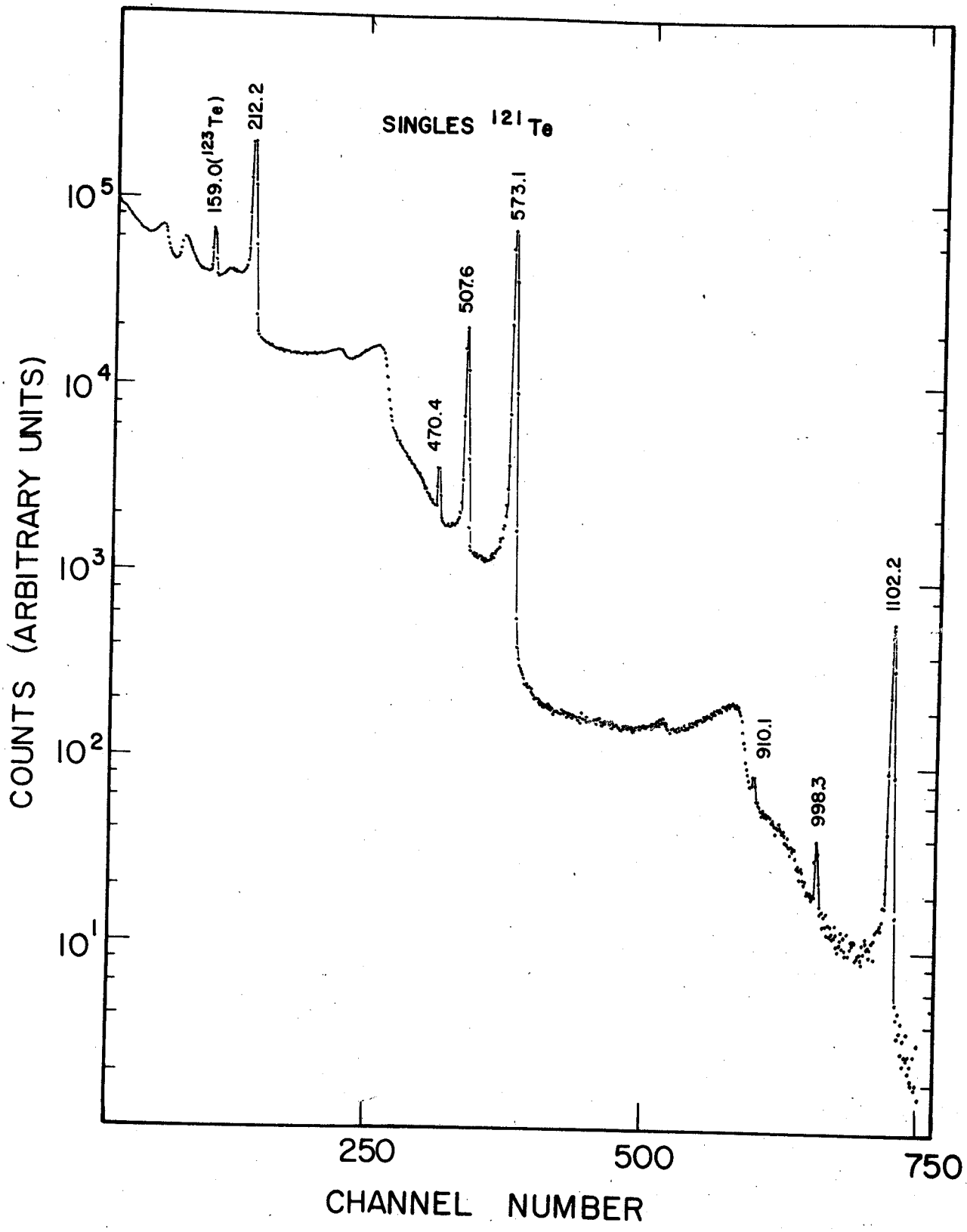


Fig. 15 Singles spectrum of $^{121}Te$, recorded with a 3 $cm^3$ Ge(Li) detector after the $^{119m}Te$ had decayed away.

results obtained by Auble et al. (9) using only scintillation detectors.

In our investigation of the $^{119}$Te spectra, no evidence was found for gamma rays in the 1500-1900 keV region that were stronger than 0.3% of the 1213 keV line. Also, upper limits for intensities of the possible 2350 and 2570 keV gammas can be reduced by at least a factor of three from the values which had been reported by other investigations (37). A sum peak of 2360 keV was, however, observed with the 12 $cm^3$ and with the 7 $cm^3$ Ge(Li) detectors and a typical one is shown in Figure 14e. Relative intensities of the 684, 768, 788 and 843 keV gamma rays in $^{119g}$Te were obtained from coincidence experiments since these weak transitions are masked by Compton backgrounds in singles spectra. A very weak gamma ray of 1260 keV was present in some of the singles spectra. It did not, however, decay with a half-life that was characteristic of the $^{119m}$Te and $^{119g}$Te and is therefore attributed to another activity.

3.2.2.B.--Gamma-gamma Coincidence Studies--Gamma-gamma coincidence experiments were performed using a 7.6 X 7.6 cm NaI(Tl) detector as the gating crystal, while spectra taken with one of the Ge(Li) counters were displayed on the 1024 channel analyser. The 1 MeV region of the gamma ray spectrum of $^{119m}$Te was scanned with the NaI(Tl) spectrometer in a series of 100-200 keV

steps, starting at 1370 and ending at 900 keV. In other coincidence experiments, the gates were set on the 153-164 and 270 keV photopeaks. The results are displayed in Figures 16 and 17, and are summarized in Table 9.

Two types of coincidence experiments were performed with the 16 hour $^{119g}$Te activity. First, a spectrum was taken in coincidence with an integral gate set above 450 keV. This discriminator setting was chosen to minimize effects of scattering between detectors, which were oriented at 180 degrees in this case. The absence of the 1338, 1413, and 1749 keV gammas from this spectrum indicates that these are ground state transitions that are directly fed by electron capture. The relative intensities of any possible gamma rays feeding these levels must be assigned to be less than 0.1.

Second, a spectrum was taken in coincidence with a region including the 644 and 700 keV photopeaks. A coincidence between this region and 1100 keV has been previously detected by Sorokin et al. (40) using scintillation counters. Our experiment resolved the 1100 keV region into lines of 1105, 1120 and 1177 keV. Furthermore, weak peaks at 684, 768, 788 and 843 are also present. All of the above gamma rays retained their relative intensities, to within statistical error, in a second spectrum that was recorded seven hours later. Subsequent experiments, gating on either side of the

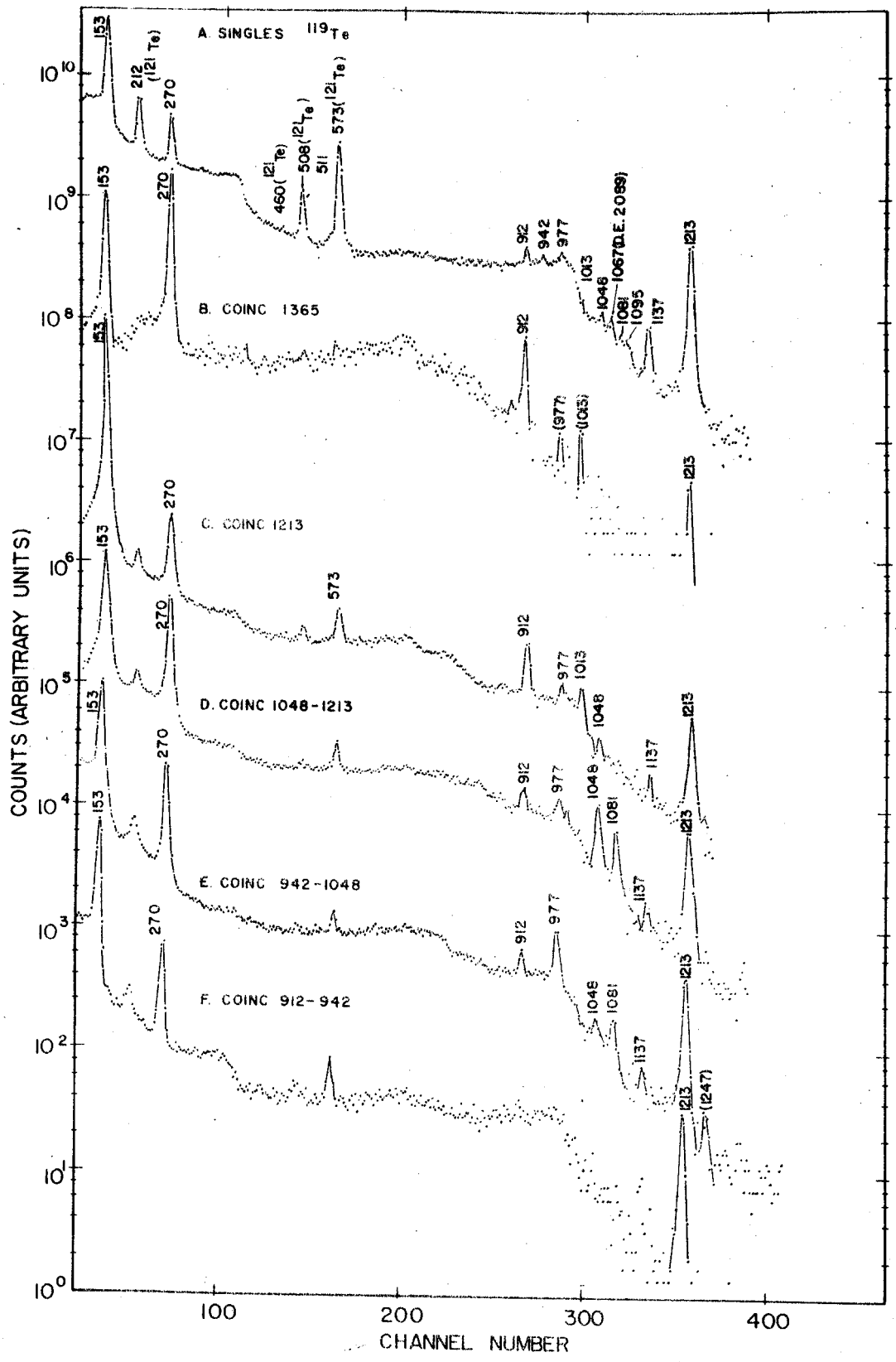


Fig. 16 Gamma ray spectra of $^{119m}$Te in coincidence with various segments of the 900-1400 keV region. These spectra were taken with a 3 cm$^3$ Ge(Li) detector and a 7.6 cm x 7.6 cm NaI(Tl) crystal. A singles spectrum is given for reference. The spectra have been arbitrarily displaced vertically for ease of presentation. The energy scales have been adjusted to be equal with the MSU CDC3600 computer.

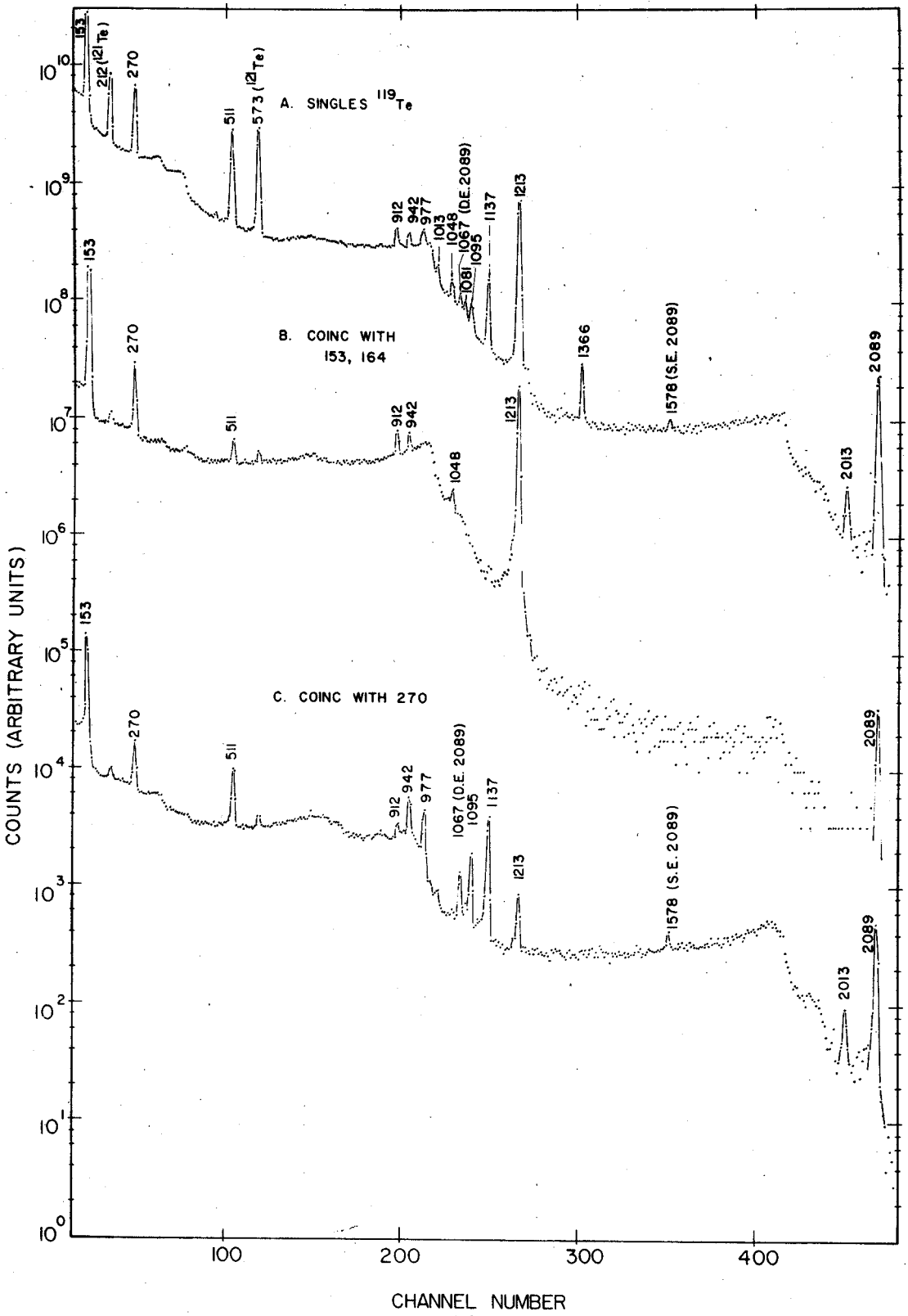


Fig. 17 Gamma ray spectra of $^{119m}$Te in coincidence with the 153 and 270 keV regions. The Ge(Li) counter used in this case had a 7 cm$^3$ active volume, while the NaI(Tl) crystal was the same as for fig. 16.

Table 9.--$^{119m}$Te Gamma-Gamma Coincidence Relationships.

| Figure | Gammas in Gate[a] (keV) | Ge(Li) Spectra: Coincident Gammas (keV) | Ge(Li) Spectra: Coincidence with (keV) |
|---|---|---|---|
| 16B | 1366, 1249 | 153, 1013 | 1213 |
| | 1213 | 270 | 2089 Compton |
| | | 912 | 1366, 1213 |
| | | 976 | 1249 |
| 16C | 1213, 1137 | 212, 508, 573 | chance ($^{121}$Te) |
| | 1249 | 153, 912, 1013 | 1213 |
| | | 270 | 1137, 2089 Compton |
| | | 976 | 1249 |
| | | 1213 | chance |
| 16D | 1048, 1067[b] | 153, 912 | 1213 |
| | 1081, 1095 | 270 | 1095, 1067 (D.E. 2089) |
| | 1137, 1213 | | 2089, 1137 Compton |
| | | 1048 | 1081 |
| | | 1081 | 1048 |
| 16E | 912, 942, 976, 979, 1013, 1048 | 153 | 912, 1213 Compton |
| | | 270 | 976, 2089 Compton |
| | | 912 | 1213 Compton |
| | | 1048 | 1081 |
| | | 1213 | chance |
| | | (1249)[c] | 976 |
| 17B | 270 | 153, 942, 977 | |
| | | 1067, 1095 | 270 |
| | | 1137, 2013, 2089 | |
| | | 270 | underlying Comptons |
| | | 1213 | chance |
| 17C | 153, 164 | 912 | 153, 164 |
| | | 942, 1213 | 153 |
| | | 1048 | 164 |

[a]Includes photo peaks only partly within gate.

[b]Double escape peak of 2089 keV gamma.

[c]A later experiment, gating on the 977 keV region, definitely established the 977-1249 and 977-117 keV cascades. The later was confirmed in a triple coincidence experiment.

644-700 keV doublet, revealed the 684, 768, 843, 1105 and 1177 keV lines to be in coincidence with the 644 keV transition, and the 788 and 1120 in coincidence with the 700 keV gamma. These results are shown in Figure 18.

Results of triple coincidence experiments with the split NaI(Tl) annulus (26) and a 7 $cm^3$ Ge(Li) detector are shown in Figure 5 and are consistent with other coincidence data and the proposed decay scheme. Spectrum B of Figure 5 shows gamma rays in triple coincidence with simultaneous pulses in the 153 and 1212 keV regions. As can be seen below, the 912 keV gamma ray is the only one in true triple coincidence with both photopeaks. The presence of the other gamma rays can be accounted for by a true coincidence with either gate, plus a chance coincidence, due to the use of a strong source, with the second gate. Similarly, in spectrum C of Figure 5, for which the two gates were set at 270 and 940-1150 keV, the 977 keV doublet and the 871 and 117 keV lines are the only true coincidences among the photopeaks.

3.2.2.C.--The Proposed Decay Schemes of $^{119g}Te$ and $^{119m}Te$--Based on evidences from coincidence data, energy sums and relative intensities, consistent decay schemes can be constructed for both $^{119g}Te$ and $^{119m}Te$. While the placement of the strongest transitions remains, in general, unchanged from previous work (37,38),

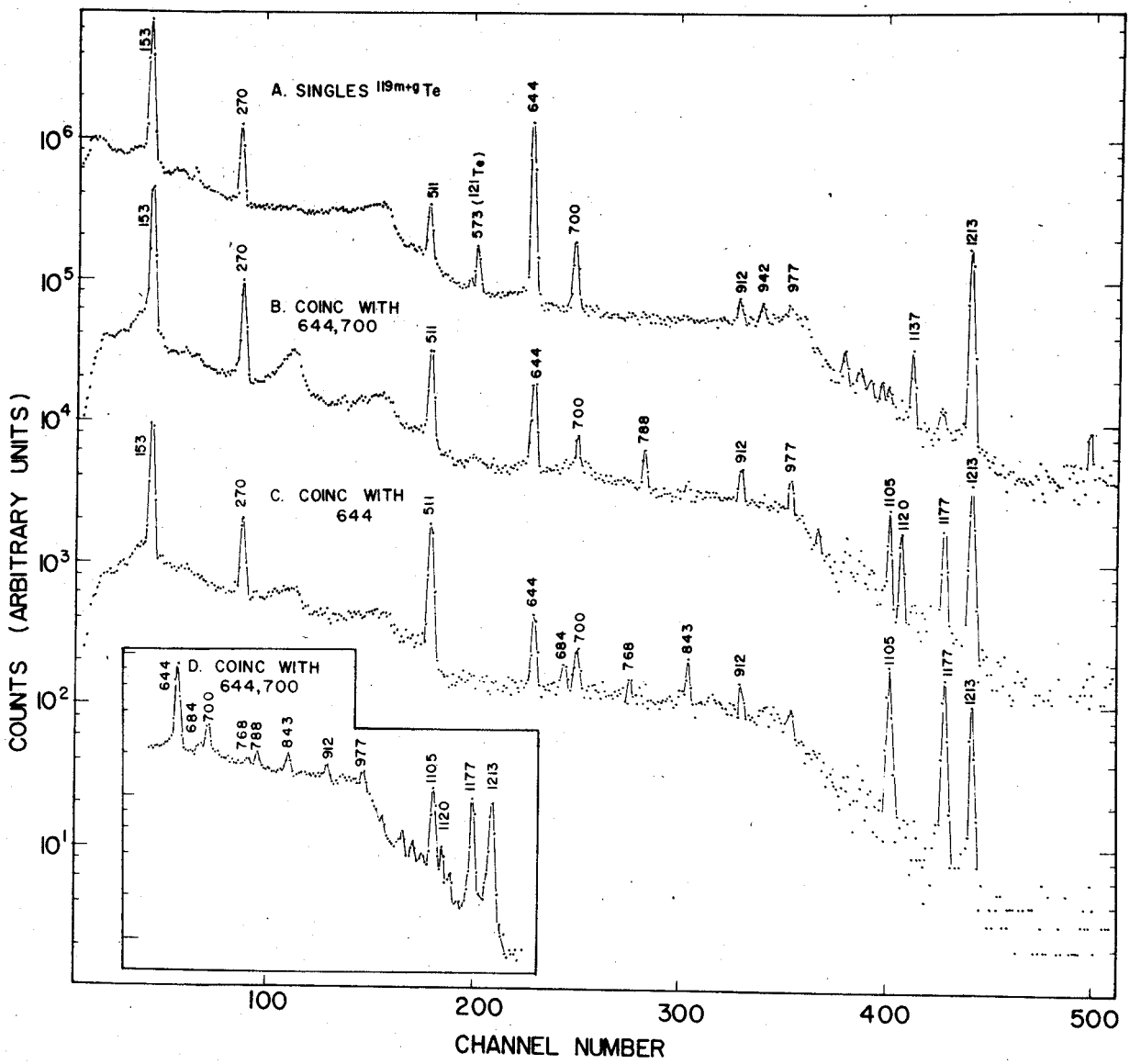


Fig. 18 Gamma ray spectra in coincidence with the 644-700 keV region in $^{119g}$Te. The 7cm$^3$ Ge(Li) detector and one half of a 20.3 cm x 20.3 cm NaI(Tl) split annulus crystal were used to record these spectra. Spectra B and C were recorded with the NaI(Tl) detector gated on the high and low sides of the 644-700 keV doublet, respectively. Spectrum D was obtained from an earlier source and shows a segment of the spectrum in coincidence with the 600-750 keV region.

the accommodation of the new gamma rays requires additional levels. The proposed level schemes are shown in Figures 19 and 20, and are in good agreement with results recently obtained by Graeffe et al. (45).

3.2.2.C.1.--Levels populated in decay of $^{119g}$Te.--Levels at 644.1 and 699.6 keV have been proposed previously (37), and are confirmed in our investigations by the high intensities of the 644.1 and 699.6 keV transitions and the absence of a 644-700 keV cascade. Gamma rays of 1105.6, 1120.0, 1176.8, 1338.7, 1412.8, and 1749.1 keV were found to decay, within experimental error, with the same halflife as the 644 keV transition. The last three were absent from the "any-coincidence" spectrum, implying levels at 1338.7, and 1412.8 and 1749.1 keV. As confirmed by coincidence data, the 1413 and 1749 keV levels also depopulate to the 644 keV state via the 768 and 1105 keV transitions, respectively. Additional levels, based on the 644-843, 700-788, 644-1177, and 700-1120 keV cascades, are placed at 1487 and 1820 keV. Another level is suggested at 1328 keV by the 644-684 keV cascade.

Positron feeding to the 664 and 700 keV levels was measured to occur in approximately 1% and 0.1% of the decays of $^{119g}$Te, respectively. No evidence was found for significant beta decay to the ground state of $^{119}$Sb.

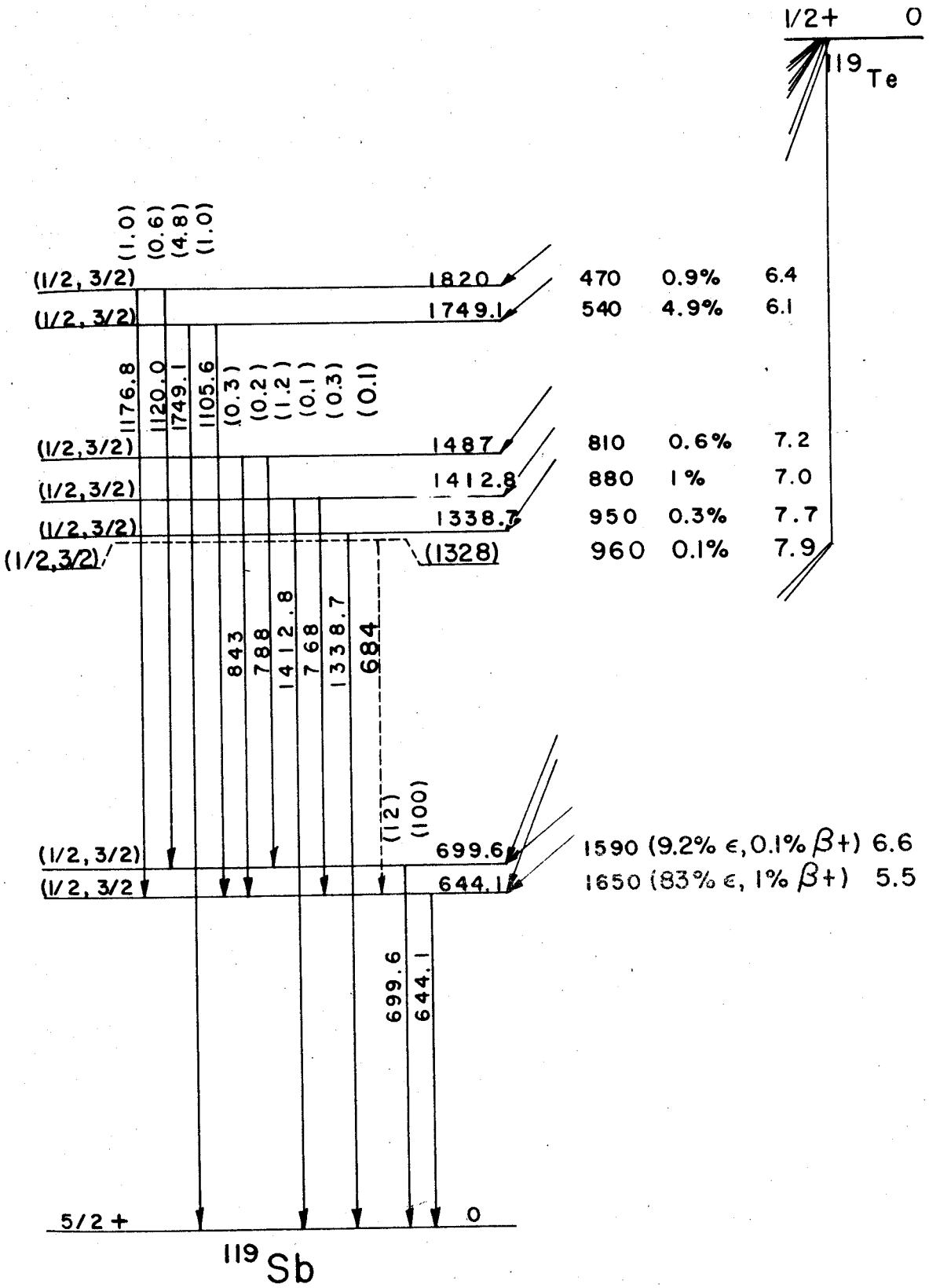


Fig. 19 Proposed decay scheme of $^{119g}$Te.

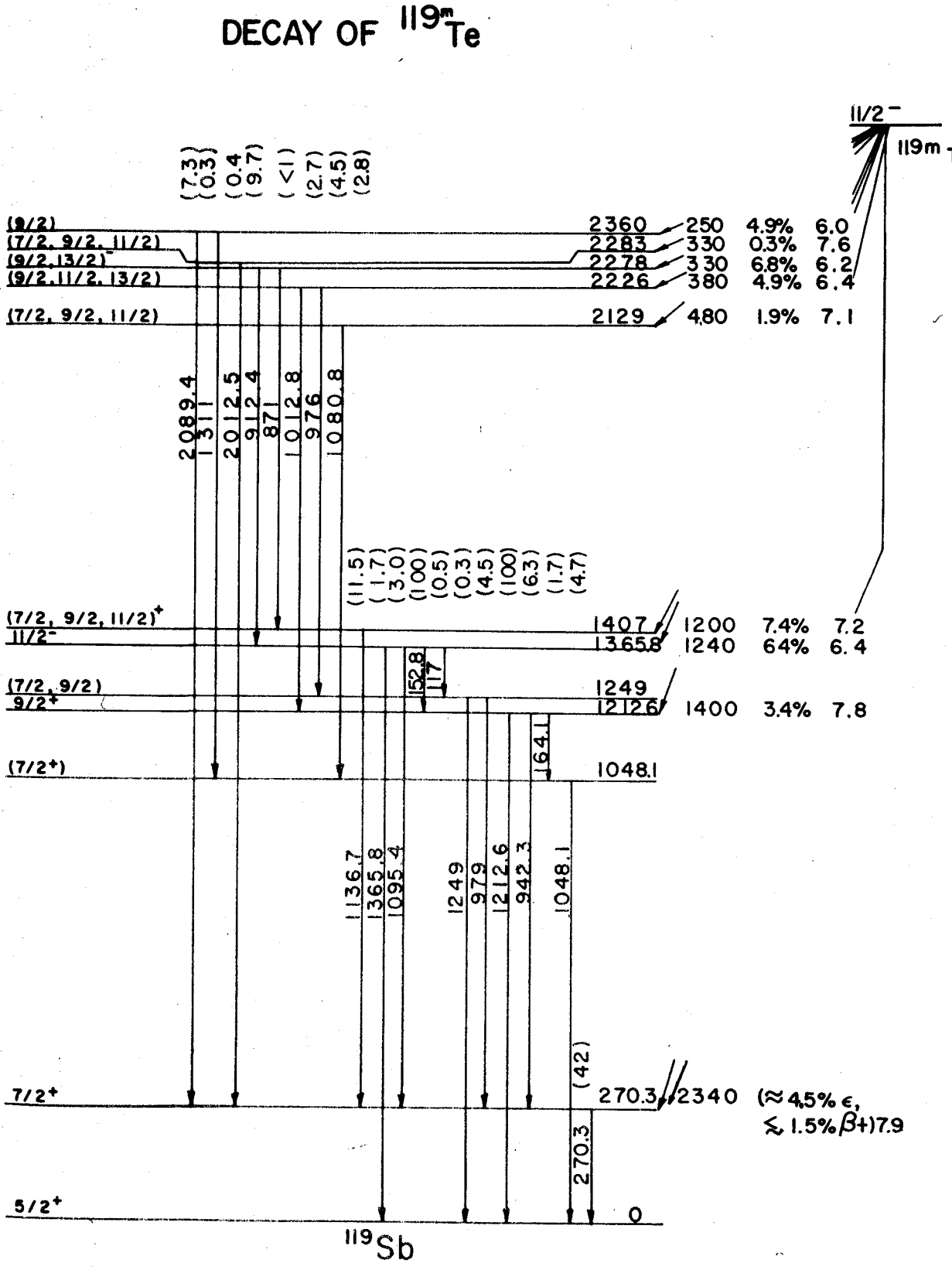


Fig. 20 Proposed decay scheme of $^{119m}Te$.

3.2.2.C.2.--Levels populated in the decay of $^{119m}$Te.--Levels corresponding to our 270.3, 1048.1., 1212.6, 1365.8, 2278 and 2360 keV states have been proposed previously (37,38), and are confirmed by our results. The levels at 270, 1213, and 1366 keV are confirmed by the 270-942, 270-1095 and 1213-153 keV cascades and the cross-over transitions to ground. The level at 1213, rather than 153 keV, is implied by a 153-942 keV cascade from the 1366 to the 270 keV level. Further evidence supporting this order is supplied by the fact that both the 912 and 1013 keV transitions are in coincidence with the 1213 keV gamma, but only the 912 keV gamma is in coincidence with the 153 keV transition. The 912 keV line was also seen in strong coincidence with the gating region at 1366 keV (which included the 1366 keV line as well as the 1213 and 153 keV sum-peak), while the 1013 keV transition was barely evident. This suggests additional levels at 2226 keV depopulating to the 1213 via the 1013 keV line, and at 2278 keV, depopulating to the 1366 via the 912 keV transition.

The intermediate level of the 1081-1048 keV cascade is placed at 1048 keV because of relative intensity arguments. Furthermore, some evidence for a coincidence between the 1048 keV line and 150 keV region confirms the previous placement (37,38) of the 164 keV transition as depopulating the 1213 keV level. A level is placed at 2129 keV because of the absence of the 1081 keV line

from all other coincidence spectra except those having gates which included the 1048 keV gamma ray. An additional level is placed at 1249 keV. It is fed from the 2226 keV level by a 976 keV transition and decays to the 270 keV state via a 979 keV transition. The very weak 1249 keV cross-over to ground then accounts for the trace of the 976 keV transtion present in coincidence with the 1200 keV region. Additional evidence from the triple coincidence data (Figure 5) suggests the existence of a 117 keV transition between the 1366 and 1249 keV levels.

From the existence of the 1137-270 keV coincidence, and from the absence of the 1137 keV line from other coincidence spectra, a level is placed at 1407 keV. That this is not the same as the 1413 keV state populated by $^{119g}$Te is confirmed by the fact that the 1413 keV gamma decays with the $^{119g}$Te half-life and the 1137 keV gamma with that of the $^{119m}$Te. Also, the energy measurements in this investigation are considered to be far more accurate than $\pm$ 6 keV. The 1407 keV state is also fed by an 871 keV transition from the 2278 keV state. This was demonstrated in a triple coincidence experiment using the split NaI(Tl) annulus and the 7 cm$^3$ Ge(Li) detector.

Finally, the 2089-270 keV cascade had been identified previously (37), and was confirmed in our

investigation, placing a state at 2360 keV. A sum peak corresponding to this cascade, seen with one of the larger Ge(Li) detectors, is shown in Figure 14e. The weak line at 2013 keV can also be seen in coincidence with the 270 keV transition, placing a level at 2283 keV. Since the errors in energy measurements are typically less than 1 keV, the 2278 and 2283 keV levels are believed to be separate states.

Weak evidence exists for the 1311 keV transition. Because of its very low relative intensity no conclusive experiments involving it are feasible at this time. However, on the basis of energy sums, it is tentatively placed between the 2360 and 1048 keV levels.

Only the 270 keV level was observed to be possibly populated by positron decay. Because pair production events caused by the 2013 and 2089 keV transitions are also in coincidence with the 270 keV gamma, only an upper limit of 1.5% of the total decays of $^{119m}$Te can be placed on the positron feeding to this level.

3.2.2.D.--Results of the Angular Correlation Experiments and Interpretation of the Level Scheme of $^{119}$Sb.--Gamma-gamma angular correlation functions obtained in this investigation for most of the cascades are shown in Figures 21 and 22. The numerical results are summarized in Table 10, where a comparison is also made with values obtained by other investigators. A

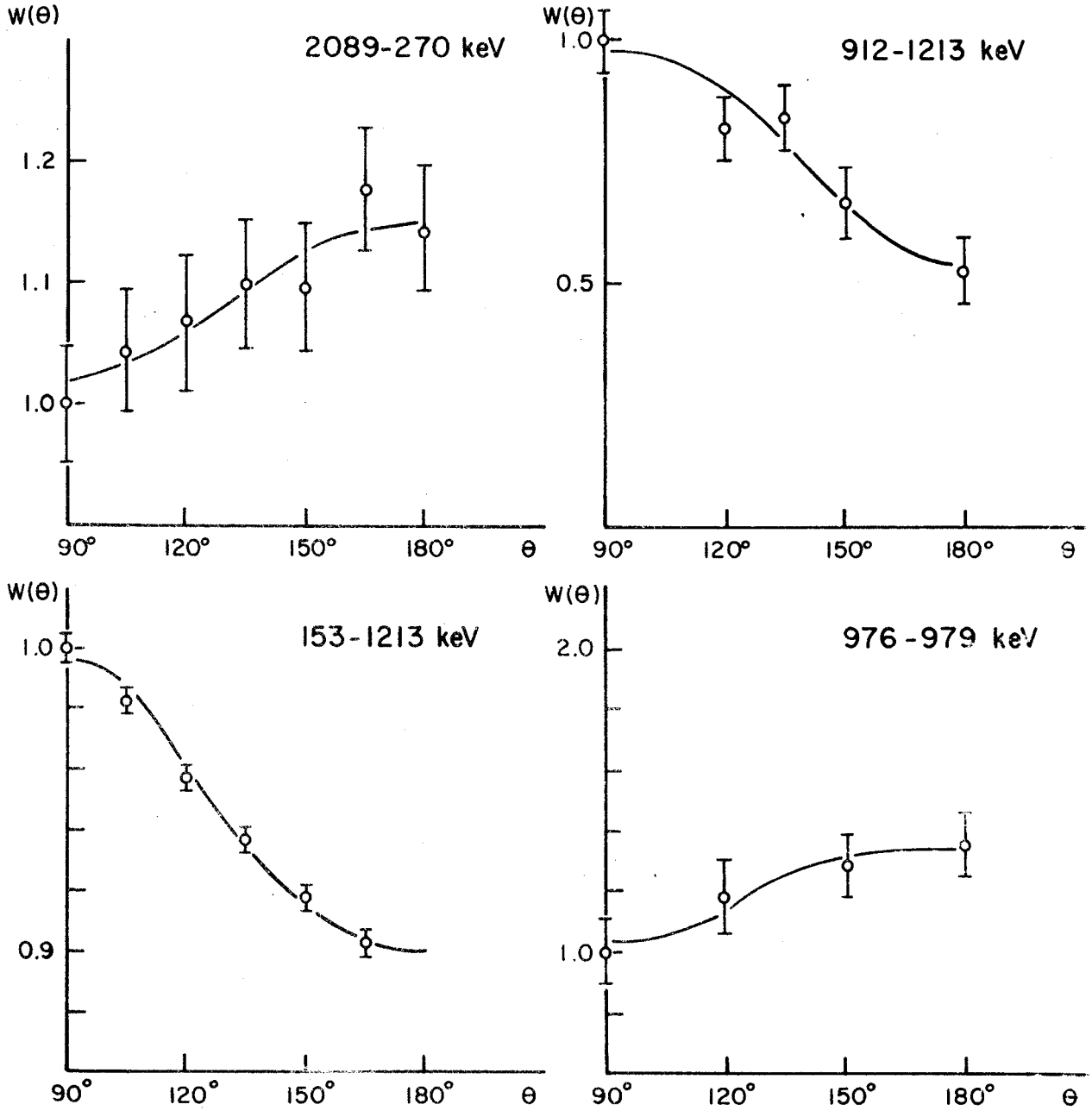


Fig. 21 Experimental correlation functions for four gamma ray cascades in $^{119}$Te. The errors to individual points are assigned primarily on the basis of statistics. The solid line is a least squares Legendre polynomial fit to the data points.

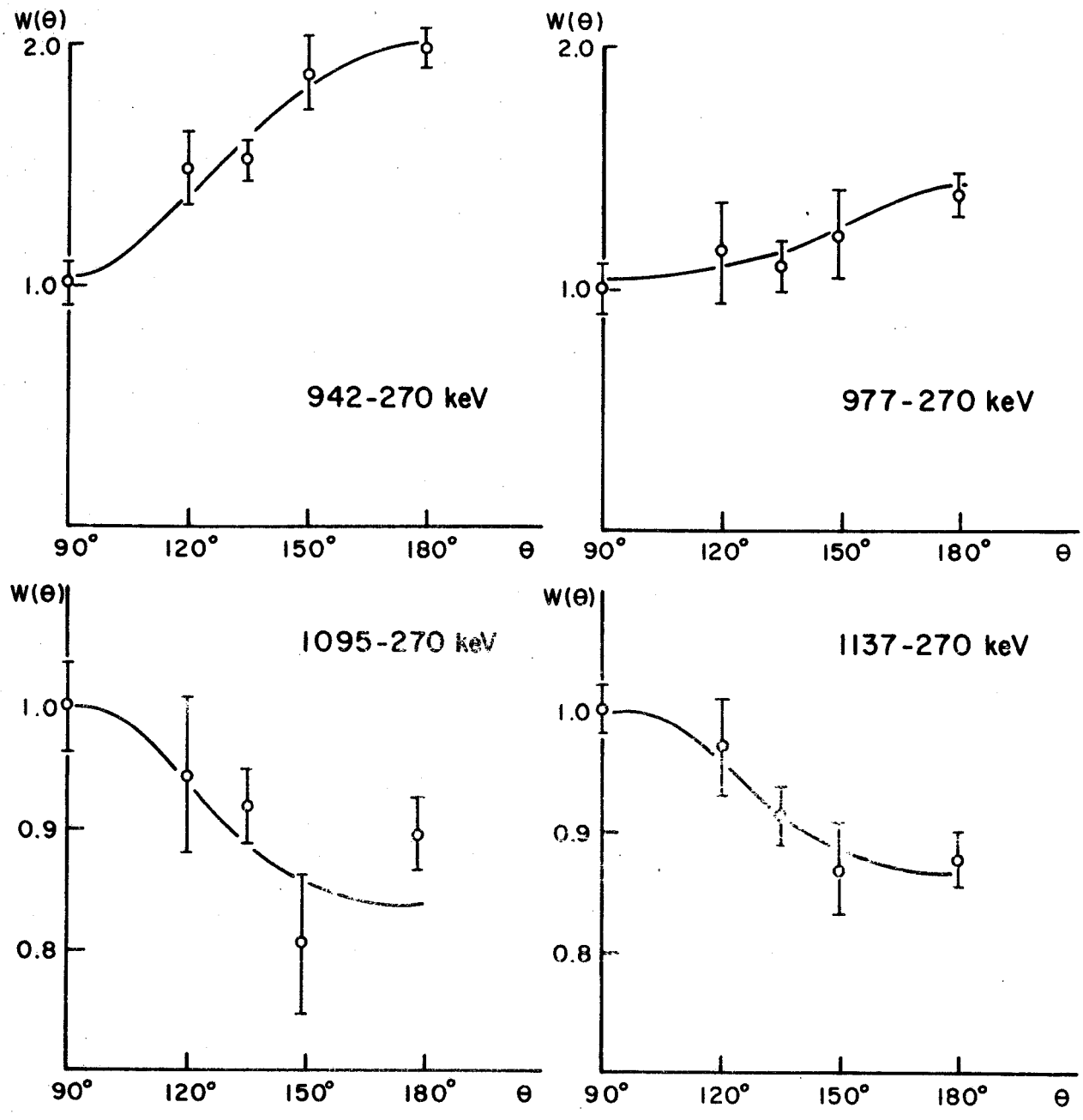


Fig. 22 Same as fig. 21 for four additional cascades. The differences in the magnitudes of the error bars for points in a given set arise from the fact that the results from several runs with different angular increments have been combined.

Table 10.--Summary of $^{119}$Te Gamma-Gamma Angular Correlation Data

| Cascade Energies (keV) | Correlation Coefficients $A_2$ | $A_4$ | Assigned Spin Sequence [a] | Mixing Ratios [a] $\delta_1$ | $\delta_2$ |
|---|---|---|---|---|---|
| 153-1213 | $-0.071 \pm 0.007$ | $0.001 \pm 0.01$ | 11/2(1,2)9/2(2)5/2 | $-0.04 \leq \delta_{153} \leq 0.04$ | $-0.08 \leq \delta_{1213} \leq -0.03$ |
| | $-0.069 \pm 0.005$[b] | $0.002 \pm 0.005$[b] | | | |
| | $-0.062 \pm 0.004$[c] | $-0.002 \pm 0.005$[c] | | | |
| | $-0.065 \pm 0.006$[d] | $0.0006 \pm 0.006$[d] | | | |
| 942-270 | $0.56 \pm 0.1$ | $-0.10 \pm 0.1$ | 9/2(1,2)7/2(1,2)5/2 | $-3.2 \leq \delta_{270} \leq -0.1$ | $0.2 \leq \delta_{942} \leq 6.0$[f] |
| | $0.273 \pm 0.011$[ce] | $0.013 \pm 0.015$[ce] | | | |
| 153-942 | $0.39 \pm 0.15$ | $0.16 \pm 0.2$ | 11/2(1,2)9/2(1,2)7/2 | $-1.2 \leq \delta_{942} \leq -0.6$[f] | $0.03 \leq \delta_{153} \leq 0.04$ |
| 1095-270 | $-0.16 \pm 0.003$ | $0.09 \pm 0.1$ | 11/2(2,3)7/2(1,2)5/2 | $-0.3 \leq \delta_{1095} \leq 0.1$ or $-2.5 \leq \delta_{1095} \leq -1.3$ | $-5.0 \leq \delta_{270} \leq 0.1$ |
| | $-0.041 \pm 0.004$[c] | $0.05 \pm 0.007$[cg] | | | |
| 1137-270 | $-0.12 \pm 0.02$ | $0.04 \pm 0.1$ | h | | |
| 2089-270 | $0.019 \pm 0.02$ | $-0.02 \pm 0.1$ | 9/2(1,2)7/2(1,2)5/2 | | |
| | $0.083 \pm 0.015$[b] | $0.012 \pm 0.015$[b] | | | |
| | $0.124 \pm 0.015$[c] | $0.058 \pm .023$[c] | | | |
| 977-270 | $0.25 \pm 0.05$ | $0.09 \pm 0.1$ | h | | |
| 912-1213 | $-0.40 \pm 0.08$ | $0.07 \pm 0.1$ | h | | |
| 1013-1213 | $-0.26 \pm 0.1$ | $-0.16 \pm 0.2$ | h | | |
| 976-979 | $0.23 \pm 0.05$ | $-0.09 \pm 0.1$ | h | | |
| 9.2-153 | $0.53 \pm 0.2$ | $-0.10 \pm 0.2$ | h | | |

[a]Mixing ratios and spin sequences determined from the present correlation data. Only the internal conversion coefficient, of the 153 keV transition, has been used to restrict the choices of the spin sequences and mixing parameters.

[b]Reference 39. [c]Reference 44. [d]Reference 45.

[e]These correlation coefficients were determined in Reference 44, ignoring data points near 180° angle because of the presence of positrons in a contaminant. This positron emitting contaminant was not present in the present data.

[f]Sign change because of the change in order of emission of the 942 keV gamma in these two cascades (61).

[g]The 1095 keV peak was not considered to be a doublet in these data (44).

[h]Unique spin assignment not possible from this study.

summary of the multipolarities and mixing ratios which are suggested by these results is given in Table 11. Also listed in the same table are multipolarities assigned in previous investigations.

Because of the large uncertainties in the $A_4$ values, all of the interpretations of the decay scheme were based on the $A_2$ values only. In all cases the experimental and theoretical $A_4$ coefficients agreed to within the experimental uncertainties. Although, in general, any one experimental correlation function is consistent with more than one set of spin assignments, combining the results for several cascades involving common levels has strongly suggested unique values for some of the states. The spin values assigned from this study are those in the decay scheme shown in Figure 20. A summary of the interpretation is given below.

3.2.2.D.1.--The 1366, 1213, 270 and 0 keV States.--The only two spin sequences for the 1366, 1213, 270 and 0 keV levels which are consistent with log ft values, multipolarity assignments from conversion electron studies (38, 39, 45) and previous angular correlation measurements (39, 44, 45) are $11/2^-$, $9/2^+$, $7/2^+$, $5/2^+$, or $9/2^-$, $7/2^+$, $7/2^+$, $5/2^+$, respectively. Of the cascades studied in this investigation only that involving the 153 and 942 keV transitions which depopulate

Table 11.--Comparison of Mulipolerities Assigned by Various Investigators.

| Transition (keV) | Proposed Multipolarity | | | |
|---|---|---|---|---|
| | Svedberg et al.[a] | Graeffe et al.[b] | Singru et al.[c] | Present |
| 153 | E1 | E1 | E1 | E1,(≤0.1%M2) |
| 164 | M1 | M1,E2 | | |
| 270 | M1 | M1,E2 | M1,<40%E2 | M1,(≤20% or 80 to 90% E2) |
| 912 | | M1,E2 | M1,E2 | M1,(20 to 70% E2) |
| 942 | M1 | M1,E2 | | M1,(20 to 60% E2) |
| 975 | M1 | | | d |
| 979 | | | | d |
| 1013 | | M1,E2 | | d |
| 1048 | M1 | M1,E2 | | |
| 1081 | | E1 | | |
| 1096 | M2 | M2 | | M2 |
| 1137 | M1 | E1 | | M1, E2 |
| 1213 | E2 | M1,E2 | M1,E2 | E2,(≤0.1%M3) |
| 1366 | E3 | E3 | | E3 |
| 2089 | | | | E1 or M1,E2 |

[a]Reference 38. [b]Reference 45. [c]Reference 44.

[d]Results inconclusive.

the 1366 and 1213 keV levels, respectively, yields a correlation function which is consistent with only the former spin sequence. However, the 942-270 keV cascade produced an experimental $A_2$ value which required a most liberal allowance for experimental error in order to be consistent with the latter sequence, whereas this $A_2$ value is in agreement with theoretical values obtained from the first spin sequence.

Although the results of these angular correlation measurements strongly suggest the spin sequence of $11/2^-$, $9/2^+$, $7/2^+$, and $5/2^+$, for the 1366, 1213, 270 and 0 keV levels, respectively, a number of additional remarks should be made. In order to produce an $A_2$ value which is as large as the measured value, even with a liberal error, the E1 153 keV transition must have approximately a 0.1% M2 admixture. Because of this M2 admixture in the 153 keV transition, there must also be an M3 admixture of comparable magnitude in the predominately E2 1213 keV transition. While the E1 + M2 admixture is not too surprising, to the best of our knowledge, an E2 + M3 combination has never been observed.

As can be seen in Table 10, the mixing parameter for the 942 keV transition changes sign in the 942-270 keV as opposed to the 153-942 keV correlation. This is consistent with a well known triple cascade theorem (61).

3.2.2.D.2.--Other Levels.--Except for the case of the four levels discussed above, at least two possibilities still remain in the spin assignments to the other states. It should be noted that, with possibly one exception, the correlation measurements are consistent with the most recent conversion electron study assignments (45).

The possible discrepancy exists for the case of the 1407 keV state, where a $9/2^-$ spin assignment has been made previously (45). The negative $\delta_{270}$, which has already been established, does not permit the observed $A_2$ value for the 1137-270 keV cascade unless the proposed E1 transition is appreciably (a few per cent) M2 admixed. Either a $7/2^+$, $9/2^+$, or $11/2^+$ assignment would be consistent with the correlation results.

The 1013-1213 correlation leaves 9/2, 11/2, 13/2 as the possible spin assignments for the 2226 keV level.

From correlation measurements on the 912-153 and 912-(153)- 1213 keV cascades, the spin of the 2278 keV level must be $9/2^-$ or $13/2^-$. The 912 keV transition is from 20 to 70% E2.

From the 2089-270 keV correlation, an $11/2^+$ assignment can be ruled out for the 2360 keV state, and $11/2^-$ is unlikely since then the 2089 keV gamma would have to be M2 with about a 20% E3 admixture.

A spin of 9/2 is the most probable value, making the 2089 keV transition almost pure E1 or M1.+ E2.

No reliable evidence was obtained for making spin assignments to the 1048, 1250, 2129, and 2284 keV states.

## 3.2.3. Decay Scheme of $^{117g}$Te

3.2.3.A.--The Gamma Ray Singles Spectrum.--Gamma ray singles spectra were recorded with several Ge(Li) detectors. Below 1800 keV, a 0.8 $cm^3$ counter with $\lesssim$ 3.0 keV FWHM resolution for the 662 keV gamma of $^{137}$Cs was used. The efficiency for detection of weak high energy transitions was increased with a 7 $cm^3$ counter whose resolution was $\approx$ 4.5 keV FWHM. Portions of typical singles spectra are shown in Figures 23 and 24. A list of transitions and their relative intensities is given in Table 12.

Halflife measurements were performed on the 720, 1091, 1278 (D.E. of 2300), 1717, and 2300 keV lines. Two series of 8 min runs were taken--the first set spanning about 80% of a halflife, the second about 1.5 halflives. Corrections were made for dead time and source decay. The mean value obtained was 1.14 hours, with an average deviation of 0.08 hrs from the mean. The value of 1.14h is in agreement with values of 61$\pm$2 min, 1.1$\pm$0.1h, 1.1$\pm$0.1h and 65$\pm$5 min reported by reference 32, 33, 34, and 35 respectively.

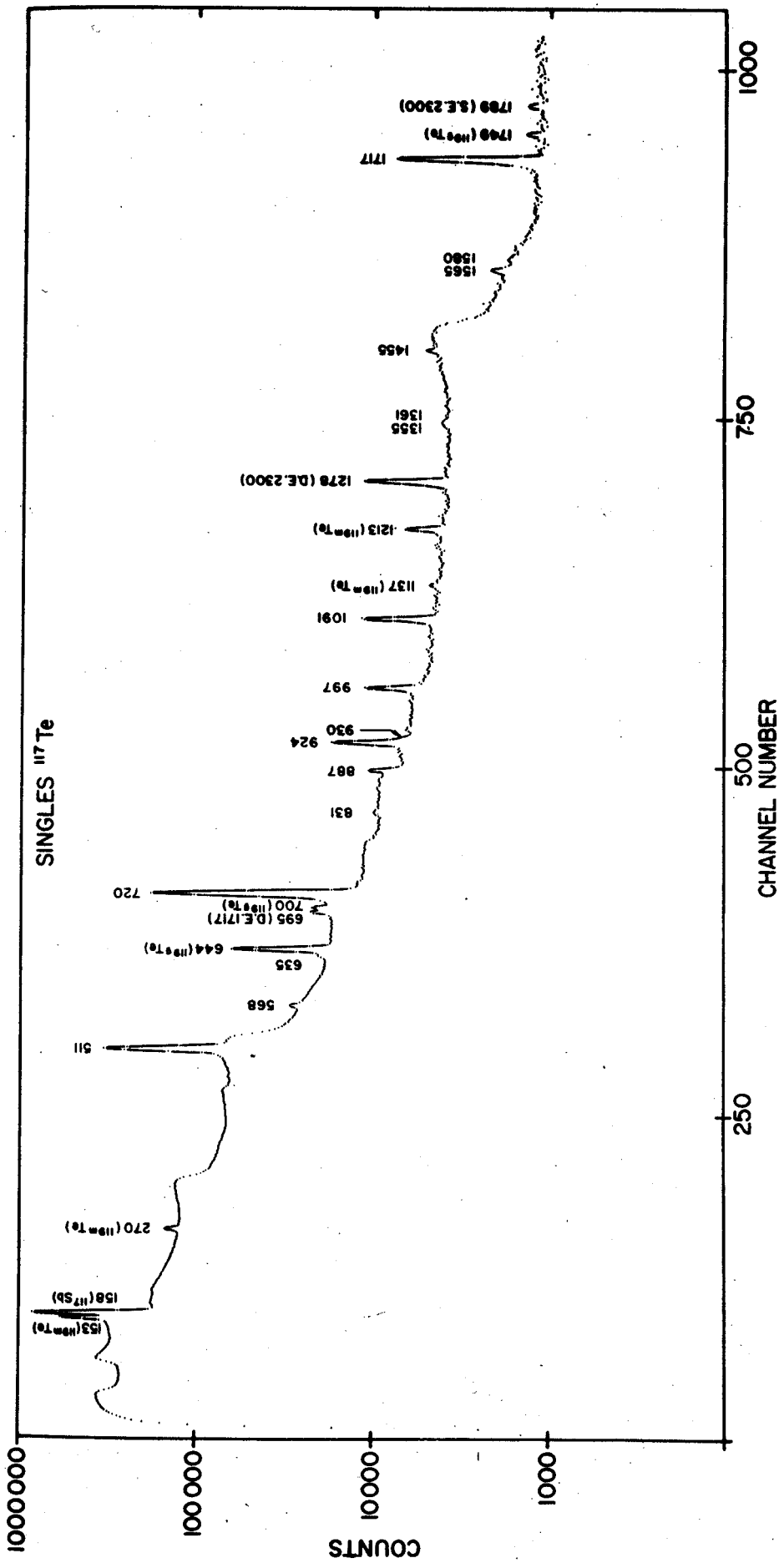


Fig. 23 Singles spectrum of $^{117}$Te below approximately 1800 keV, recorded with a 3 cm$^3$ Ge(Li) detector.

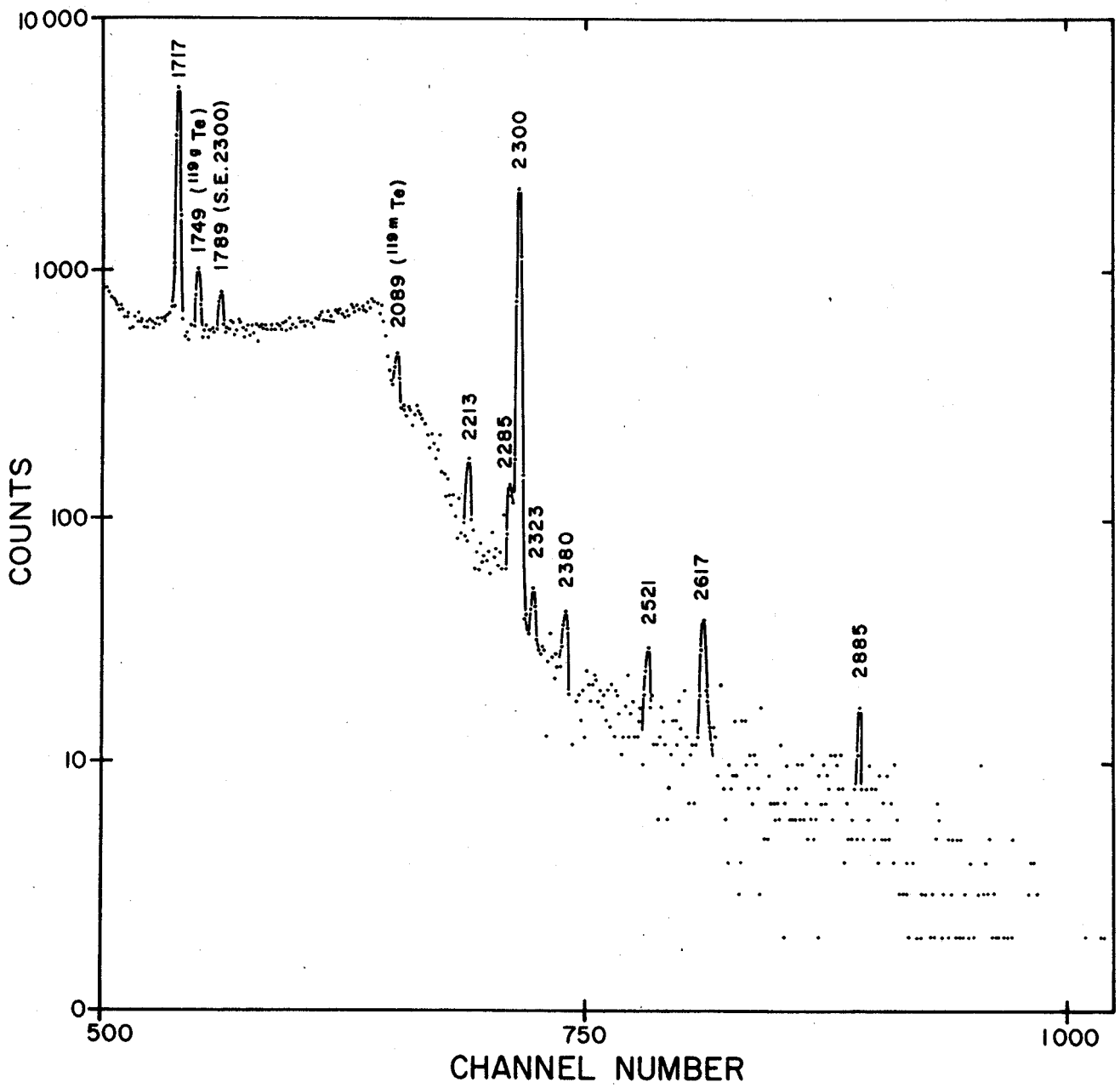


Fig. 24 High energy portion of a singles spectrum of $^{117}Te$, recorded with a 7 $cm^3$ Ge(Li) detector. This spectrum was recorded after approximately one halflife of $^{117}Te$ to allow traces of a $^{34}Cl$ contaminant to decay out. Several spectra were recorded from sources of comparable age, and were summed to give the above spectrum. Lines at 2323, 2521 and 2617 keV are of unknown origin but decay with a halflife longer than that of $^{117}Te$.

Table 12.--Energies and Relative Intensities of Gamma Rays Observed in the Decay of $^{117g}$Te.

| Energy (keV) | Uncertainty (keV) | Relative Intensity[a, b] |
|---|---|---|
| 568.8 | ±0.5 | 1.3 |
| 634.6 | 0.5 | 0.8 |
| 719.8 | 0.4 | 100 |
| 830.8 | 0.5 | 0.9 |
| 886.8 | 0.5 | 2.4 |
| 923.9 | 0.4 | 9.4 |
| 930 | 1.0 | 0.5 |
| 996.7 | 0.4 | 6.1 |
| 1090.8 | 0.4 | 10.5 |
| 1354.6 | 0.7 | 0.6 |
| 1361.0 | 0.7 | 0.6 |
| 1454.8 | 0.4 | 1.2 |
| 1565.2 | 0.6 | 1.3 |
| 1579.9 | 1.5 | 0.8 |
| 1716.5 | 0.4 | 23 |
| 2213 | 1.0 | 0.6 |
| 2285 | 1.0 | 0.7 |
| 2300.0 | 0.5 | 16 |
| 2380[c] | 1.5 | 0.2 |
| 2885[c] | 2.0 | 0.1 |

[a]Uncertainties in relative intensity are estimated as ±10% for the strong transitions.

[b]Gamma intensity only.

[c]Assignment to $^{119g}$Te tentative.

3.2.3.B.--Gamma-Gamma Coincidence Results.--Coincidence experiments were limited by the 1.1h halflife. Besides conventional Ge(Li)-NaI(Tl) coincidence experiments, three other types of coincidence counting were performed with the 20.3 cm x 20.3 cm NaI(Tl) split annulus. First an "any-coincidence" spectrum, employing an integral NaI(Tl) gate above the 511 keV photopeak, was recorded. A second type of experiment, complementary to the "any-coincidence," was to count only those pulses from the Ge(Li) counter which were not incoincidence with a signal from the NaI(Tl) crystal. A third type of coincidence experiment performed with the split annulus was to simultaneously gate on 511 keV photons in each half, and count the resulting coincident Ge(Li) spectrum. This established any positron fed levels and indicated double escape peaks of high energy gamma rays. This spectrum is shown in Figure 25.

Other coincidence spectra were recorded with the NaI(Tl) detector scanning essentially all of the spectrum above 600 keV. To compensate for the short halflife, strong sources were used at the start of all coincidence counting, leading to an appreciable number of chance events. Hence, interpretations of the coincidence spectra must be based not necessarily on the presence of a given line but by its relative enhancement from singles relative to other lines.

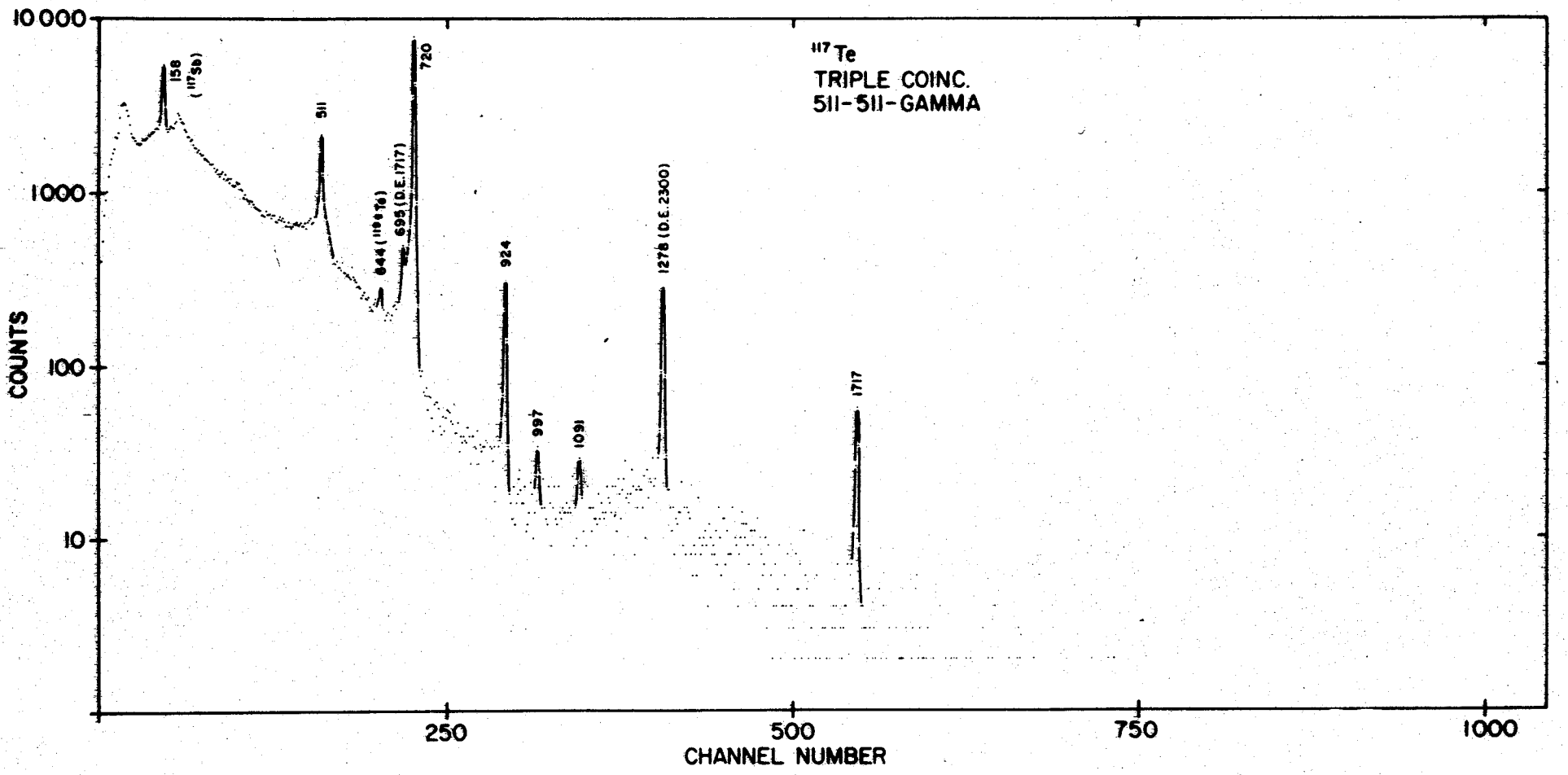


Fig. 25 Results of a triple coincidence experiment on $^{117}Te$ recorded with a 20.3 cm x 20.3 cm NaI(Tl) split annulus and a 7 $cm^3$ Ge(Li) detector. Each half of the annulus was gated on the 511 keV photopeak, while the result-

Because counting could be done for only relatively short periods at a time, most coincidence spectra exhibit regions with large statistical fluctuations. In order to ascertain whether a number of possible peaks were more than background fluctuations, most of the coincidence runs were repeated with different sources. Coincidence evidences were obtained for all lines of less than 1800 keV energy which could be observed in singles spectra. In addition, several other possible gamma rays were suggested by some coincidence experiments, but these did not reproduce well enough to warrant their placement in the decay scheme.

The results of the coincidence studies are summarized in Table 13. Several typical spectra are shown in Figure 26.

3.2.3.C.--Positron-Gamma Coincidence Results.--Positron-gamma coincidence spectra were recorded with a 3.8cm X 0.5cm plastic scintillator (Pilot B) and a 7.6cm X 7.6cm NaI(Tl) detector. Gating regions in the NaI(Tl) spectrum were selected at 511, 720, 924, and 1717 keV. The resulting coincident positron spectra confirmed that there is no significant positron decay to the ground state of $^{117}$Sb.

Because of source thickness, window thickness, and the inherently poor resolution of plastic scintillators, reliable spectral shapes of the Fermi

Table 13.--$^{117}$Te Gamma-Gamma Coincidence Relationships.

| Figure | Gamma in NaI(Tl) gate (keV) | Coincident gammas in Ge(Li) spectrum (keV) |
|---|---|---|
| 25 | 511-511[a] | 720, 924, 997, 1091, 1717 |
| 26B | 720 | 635, 997, 1091, 1565, 1580 |
| 26C | 887 | 924 |
| 26C | 924 | 887, 1361 |
| 26C | 930 | 1355 |
| 26D | 1355 | 930 |
| 26D | 1361 | 924 |
| 26D | 1455 | 831 |
| 26E | 1717 | 568 |
| [b] | >1850 | none observed |

[a]Triple coincident experiment.

[b]Spectrum not shown.

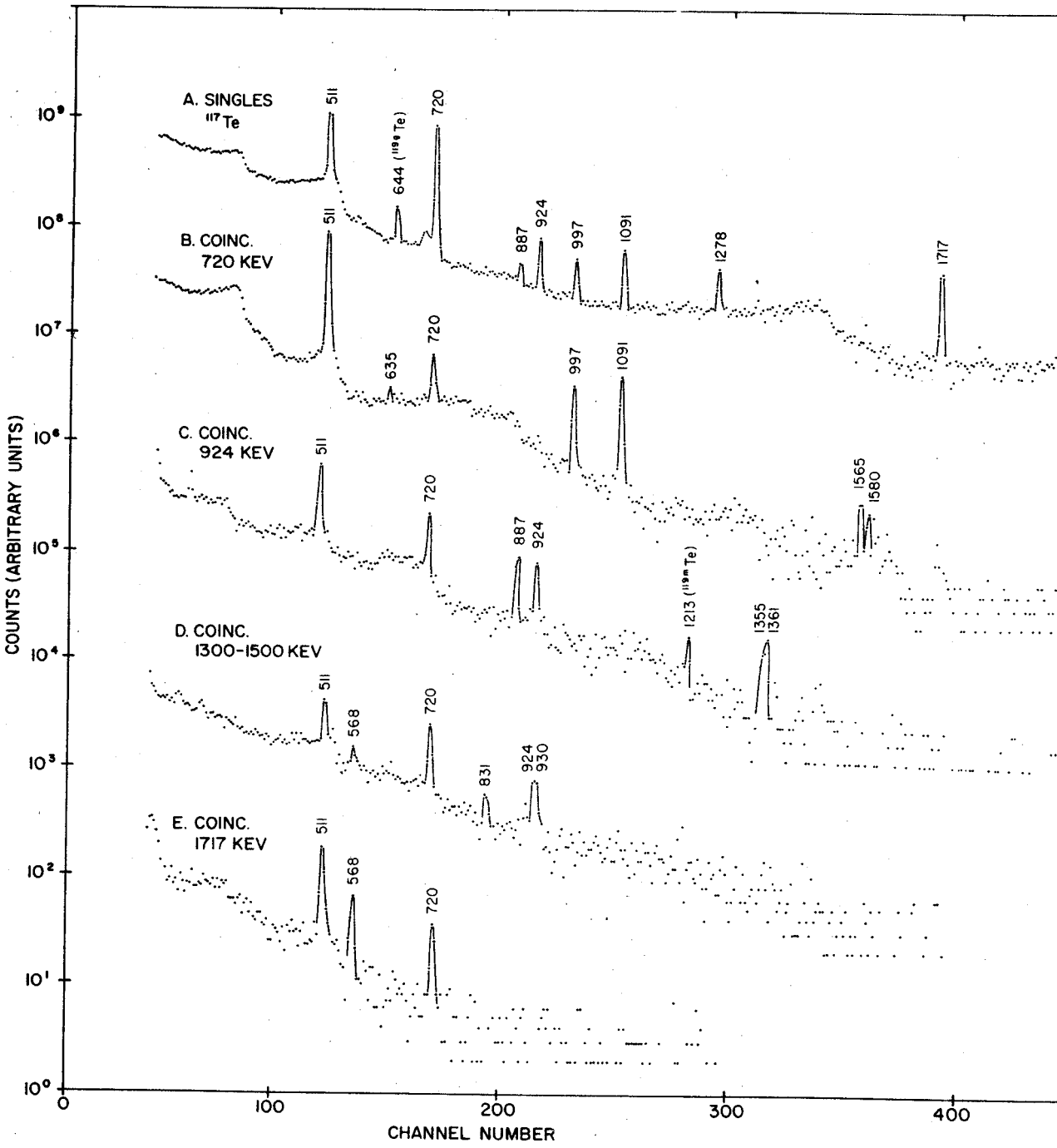


Fig. 26 Coincidence spectra of $^{117}$Te obtained with a 7 cm$^3$ Ge(Li) counter and a 7.6 x 7.6 cm NaI(Tl) crystal.

plots could not be obtained. However, all of the positron endpoint measurements indicated the beta disintegration energy to be 3550±100 keV.

No significant secondary low energy positron groups were observed in any of the coincidence spectra. This is in agreement with the results of the 511-511-gamma triple coincidence experiment shown in Figure 25.

3.2.3.D.--The Proposed Decay Scheme of $^{117g}Te$--Coincidence results, energy sums and relative intensity considerations allow all of the strong transitions (relative intensity >1.0) to be placed unambiguously. The proposed decay scheme, shown in Figure 27, accommodates all of the gamma rays observed in this investigation. It should be stressed, however, that because of the short halflife, a number of the very weak high energy transitions that were observed could not be conclusively assigned to the decay of $^{117g}Te$. Because of the very low count rates, only upper and lower limits of about 2h and 30 min, respectively, can be placed on the halflives of these gamma rays. Of these, the 2380 and 2885 keV lines are the most likely candidates for positions in the $^{119g}Te$ decay scheme-probably as ground state transitions. The other lines, in spite of the poor statistics, appeared to decay with halflives different from 1.1 hours. One contaminant which could definitely be identified was

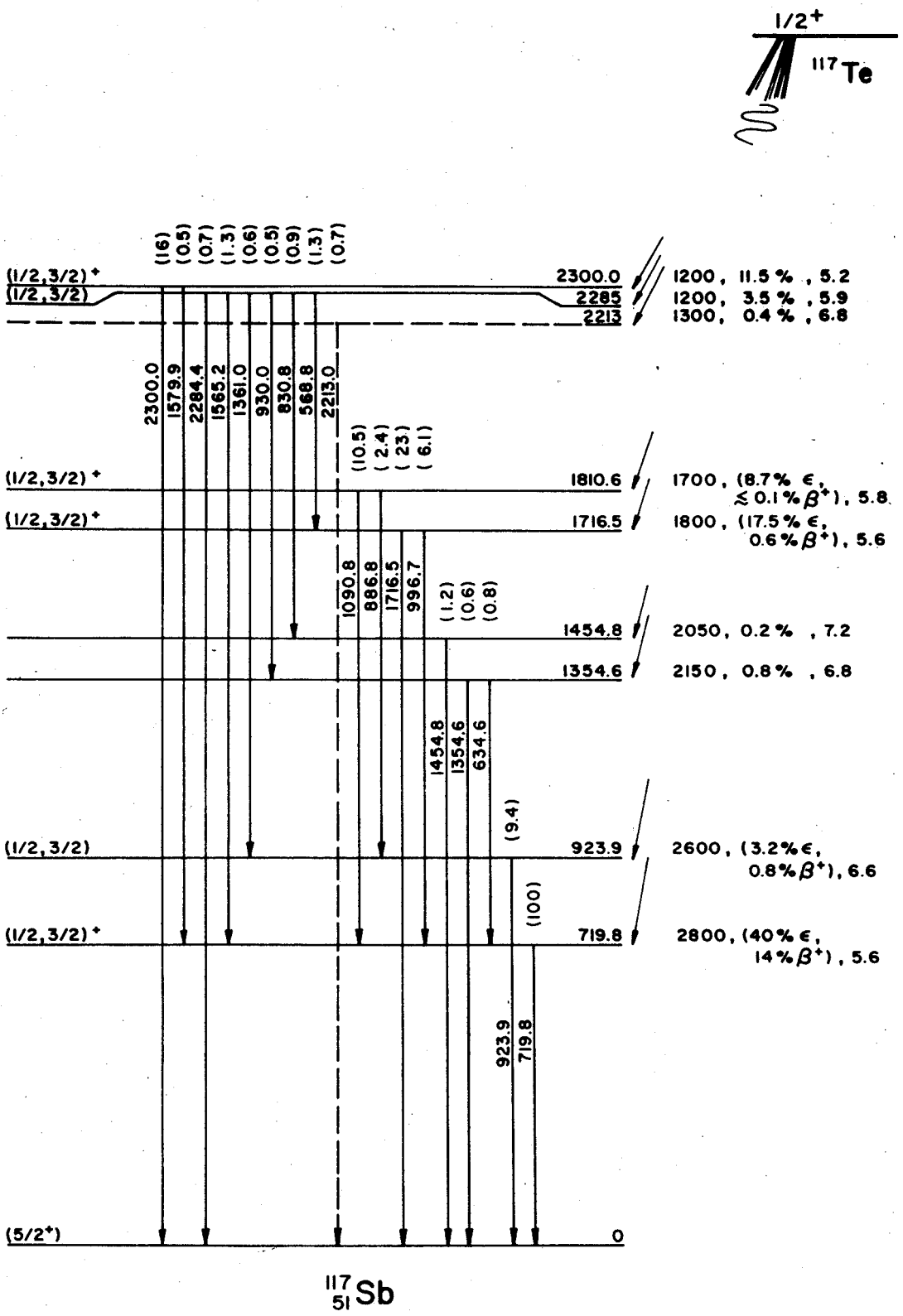


Fig. 27 The proposed decay scheme of $^{117}$Te. Weak transitions of 2380 and 2885 keV, which could not be definitely assigned to the decay of $^{117}$Te, have been omitted.

$^{34}Cl$, small traces of which were always present after rapid chemical separations of the tellurium parents from the $SbCl_3$ targets. Comparison with the $^{34}Cl$ spectrum (62) allowed several of these high energy lines to be discarded.

Three levels that are heavily fed by positrons are indicated at 720, 924, and 1717 keV by the 511-511-gamma coincidence spectrum, Figure 25. The lines at 695 and 1278 keV are assigned as double escape peaks of the 1717 and 2300 keV gamma rays, respectively. That no cascades exist among the 720, 924, and 1717 keV transitions can be seen from spectra taken in coincidence with these regions. In each case, the presence of the other two lines can be accounted for by chance coincidences and underlying Comptons in the gate.

Strong coincidences between the 720 keV region and the 997, 1091, and 1565 keV gamma rays, and between the 924 keV region and the 887, 1355, and 1361 keV lines confirm the 1717 keV level and suggest additional levels at 1811 and 2285 keV. Further evidence for the level at 2285 keV is provided by a 2285 keV transition, by the suggested presence of 924-1361 and 930-1355 keV cascades and by the presence of the 831 keV line in coincidence with the 1455 keV region. The intermediate levels of the above two cascades are placed at 1355 and 1455 keV from relative intensity considerations.

The 1355 keV levels may also depopulate to the 720 keV state as is suggested by the trace of the 635 keV line in coincidence with the 720 keV region. The 1455 keV level has not been found to involve any transitions other than the 831-1455 keV cascade. Some fragmentary evidence has suggested the 1455 keV transition to have a half life that is slightly longer than 1.1hours. However, most of the discrepancy can be accounted for by poor statistics.

Additional coincidence data show the 569 keV transition takes place from the 2285 keV state to the 1717 keV level. The absence of the strong 2300 keV line from the "any-coincidence" spectrum indicates a state at 2300 keV. The 2300 keV state also depopulates to the 720 keV state, as is evidenced by the trace of the weak 1580 keV line in coincidence with the 720 keV region.

No coincidence experiments involving the high energy transitions are feasible at this time. Estimates from singles and coincidence counting rates indicate that at least a 24 hour counting time would be necessary with fresh sources produced at frequent intervals, to obtain conclusive coincidence data for any of the lines above 2300 keV.

A very striking similarity exists between the decay scheme of $^{117}Te$, Figure 27, and that of $^{119g}Te$, Figure 19. A comparison of the two figures shows the

two schemes to be alike in energy level structure and in beta decay branching ratios. This suggests the decay of $^{117}$Te to be that of a low spin parent. The ground state spin of $^{117}$Te is known to be $1/2^+$ from atomic beam measurements (63). If this is indeed the decay of the ground state, then tentative spin and parity assignments can be made for some of the levels on the basis of log ft values. States at 720, 1717, 1811 and 2300 all have $4.0 \leq$ log ft $\leq 5.8$, indicating allowed beta decay (64). Hence, these states should all have positive parity and J = 1/2 or 3/2. Slightly higher log ft values for the remainder of the levels indicate allowed or first forbidden beta transitions, implying J = 1/2, 3/2 for these.

That these assignments for the 720 and 924 keV states are consistent with other data and systematics in this region will be discussed in the following sections.

3.2.3.E.--The Search for $^{117m}$Te.--3.2.3.E.1.--Systematics of Odd A Tellurium and Antimony States.--As shown in Figure 28, excited states of $J = 3/2^+$ and $11/2^-$ can be seen to migrate upward in energy with decreasing neutron number, in $^{125}$Te, $^{123}$Te and $^{121}$Te. Isomeric transitions, originating at the $11/2^-$ states, are known to occur in all three isotopes (15). However, while $^{119m}$Te is known to exist, no isomeric transition

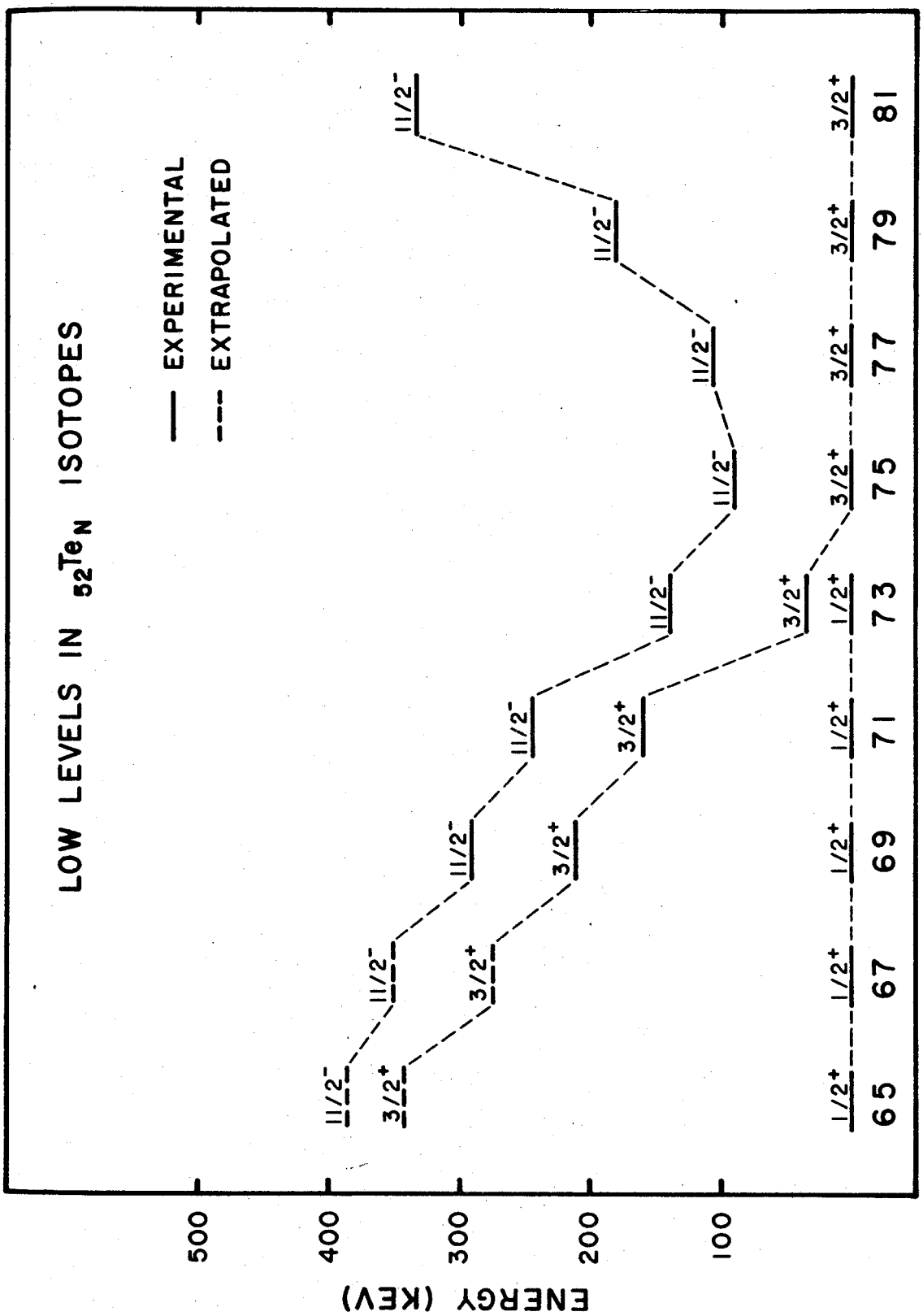


Fig. 28 Low lying levels in $_{52}Te_N$ isotopes. The $3/2^+$ and $11/2^-$ levels for $^{117}Te$ and $^{119}Te$ are located by

has been observed in our study or by other investigations (37, 45).

Two plausible explanations for this phenomenon can be obtained if one relies on the shell model systematics in this region. As can be seen in Figure 28, the separation of the $11/2^-$ and $3/2^+$ levels decreases to less than 100 keV as one approaches $^{119}Te$ from the right. The single particle estimate for M4 transition probabilities of less than 100 keV in energy, indicates a halflife of a few years, much too long to compete with 4.7 day beta decay. In the case of $^{117}Te$, the $3/2^+$ level may be even closer to, or possibly higher than the $11/2^-$ state.

Systematics of antimony levels (15), Figure 29, suggest a $7/2^+$ state at approximately 530 keV in $^{117}Sb$. A state at this energy, tentatively identified as having spin 7/2, has been observed via ($^3He$,d) reactions by Bassani et al (54), Ishimatsu et al. (55), and Barnes et al. (56). Analagous to the decay of $^{121m}Te$ and $^{119m}Te$, $^{117m}Te$ should decay via a first-forbidden unique beta branch to the 530 keV $7/2^+$ state in $^{117}Sb$ with a partial halflife of several days. However, this may be much too slow to compete with allowed or other first-forbidden beta groups which are expected to be present from systematics and the large decay energy. Especially if, as in $^{119}Sb$, high spin negative parity states are present, the beta decay process could be very rapid.

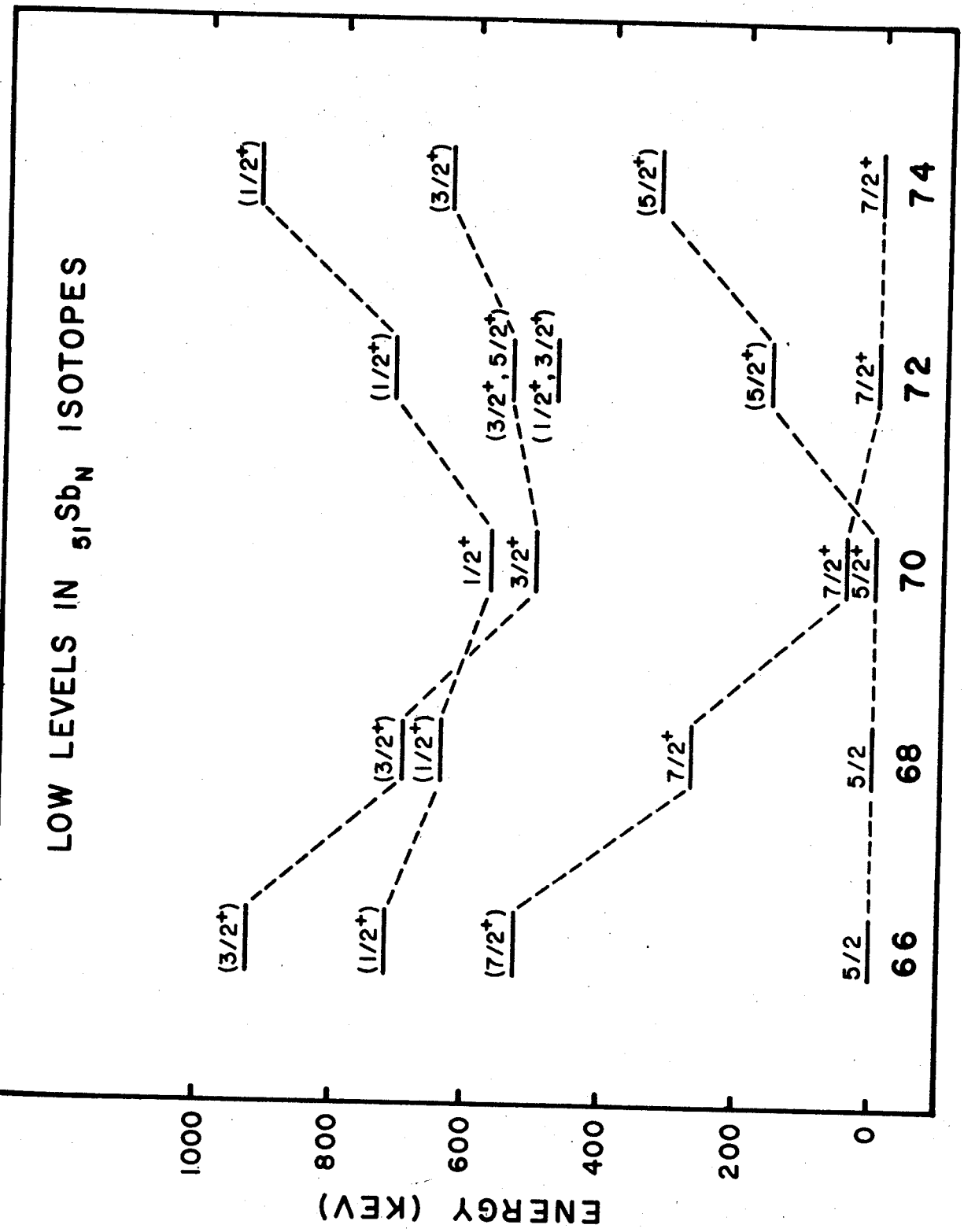


Fig. 29 Low lying levels in $_{51}Sb_N$ isotopes as observed in β-γ decay (9,45) and $^3$He,d) and (d,d') experiments

An alternative explanation for the absence of an identifiable $^{117m}$Te activity can be sought from the case of $^{115}$Te. A 275 keV M3 transition in $^{115}$Te has been reported to have a halflife of approximately 0.1 sec., suggesting a $7/2^+$ excited state (65,66). Hence it is possible that a $7/2^+$ level may exist below the $11/2^-$ state in $^{117}$Te, making deexcitation of the $11/2^-$ state comparatively rapid.

3.2.3.E.2.--Experimental Results.--Attempts to identify an isomeric activity $^{117m}$Te were primarily based on a search for a 530 keV gamma ray depopulating a spin $7/2^+$ state of this energy as predicted from systematics and observed via ($^3$He,d) reactions (54-56). First, no evidence was observed for any gamma ray activity having a halflife longer than about 2 minutes but shorter than 1 hour.

Second, a thin target of antimony metal was bombarded to produce the highest available ratio of $^{117}$Te to $^{119}$Te. The chemically extracted activities were followed for several days. A very weak, but unquestionable, peak at 530 keV became evident as the 16h $^{119g}$Te activity decayed away. Since this line was present in a spectrum recorded immediately after subsequent specific tellurium chemistry, it must be associated with the decay of some tellurium parent.

Third, a search was made for the 2.5h daughter of $^{117}Te$. The antimony daughters of $^{118}Te$ and $^{119}Te$ were periodically extracted from the source, but the prominent 160 keV transition in the decay of $^{117}Sb$ could not be identified in the samples. However, the amount of activity expected was extremely small, and could have been masked by the presence of small amounts of $^{119}Te$ impurity.

Fourth, assuming that any $^{117m}Te$ would be produced in approximately the same ratio to $^{117g}Te$ as $^{119m}Te$ is produced to $^{119g}Te$, a far greater amount of the 530 keV gamma activity should have been present if this transition does indeed originate from $^{117m}Te$. Also, because of the large beta disintegration energy, a far richer gamma ray spectrum can be anticipated. That most of the beta decay of $^{117m}Te$ would go directly to the ground state of $^{117}Sb$ (third order forbidden transtion) is very unlikely on the basis of systematics in this region.

Hence, while the existence of an isomeric state $^{117m}Te$, with an appreciable halflife, cannot be definitely excluded, it is suggested to be very unlikely. The fact that the 530 keV gamma ray is associated with a tellurium parent, or with an activity which survives specific tellurium chemistry, remains at present, a mystery. The resolution of this problem is complicated by the very low intensity of this gamma ray relative to the gamma rays of $^{119m}Te$, which are always present as contaminant.

# CHAPTER IV

# DISCUSSION OF RESULTS

Because beta and subsequent gamma decay populate only a limited set of energy levels, only a limited amount of information can be obtained from beta and gamma spectroscopy experiments. Hence it is very difficult to present a complete and fair test for nuclear models from these experiments alone. In the case of the antimony isotopes, additional information has been obtained from ($^3$He,d) experiments. Wherever possible, these results are compared to those of our investigation. Then the two sets are combined in order to make some qualitative comparisons with theoretical calculations.

## 4.1. Comparisons with Reaction Studies and Identifications of Some Corresponding States

As of this writing, at least three independent sets of different experiments have been performed to investigate the levels of odd mass antimony isotopes via the ($^3$He,d) reaction (54-56). Because of a larger experimental uncertainty in the reaction energy measurements, some quantitative discrepancies with respect to results of the gamma decay data exist in the level energies. However, several states can be identified as being common to the ($^3$He,d) results and

to the gamma ray studies. Also a number of levels exist which were populated in only one of the two types of experiments. In some cases this uniqueness can suggest possible spin values for the level.

A comparison of the various states observed in our investigation with those populated in ($^{3}$He,d) experiments is shown in Tables 14 and 15 and Figures 30 and 31 for $^{119}$Sb and $^{117}$Sb. Table 14 and Figure 30, also include states observed by Graefee et al. (45) in a recent high resolution gamma ray investigation of $^{119}$Sb. It can be seen that the results of the two independent gamma ray studies are in excellent agreement.

No published reaction data exist for the case of $^{129}$I. Hence, any discussion of this isotope must be confined to levels populated by beta decay.

From existing data, some corresponding levels can be identified in $^{117}$Sb, $^{119}$Sb and $^{121}$Sb. These states and some of their properties are listed in Table 16. The lowest of those states which have been tentatively assigned as having spin 1/2 and 3/2 have also been observed in the previously mentioned ($^{3}$He,d) reaction experiments. The 7/2+ and 5/2+ states have also been identified in the ($^{3}$He,d) reactions and in the beta decay of $^{119m}$Te and $^{121m}$Te. However, as already discussed in Section 2.3.E of Chapter III, the 7/2+ state could not be established conclusively as being present in the decay

Table 14.--Experimentally observed energy states in $^{119}Sb$.

| Present Investigation | Graeffe et al.[a] | Barnes et al.[b] | Ishimatsu et al.[c] | Bassani et al.[d] |
|---|---|---|---|---|
| ($\beta$-$\gamma$ decay) | ($\beta$-$\gamma$,d) | ($^3$He,d) | ($^3$He, d) | ($^3$He, d) |
| 0.2703 | 0.2706 | 0.261 | 0.27 | 0.268 |
| | | 0.385 | | |
| 0.6441 | 0.6443 | 0.635 | 0.66 | 0.604 |
| 0.6996 | 0.7000 | 0.695 | 0.71 | 0.668 |
| 1.0481 | 1.0483 | | | |
| 1.2126 | 1.2127 | | | |
| 1.249 | 1.2496 | | | |
| 1.328 | | | | 1.315 |
| 1.338 | 1.3385 | 1.335 | | |
| 1.3658 | 1.3658 | | 1.37 | 1.370 |
| 1.407 | 1.4066 | | | |
| | | 1.460 | | |
| 1.487 | 1.4874 | | 1.49 | |
| | | 1.640 | | |
| 1.7491 | 1.7495 | | | |
| 1.820 | 1.8222 | 1.830 | | 1.808 |
| | | 1.950 | | |
| | | 2.075 | | |
| 2.129 | 2.1293 | | | 2.118 |
| 2.225 | 2.2260 | 2.215 | | |
| 2.278 | 2.2778 | 2.280 | | 2.264 |
| 2.283 | 2.2836 | | | |
| 2.360 | 2.3603 | 2.355 | | 2.346 |
| | | 2.545 | | |
| | | | | 2.702 |
| | | | | 2.776 |

[a]Reference 45.

[b]Reference 56.

[c]Reference 55.

[d]Reference 54.

Table 15.--Experimentally observed states in $^{117}Sb$.

| Present Investigation | Barnes et al.[a] | Ishimatsu et al.[b] | Bassani et al.[c] |
|---|---|---|---|
| ($\beta$-$\gamma$ decay) | ($^3$He,d) | ($^3$He, d) | ($^3$He, d) |
| | 0.530 | 0.52 | 0.530 |
| 0.7198 | 0.725 | 0.72 | 0.700 |
| 0.9239 | 0.941 | 0.92 | 0.915 |
| | 1.337 | 1.32 | 1.328 |
| 1.355 | | | |
| | 1.389 | 1.38 | |
| 1.455 | | 1.47 | |
| | 1.570 | | |
| | 1.681 | | |
| 1.7165 | | | |
| 1.8106 | | 1.79 | 1.778 |
| | | 1.99 | 1.840 |
| | | 2.14 | 2.172 |
| (2.213) | 2.24 | 2.21 | 2.244 |
| 2.285 | | 2.28 | |
| 2.300 | 2.320 | | |
| (2.380) | | | |
| | 2.443 | 2.41 | |
| | 2.502 | 2.52 | |
| | 2.562 | | |
| | 2.629 | 2.61 | |
| (2.885) | | 2.88 | |
| | | 2.98 | |

[a] Reference 56.

[b] Reference 55.

[c] Reference 54.

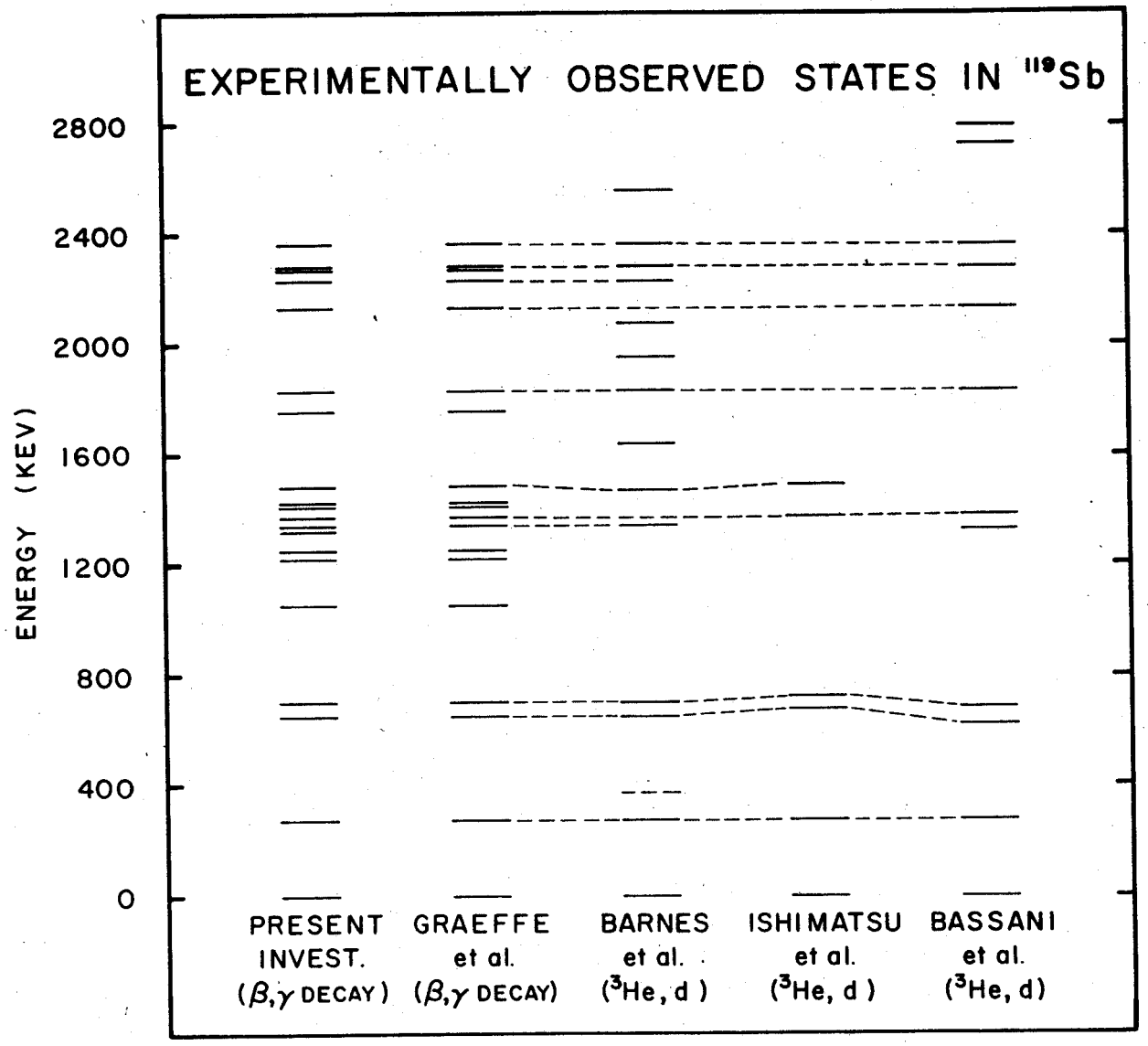


Fig. 30 Comparison of levels in $^{119}Sb$ populated by beta decay to those observed in ($^{3}He$,d) reactions (54-56). The two sets of β-γ levels were established independently and at about the same time. Both sets are shown for confirmation. Where possible, corresponding levels have been suggested.

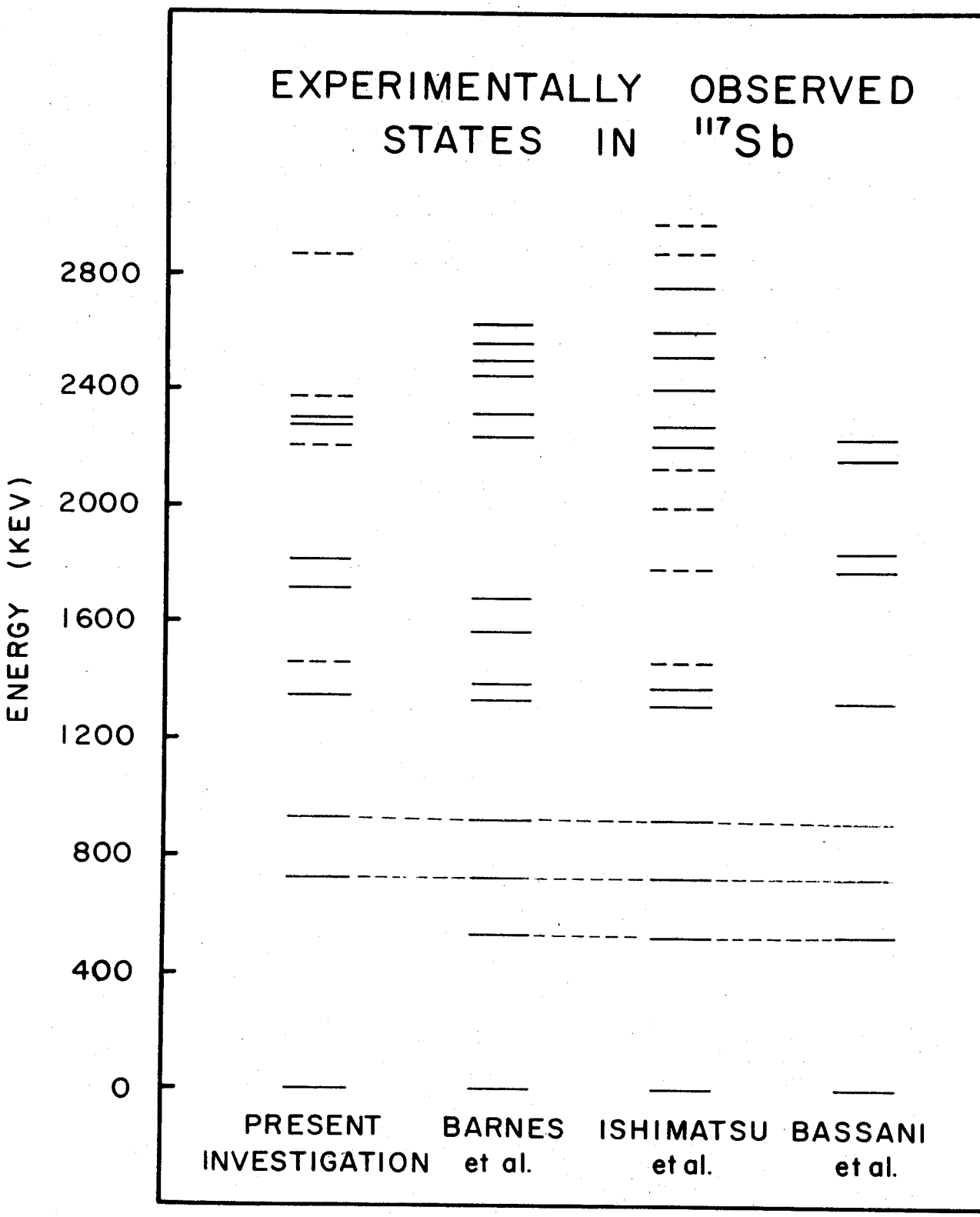


Fig. 31 Comparison of $^{117}Sb$ levels populated by beta decay to those observed in ($^{3}He$,d) reactions (54-56). The $\beta$-$\gamma$ set is less complete than that for $^{119}Sb$ because of the absence of an identifiable isomeric decay $^{117m}Te$.

Table 16.-- Properties of similar states in odd mass antimony isotopes.

| Isotope[a] | Tentative Spin | Energy (keV) | log ft | Fractional decay to[b] $1/2^+$ | $3/2^+$ | $5/2^+$ |
|---|---|---|---|---|---|---|
| 117 | $1/2^+$ | 720 | 5.6 | - | - | 1.0 |
| 119 | $1/2^+$ | 644 | 5.5 | - | - | 1.0 |
| 121 | $1/2^+$ | 573 | 6.3 | - | 0 | 1.0 |
| 117 | $3/2^+$ | 924 | 6.6 | 0 | - | 1.0 |
| 119 | $3/2^+$ | 700 | 6.6 | 0 | - | 1.0 |
| 121 | $3/2^+$ | 508 | 7.0 | - | - | 1.0 |
| 117 | $1/2^+,3/2^+$ | 1717 | 5.6 | 0.21 | 0 | 0.79 |
| 119 | $1/2^+,3/2^+$ | 1749 | 6.1 | 0.17 | 0 | 0.83 |
| 117 | $1/2^+,3/2^+$ | 1811 | 5.8 | 0.70 | 0.30 | 0 |
| 119 | $1/2^+,3/2^+$ | 1820 | 6.4 | 0.63 | 0.37 | 0 |

[a]Values for $^{121}$Sb taken from Reference 9.

[b]Normalized to 1.0 for total gamma decay of level.

[c]Dash (-) indicates decay energetically not possible.

of a possible $^{117m}$Sb to $^{125}$Sb, as can be seen in Figure 29. In fact, if a least squares parabola is fitted to the energies of these states, relative to a state with a given spin, as for example the 5/2+, the points typically deviate by less than 1% from the curve. A similar situation holds in the case of the odd mass iodine isotopes. No theoretical explanation of this phenomenon is available at present. Attempts to correlate it with the parabolic dependence of semi-empirical mass formulas have not proven very satisfactory.

The two levels in the 1700 and 1800 keV region can be compared for $^{117}$Sb and $^{119}$Sb. From the similar energies, log ft values, and decay branches to other levels it appears very likely that the 1717, 1811 and the 1749, 1820 keV pairs represent analagous states in $^{117}$Sb and $^{119}$Sb, respectively. It appears that an 1800 keV state may also have been excited in some of the ($^{3}$He,d) experiments.

Similar considerations can be applied to properties of several states in the odd mass iodine isotopes. These states are listed in Table 17. In this case, however, the decay properties do not allow as sharp a correspondence to be made as was possible for the antimony isotopes. It should be noted that some of the differences in the decay branches may be attributable to differences in energetics.

Table 17.--Properties of similar states in odd mass iodine isotopes.

| Isotope[a] | Tentative Spin | Energy (keV) | log ft | Fractional decay to[b,c] $7/2^+$ | $5/2^+$ | $3/2^+$ |
|---|---|---|---|---|---|---|
| 125 | $3/2^+$ | 188 | 6.3[d] | 0.02 | 0.98 | - |
| 127 | $3/2^+$ | 203 | 10.2 | 0.09 | 0.91 | - |
| 129 | $3/2^+$ | 278 | 7.5 | 0.61 | 0.39 | - |
| 131 | $3/2^+$ | 493 | $\geq 7.5$ | 0.87 | 0.13 | - |
| 125 | $5/2^+$ | 372 | | 0 | 1.0 | 0 |
| 127 | $5/2^+$ | 417 | 7.0 | 0.12 | 0.85 | 0.03 |
| 129 | $5/2^+$ | 488 | 6.1 | 0.15 | 0.82 | 0.025 |
| 131 | $5/2^+$ | 603 | 6.2 | 0.20 | 0.80 | 0 |
| 127 | $11/2^+ 9/2^+ 7/2^+$ | 715 | 8.9 | 1.0 | 0 | 0 |
| 129 | $11/2^+ 9/2^+$ | 696 | 9.3 | 1.0 | 0 | 0 |
| 131 | $11/2^+ 9/2^+$ | 774 | 9.0 | 1.0 | 0 | 0 |
| 127 | $9/2^+ 7/2^+$ | 649 | 10.7 | 1.0 | 0 | 0 |
| 129 | $9/2^+ 7/2^+$ | 730 | 9.8 | 1.0 | 0 | 0 |
| 131 | $11/2^+ 9/2^+$ | 852 | 9.5 | 1.0 | 0 | 0 |

[a] Values for $^{125}I$, $^{127}I$ and $^{131}I$ taken from Reference 67, 10, and 11, respectively.

[b] Normalized to 1.0 for total decay from level.

[c] Dash (-) indicates decay energetically not possible.

[d] Estimated from data given in References 15 and 67.

## 4.2 Comparison with the Core-coupling Model

Some qualitative agreement with the core-coupling model can be found for the case of $^{119}$Sb and $^{129}$I. Detailed comparisons with existing calculations, however, indicate large quantitative discrepancies. The comparison has not been extended to $^{117}$Sb primarily for two reasons. First, only low spin states have been experimentally observed in beta and gamma decay studies. Second, although a few other states have been populated via ($^{3}$He,d) reactions, (54-56) the ranges of spins of these are still unknown.

### 4.2.1. Levels in $^{119}$Sb

As shown in Figures 19 and 20, the excited states of $^{119}$Sb, or at least those populated in beta decay, occur in two reasonably well-defined bands. The band in the region of ≈ 1.2 MeV could conveniently be interpreted as being due to a coupling between one phonon and the $5/2^+$ and $7/2^+$ single particle states. The first excited $2^+$ state which is pictured as being due to a one phonon vibration in $^{118}$Sn, which could be considered as the even-even core for $^{119}$Sb, occurs at 1230 keV. It should be noted that the 1366 keV state in $^{119}$Sb has been shown to have $J^\pi$ $11/2^-$, and, because of the negative parity, may arise from mechanisms other than the quadrupole phonon and the $d_{5/2}$ or $g_{7/2}$ single particle state coupling considered here. From its

presence in ($^{3}$He,d) spectra, and from the absence of other known negative parity states in this region, it is tempting to consider this level to be an $h_{11/2}$ single particle state. Additional support for this interpretation is provided by the strong beta decay branch to this level, which is not inconsistent with an $h_{11/2}$ neutron changing to an $h_{11/2}$ proton.

The remainder of the states in the 1000-1500 keV region could then be interpreted as due to the $5/2^+$ and $7/2^+$ ground and 1st excited states coupling with a $2^+$ phonon. Because the 1213 and the 1048 keV states depopulate primarily to the ground $5/2^+$ while the 1407 and 1249 decay to the 270 keV $7/2^+$ state, it is tempting to assign these pairs as the $9/2^+$ and $7/2^+$ members of the respective coupling multiplets. Four states, each of spin 1/2 or 3/2, exist in the 1328-1487 keV range. These could conveniently supply the remaining low spin members of these multiplets. However, the level order would be different from that calculated by Choudhury (62) for the $5/2^+$ single particle case. The missing $5/2^+$ states are not expected to be populated significantly by direct beta decay, since these would require second and third order forbidden transitions from $^{119g}$Te and $^{119m}$Te, respectively.

Assuming that the $5/2^+$ states, if they exist, would occur in this approximate energy range, one can

easily construct two multiplets whose centers of gravity come about 1100-1200 keV above the 270 keV and ground states, respectively. Comparison with the 1230 keV energy of the first $2^+$ state in $^{118}Sn$ shows this to be in agreement with the Lawson and Uretsky center of gravity theorem (18) as interpreted by deShalit (2). Construction of tentative partial multiplets in the 2100-2400 keV region, which is approximately at twice the energy of the one phonon bands, gives further support for a phonon-particle interpretation.

A particle-phonon coupling interpretation of this nature is also supported by the reaction data (54-56). Very weak excitation of states in the 1 MeV region was observed by all investigators, suggesting little single particle character for most of these levels. Inelastic scattering experiments (56) with heavy ions have suggested a collective nature for states in this energy range in neighboring $^{121}Sb$ and $^{123}Sb$. Results of DWBA calculations (54) are in agreement with observed cross sections for the $5/2^+$ and $7/2^+$ states, but are progressively too large (with increasing mass number) for the $1/2^+$ and $3/2^+$ levels. This suggests that while all four of these states may be primarily of single particle character, the single particle component in the wave functions for the $1/2^+$ and $3/2^+$ levels decreases as more neutrons are added. It has

been pointed out (56) that the wave functions for the $5/2^+$ and $7/2^+$ levels probably contain large $d_{5/2}$ and $g_{7/2}$ components. The other states in the 1.5-2.5 MeV range and the low lying $1/2^+$ and $3/2^+$ levels, which have been strongly excited in ($^3$He,d) reactions, then would have appreciable $s_{1/2}$ and $d_{3/2}$ components in their wave functions.

Despite the good qualitative agreement which can be forced between experimental results and the core-particle coupling theory, incompleteness and inadequacies in the naive formulation of the theory are readily apparent. First, because of rapid phonon de-excitations, there should exist very little cross-talk between multiplets built on the $5/2^+$ and those built on the $7/2^+$ states. Experimental evidence contradicts this. Not only do several states in the first band decay to both the $7/2^+$ and the $5/2^+$ levels, but also several states in the second band each de-excite to both sets of one phonon multiplets with comparable intensity.

Next, the transitions of 2013 and 2089 keV bypass the one phonon multiplet. Crossover transitions of this nature are forbidden, as they would correspond to a simultaneous two phonon de-excitation. However, crossover transitions of this type have been observed in nearby even-even nuclei (15), such as $^{116}$Sn (31), placing additional limitations on the surface vibration description of even-even nuclei.

Furthermore, states of spin $5/2^+$ in the one phonon multiplets should be populated, if not by direct beta decay, then at least by E2 transitions from $7/2^+$ and $9/2^+$ states in the second band.

The levels at 644, 700, 1749, and 1810 keV were excluded from the above beta-gamma decay considerations in order to construct, in the absence of any specific calculations, the simplest sets of multiplets giving the best qualitative agreement with the core-coupling theory. It is quite possible that these four states may also be levels belonging to the coupling multiplets, in which case there would be appreciable splitting of the coupled levels. Similarly, it is also possible that several of the low spin states in the 1400 keV range arise from particle-two phonon couplings. Even if this is the case, the preceeding qualitative arguments for (and against) the core-coupling model are only slightly affected.

As already mentioned, the calculation by Choudhury (5) for a $5/2^+$ particle-one phonon coupling gives an energy level order which is very unlikely on the basis of known levels. A second calculation, performed by Pashkevich and Sardaryan (23), applies the strong coupling treatment to $^{119}$Sb. Reasonably good agreement exists for the energies of the 270, 644, 700, and possibly the 1487 keV states. However, very large quantitative discrepancies in energy prevent any

one to one correspondences to be drawn between calculation and experiment for any of the other states.

### 4.2.2. Levels in $^{129}I$

In the case of $^{129}I$, calculations of the energies of the status have been performed by Banerjee and Gupta (3) and more recently by O'Dwyer and Choudhury (4). The results of the latter of these and of the Kisslinger-Sorensen calculations (6) are compared with experimental results in Figure 32. Neither type of calculation yields energy levels which are in particularly good quantitative agreement with the experimental values. However, when trends of levels are considered across $^{127}I$, $^{129}I$, and $^{131}I$, the calculations leave a much more favorable impression. The results of O'Dwyer *et al.* instead of Banerjee *et al.* were used because of better agreement with experiment.

Comparisons in regard to transition rates could be made with the work of O'Dwyer *et al.* (4) only since numerical results from the other calculations were not available. In the few cases where correspondences between levels could be made, and relative partial halflives compared, there was notably poor agreement. Discrepancies were as large as a few orders of magnitude.

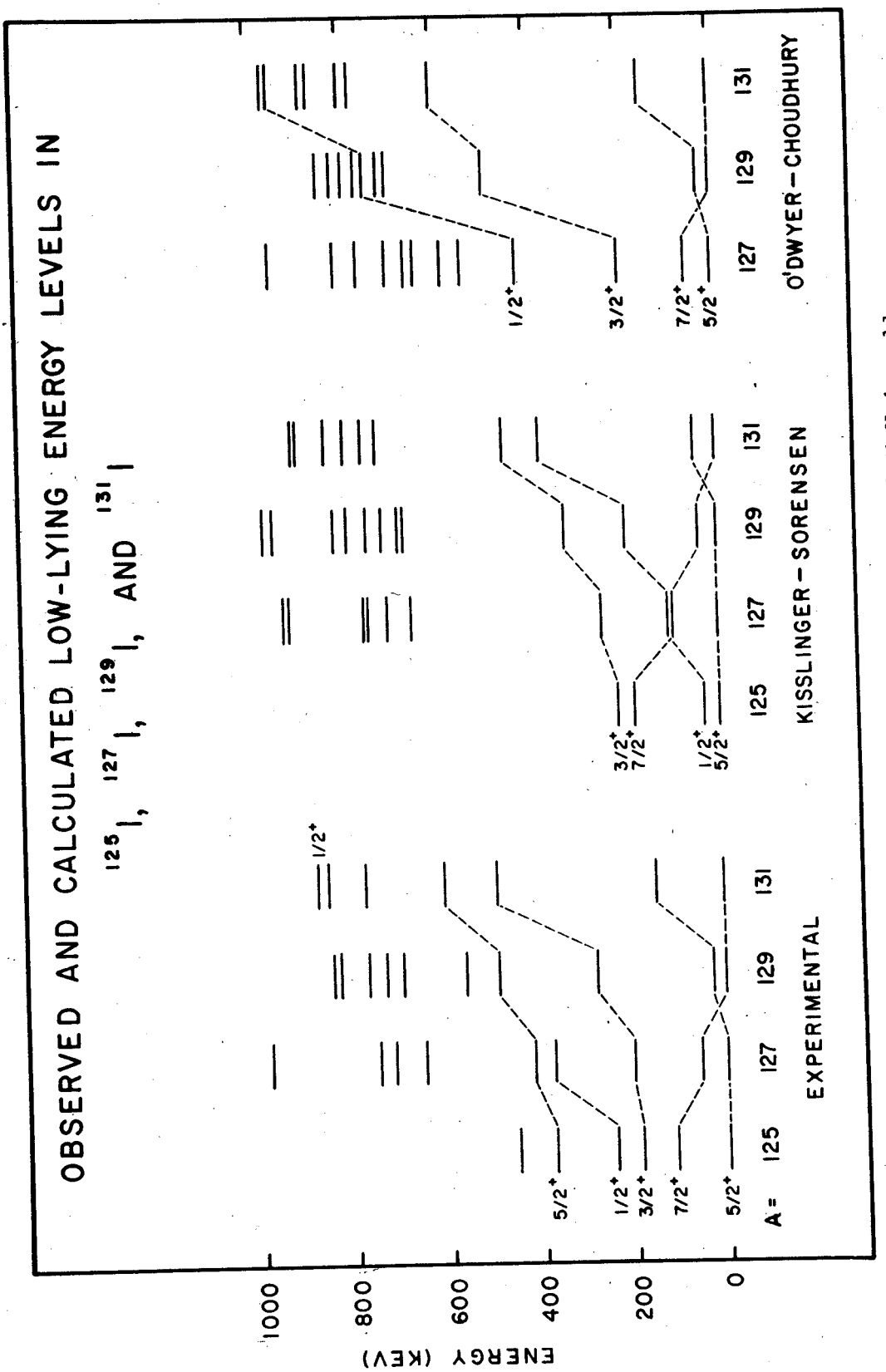


Fig. 32 A comparison of energy levels below 1 MeV in odd mass iodine isotopes. The states calculated by Kisslinger and Sorensen (6) and those calculated by O'Dwyer and Choudhury (4) are compared to experimentally observed levels. (Numerical K-S values for 125I were available for the low states only.)

It should be noted that since the iodine nucleus consists of Z = 50 + 3 protons, compared to Z = 50 + 1 for the case of antimony, greater difficulty can be anticipated in treating iodine in the weak coupling scheme. Furthermore, if the adjacent even-even tellurium nucleus is considered to be the core, then the much lower phonon energies (15) can be expected to add to the complexity in interpreting the level structure. Additional complications may be expected if one assumes that the three protons may couple according to schemes different from a zero-spin pair plus an odd proton.

## 4.3. Comparison with Pairing and Quadrupole Interaction Calculations

The Kisslinger-Sorensen calculation (6) for the odd mass antimony and iodine isotopes shows some good agreement with experimental measurements with respect to relative motion of some low lying energy levels. In this calculation, the single particle energies for the $g_{7/2}$, $d_{5/2}$, $h_{11/2}$, $d_{3/2}$, and $s_{1/2}$ states were chosen as existing at 0.26, 0.78, 2.29, 3.45, and 3.59 MeV, respectively, for mass number 115. A smooth A dependence, with two correction terms, was assigned to each of these values. The first of these correction terms is dependent upon the $\ell$-value of the shell model state as well as upon the mass number of the

nucleus. A second correction term is introduced as "a special N or Z dependent shift." Values of the other parameters such as $\lambda$,$\Delta$ and the quadrupole coupling constants are tabulated in Reference 6.

The set of low energy levels obtained in this calculation is shown in Figures 32 and 33 for the odd mass iodine and antimony isotopes, respectively. Both sets of calculated levels show impressive agreement with experimental data, shown in the same figures, when one compares the motion of the states with mass number. However, numerical discrepancies are evident. Also, the crossing of pairs of levels, such as the $7/2^+$ and the $5/2^+$ in both the antimonies and the iodines, is slightly in error.

The spin values of most of the higher excited states are not known well enough to allow similar comparisons to be drawn among these levels over several isotopes. Hence, the comparisons are limited to the low energy states only.

Electromagnetic transition probabilities can be calculated as in Section 1.5.2, with the matrix elements taken between the appropriate states. Because of phonon admixtures in many of the wave functions, the E2 transition rates are expected to be enhanced. A striking example of this is the 942 keV M1 + E2 transition between the 1213 and 270 keV states in $^{119}$Sb.

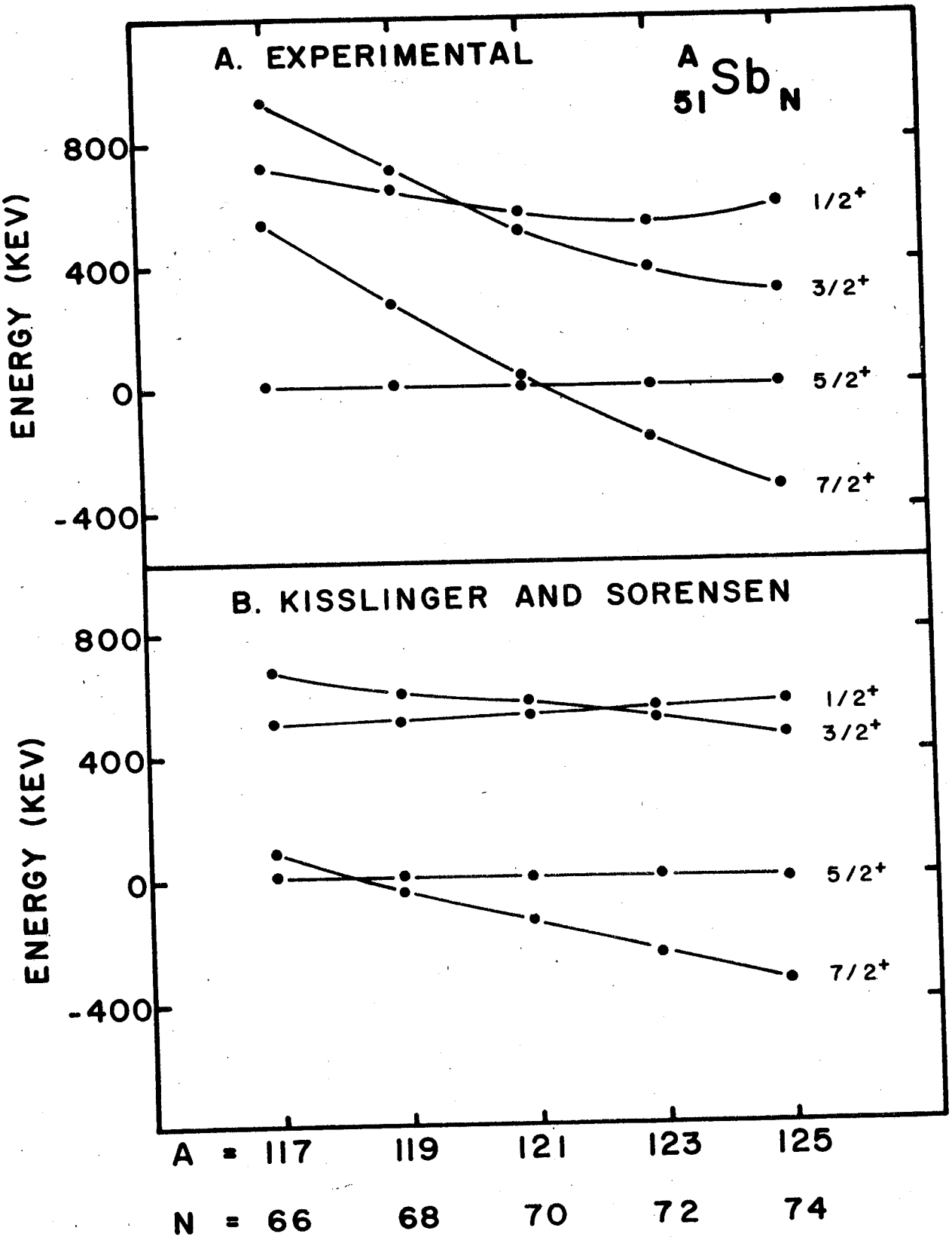


Fig. 33 A comparison of the observed low lying energy levels in the odd mass antimony isotopes with the values calculated by Kisslinger and Sorensen (6).

The angular correlation studies indicate a very large E2 component, suggesting a considerable one phonon component in both of the states involved. This is not unexpected for the 1213 keV level, but is somewhat surprising for the 270 keV state. However, the calculation does show the 270 keV state to have an appreciable one-phonon admixture.

The large phonon admixture can also be used to explain a hindrance in beta decay to certain states. This was first noted by Walters et al. (68) for the case of $^{131g}Te \longrightarrow {}^{131}I$ and later for other iodine isotopes (10, 49). The hindrance can be explained by the presence of a large phonon component in the wave functions for the daughter nuclei. In particular, the $3/2^+$ state in iodine isotopes is populated by the beta decay of a $3/2^+$ tellurium parent. The experimental log ft values are 10.2, 7.5, and $\geq$ 7.5 for $^{127}I$, $^{129}I$ and $^{131}I$, respectively. These values are much higher than would be expected for an allowed beta transition between two single particle states. A large phonon component has been predicted for these states by the Kisslinger-Sorenson calculation. However, the same approach encounters difficulty when the second $5/2^+$ state is considered.

# CHAPTER V

## CONCLUSIONS

Appreciable progress has been made in the effort to obtain information about systematic behavior of nuclei in the tin region. The new and powerful techniques of high resolution gamma ray spectroscopy, including accurate energy measurements, high resolution coincidence studies, and to some extent high resolution angular correlation measurements, have made possible the construction of more complete and less ambiguous decay schemes than was possible previously with scintillation counters alone.

One measure of the success of this investigation, and investigations in other laboratories, has been the identification of systematic motion in energy of several low lying states in both the odd mass antimony and the odd mass iodine isotopes. From the comparison of relative positions in the decay scheme and from comparisons of other properties such as log (ft) values and relative transition probabilities to other levels, it has also been possible to identify a few corresponding higher energy states in neighboring isotopes. However, in general, these correspondences are not as clearly defined because of the absence of

definite spin assignments and because of the greater density of states at higher energies. Information about spins and mixing ratios should become more readily available as more angular correlation studies are performed with large volume Ge(Li) detectors.

It is readily apparent that, despite the wealth of accurate information which can be obtained, studies of gamma rays emitted following beta disintegration must be complemented by other types of experiments. As a specific example, comparisons of levels above 1200 keV can not be extended to $^{121}$Sb because of the low beta decay energy. As a second example, high spin states in $^{117}$Sb could not be observed because of the apparent absence of a high spin isomer $^{117m}$Te.

Although recent ($^{3}$He,d) experiments have provided some additional information in this region, more experiments such as other types of pickup or stripping, reaction-gamma, and Coulomb excitation are needed to complement beta-gamma studies. Unfortunately not all of these experiments are feasible for each nucleus.

Based on gamma ray and ($^{3}$He,d) studies alone, limited comparisons with the current nuclear models can be made. The agreement appears to be somewhat better with the pairing plus quadrupole interaction calculations than with the core-coupling model. This should not be unexpected. Since more empirical parameters are used

in the pairing plus quadrupole approach, better fits to data can be anticipated. However, the large region over which this model qualitatively fits the experimental results lends strong support for this type of interaction to have some validity.

On the other hand, the core-coupling model can not be rejected completely. As has already been pointed out, a considerable amount of empirical information can be qualitatively explained with this model. It is conceivable that a refinement in the approximations used could bring calculations more in line with experiment.

# BIBLIOGRAPHY

BIBLIOGRAPHY


1. Preston, M. A. Physics of the Nucleus. Reading, Mass: Addison-Wesley Publishing Company Inc., 1963.

2. deShalit, A. Phys. Rev. 122 (1961), 1530.

3. Banerjee, B., and Gupta, K. K. Nucl. Phys. 30 (1962), 227.

4. O'Dwyer, T. F., and Choudhury, D. C. Bul. Am. Phys. Soc. 11 (1966) 321, and private communication.

5. Choudhury, D. C., K. Danske Vidensk. Selsk. mat.-fys. 28 (1954), No. 4.

6. Kisslinger, L. S., and Sorensen, R. A. Revs. of Mod. Phys. 35 (1963), 853.

7. Auble, R. L., and Kelly, W. H. Nucl. Phys. 79 (1966), 577.

8. Auble, R. L., and Kelly, W. H. Nucl. Phys. 81 (1966), 442.

9. Auble, R. L., Kelly, W. H., and Bolotin, H. H. Nucl. Phys. 58 (1964), 337.

10. Auble, R. L., and Kelly, W. H. Nucl. Phys. 73 (1965), 25.

11. Beyer, L. M., Berzins, G., and Kelly, W. H. Nucl. Phys., A93 (1967), 436.

12. Mayer, M. G., and Jensen, J. D. H. Elementary Theory of Nuclear Shell Structure. New York: John Wiley & Sons, Inc., 1955.

13. Mayer, M. G. Phys. Rev. 75 (1949), 1969.

14. Haxel, O., Jensen, J. H. D., and Suess, H. E. Phys. Rev. 75 (1949), 1766.

15. Nuclear Data Sheets. Washington, D. C.: The National Academy of Sciences-National Research Council.

16. Bohr, A., K. Danske, Vidensk. Selsk. mat.-fys. Medd. 26 (1952), No. 14.

17. Bohr, A., and Mottelson, B. R. K. Danske Vidensk. Selsk. mat.-fys. Medd. 29 (1955), No. 16.

18. Lawson, R. D., and Uretsky, J. L. Phys. Rev. 108 (1957), 1300.

19. Silverberg, L. Ark. Fys. 20 (1961), 341.

20. Nillson, S. G., K. Danske Vidensk. Selsk. mat.-fys. Medd. 26 (1952), No. 14.

Nillson, S. G., K. Danske Vidensk. Selsk. mat.-fys. Medd. 29 (1955), No. 16.

21. Newton, T. D. Canad. J. Phys. 38 (1960), 700.

22. Davydov, A. S. Bul. Acad. Sci. USSR, 28 (1964), 1476, and references cited therein.

23. Pashkevich, V. V., and Sardaryan, R. A. Nucl. Phys. 65 (1965), 401.

24. Goulding, F. S. UCRL-16231.

25. Ewan, G. T., and Tavendale, A. J. Canad. J. Phys. 42 (1964), 2286.

26. Auble, R. L., Beery, D. B., Berzins, G., Beyer, L. M., Etherton, R. C., Kelly, W. H., and McHarris, W. C. Nucl. Inst. and Meth. (to be published).

27. Rice, T. private communication.

28. Heath, R. L., Black. W. W., and Cline, J. E. preprint (1966).

29. Heath, R. L. IDO-16880-1 (August, 1964).

30. Bolotin, H. H., Li, A. C., and Swarzchild, A. Phys. Rev. 124 (1961), 213.

31. Yates, M. J. L. In Alpha-Beta-, and Gamma-Ray Spectroscopy, edited by K. Siegbahn. Amsterdam: North-Holland Publishing Co., 1965), Appendix 9.

32. Fink, R. W., Andersson, G., and Kantele, J. Arkiv for Fysik 19 (1961), 323.

33. Vartanov, N. A., Ryukhin, Y. A., Selinov, I. P., Chikladze, V. L., and Khylelidze, D. E. Soviet Physics JETP 14 (1962), 215.

34. Butement, F. D. S., and Quaim, S. M. Inorg. Nucl. Chem. 27 (1965), 1729.

35. Khulelidze, D. E., Chikhladze, V. L., Vartanov, N. A., and Ryukhin, Y. A. Izv. Akad. Nuak SSSR 26 (1962), 1036.

36. Gupta, R. K., Pramilla, G. C., and Srinivasa Raghavan, R. Nucl. Phys. 32 (1962), 669.

37. Kantele, J., and Fink, R. W. Nucl. Phys. 43 (1963), 187.

38. Svedberg, J., and Andersson, G. Nucl. Phys. 48 (1963), 313.

39. Ramayya, A. V. Nucl. Sci. Abst. 19-21450 (1965), 2622.

40. Sorokin, A. A., Shtal, M. Z., and Rybakov, V. N. Izv. Akad. Nauk SSR, Ser. Fiz. 29 (1965), 819.

41. Graves, W. E., and Mitchell, A. G. C. Phys. Rev. 101 (1956), 701.

42. Ramayya, A. V., Yoshizawa, Y., and Mitchell, A. G. C. Nucl. Phys. 56 (1964), 129.

43. Devare, S. H., and Devare, H. G. Phys. Rev. 134 (1964), B705.

44. Singru, R. M., Devare, S. H., and Devare, H. G. preprint (1966).

45. Graeffe, G., Hoffman, E. J., and Sarantites, D. G. (to be published).

46. Bornemeier, D. D., Potmis, V. R., Ellsworth, L. D., and Mandeville, C. E. Phys. Rev. 138 (1965), B525.

47. Gupta, S. L., and Saha, N. K. Nucl. Phys. 73 (1965), 461.

48. Hurley, J. P., and Mathiesen, J. M. Nucl. Phys. 73 (1965), 328.

49. Bemis, C. E., and Fransson, K. Phys. Letters 19 (1965), 567.

50. Walters, W. B., and Gordon G. E. Private communications (1966).

51. Berzins, G., Beyer, L. M., Kelly, W. H., Walters, W. B., and Gordon, G. E. Nucl. Phys. A93 (1967), 546.

52. Eastwood, T. A. Unpublished results, private communication (1966).

53. Berzins, G., Kelly, W. H., Graeffe, G., and Walters, W. (To be published).

54. Bassini, G., Conjeaud, M., Gastebois, J., Harer, S., Laget, J. M., and Picard, J. Phys. Letters 22 (1966), 189.

Bassani, G., Conjeaud, M., Gastebois, J., Harer, S., Laget, J. M., and Picard, J. Unpublished Report.

55. Ishimatsu, T., Yagi, K., Omura, H., Nakazima, Y., Nakagawa, T., and Orihare, H. Bul. Inter. Conf. Nucl. Phys. (September, 1966), 16.

Ishimatsu, T. Private Communication.

56. Barnes, P. D., Ellegaard, C., Herskind, B., and Joshi, Physics Letters, 23 (1966), 266.

57. Merritt, J. S., and Taylor, J. G. V. Anal. Chem. 37 (1965), 351.

58. Andersson, G., and Hagebo, E. Arkiv. Fysik 22 (1962) 349.

59. Moszkowski, S. A. Phys. Rev. 82 (1951), 35.

60. Berzins, G., and Kelly, W. H. Nucl. Phys. A92 (1967) 65.

61. Ofer, S. Phys. Rev. 114 (1959), 870.

62. Beery, D. B., and Kelly, W. H. (To be published).

63. Axensten, S., Liljegren, G., and Lindgren, I. Arkiv. Fysik, 20 (1961), 473.

64. Nuclear Data (edited by K. Way), 1 (1966), B1-1-V11.

65. Khulelidze, D. E., Chikhladze, V. L., Onufriev, V. G Kushakevich, Y. P., and Dyatlow, V. K. JETP, 47 (1964), 1167.

66. Demin, A. G., and Rozman, I. M. JETP, 45 (1963), 13

67. Geiger, J. S. Unpublished report (1967).

68. Walters, W. B., Bemis, C. E. Jr., and Gordon, G. E. Phys. Rev. 140 (1965), B268.

69. DeBenedetti, S. Nuclear Interactions. New York: John Wiley & Sons, Inc., 1964.

70. Konopinski, E. J., and Rose, M. E. In Alpha-Beta-, and Gamma-Ray Spectroscopy, loc. cit., Ch. XXIII.

71. Wapstra, A. H., Nijgh, G. J., and VanLieshout, R. Nuclear Spectroscopy Tables. Amsterdam: North-Holland Publishing Co., 1959.

72. Fraunfelder, H., and Steffen, R. M. In Alpha-Beta-, and Gamma-Ray Sepctoscopy, loc. cit., Ch. XIX.

73. Fagg, L. W., and Hanna, S. S. Rev. Mod. Phys. 31 (1959), 711.

# APPENDICES

# APPENDIX A

# APPENDIX A

## Beta and Gamma Decay Selection Rules

Only a limited number of possible energy levels are expected to be populated in beta and subsequent gamma decay. It is the purpose of this section to give a brief summary of the selection rules that are most commonly used in studies involving the beta and gamma decay processes.

### I.5.1. Beta Decay

The general expression for the transition probability in the beta decay process can be written as (69):

$$\lambda = \frac{\ln 2}{t_{1/2}} = 2\pi \, |M|^2_{ave} \int_0^{E_o} \rho_F(E) \, F(\pm Z, E_o) \, dE \int d\Omega_e \int d\Omega_\alpha$$

where

$|M|_{ave}$ is the matrix element between initial and final states, $\rho_F(E)$ is the statistical factor describing the energy spectrum of the electrons, $F(\pm Z,E)$ is a correction factor arising from the fact that the created electron or positron must be described by a Coulomb wave function rather than a plane wave, $t_{1/2}$ is the halflife, and the subscripts $\mu$ and e refer to the neutrino and electron, respectively.

The correction factors $F(\pm Z,E)$ and $F(K)$ for $\beta^{\mp}$ emission and K capture, respectively, can be numerically evaluated (69, 70). The matrix element $|M|_{ave}$ is dependent upon both the leptonic and nuclear wavefunctions and reflects the ease with which a beta transition may take place between the given states.

It is useful to define a quantity f for $\beta^{\mp}$ emission and K capture as

$$f_{\pm} = \frac{1}{m^5} \int_o^{po} F(\pm z,E)\, p^2\, (E_o - E)^2\, dp$$

$$f_k = \frac{4\pi}{m^5} (z\, e^2 m)^3\, E_o^3$$

Then the product of f and the halflife $t_{1/2}$ can be written as

$$ft_{1/2} = \frac{A}{|M|^2_{ave}}$$

where A consists of various constants from statistical and Coulomb corrections. It has been found empirically that the order of forbiddenness of a transition can be characterized by the ft., or more conveniently, the log ft value. A set of rules can be summarized as follows (64):

1. For odd A, if log ft $\leq$ 4.0, then $\Delta J = 0$, $\Delta\pi$ = no and the transition is called super-allowed.

2. For Z < 80 if log ft $\leq$ 5.8, the transition is allowed with $\Delta J = 0,1$ and $\Delta\pi$ = no.

3. If $5.8 \leq \log ft \leq 10.6$, the transition is allowed, or first forbidden with $\Delta J = 0,1$ and $\Delta\pi$ = yes.

4. If $10.6 \leq \log ft \leq 15$, the transition may be allowed, first-forbidden, or second-forbidden.

5. A beta transition is first forbidden unique ($\Delta J = 2$, $\Delta\pi$ = yes) if $\log f_1 t \leq 7.6$ and if the Fermi plot has appreciable curvature corresponding to a shape factor $(p^2 + q^2)$, where p and q are the electron and neutrino momenta, respectively. The function $f_1$, has been defined as (71):

$$f_1 = [a\,(E_o^2 - 1) - b\,(E_o - 1)]\,f$$

where a and b are (tabulated) constants, $E_o$ is the maximum electron energy in mass units, and f has been defined above.

I.5.2. Gamma Decay

When a nucleus in a state $|iJ_i\pi_i>$ with angular momentum $J_i$ and parity $\pi_i$ makes a transition via the electromagnetic interaction to a state $|fJ_f\pi_f>$, conservation of angular momentum requires that the resulting gamma ray carry off angular momentum J such that

$$J = |J_f - J_i|,\ |J_f - J_i + 1| \ldots\ J_f + J_i, \text{ but } J \neq 0$$

Hence, for a given type of transition, photons with several different J values may be permissible. However, as is shown later, only one or two of these values are observed in transitions in practice. Moreover, parity conservation

requires that $\pi = \pi_i \pi_f$ be the parity of the radiation.

According to the superposition principle, an arbitrary function may be expanded in terms of other functions which form a complete orthogonal set. Since nuclear states are eigenstates of J and $\pi$, it is useful to describe the electromagnetic field in terms of angular momentum eigenfunctions. The well-known solutions to the scalar wave equation (69)

$$(\nabla^2 + k^2)\ U = 0$$

are

$$U_\ell^m\ (kr) = j_\ell\ (kr)\ Y_\ell^m\ (\theta, \phi)$$

where $j_\ell$ and $Y_\ell^m$ are the spherical Bessel functions and the spherical harmonics, respectively, the latter being eigenfunctions of angular momentum.

The corresponding vector wave equation for the spatial component A of the electromagnetic potential $\mathcal{A}$ (where $\mathcal{A} = \underline{A}(\underline{r})\ T(t)$),

$$(\nabla^2 + k^2)\ \underline{A} = 0$$

has considerably more complicated solutions. Two solution $A_\mu$, which satisfy this equation, can be expressed in terms of the angular momentum operator $\underline{L} = -i \hbar\ \underline{r} \wedge \underline{\nabla}$ and of the solutions to the scalar equation as

$$A^{M}_{\varepsilon L} = \sqrt{\frac{2}{J(J+1)}}\ \frac{1}{kr}\ \underline{\nabla} \wedge \underline{L}\ U^{M}_{J}\ (kr)$$

$$A^{M}_{\mathcal{m}L} = \sqrt{\frac{2}{J(J+1)}}\ \frac{k}{kr}\ \underline{L}\ U^{M}_{J}\ (kr)$$

These are referred to as the electric ($\varepsilon$) and magnetic ($\mathcal{m}$) modes of the vector potential.

One important conclusion can be reached by inspecting the expressions for $A^{M}_{\mu J}$. Because of the extra vector operator in the first of these, the two expressions are of opposite parity. Hence, for a given value of J, any operator which involves $A^{M}_{\mu J}$ can be expected to have non-zero matrix elements in only one of these two modes. The orbital parity arising from the spherical harmonies, $Y^{M}_{J}$, is $(-1)^{J}$. Hence, the vector potential has parity $(-1)^{J}$ for the magnetic mode and $-(-1)^{J}$ for the electric mode.

The electric and magnetic fields in either mode can be obtained by

$$\underline{E}^{M}_{\mu J} = -\frac{1}{c}\ \frac{\partial}{\partial t}\ \underline{A}^{M}_{\mu J} = \pm ik\ \underline{A}^{M}_{\mu J}$$

and

$$\underline{H}^{M}_{\mu J} = \underline{\nabla}_{\wedge}\ \underline{A}^{M}_{\mu J}$$

The interactions between the electromagnetic field and N particles can be expressed as

$$H_{int} = \sum_{i=1}^{N} \left[\frac{e_i}{mic}\ \underline{p}_i \cdot \underline{A}\,(r_{\underline{i}}) + \mu_i\ \underline{s}_i \cdot \underline{H}\,(r_{\underline{i}})\right]$$

where $e_i$, $m_i$, $p_i$, $\mu_i$, and $s_i$, refer to the charge, mass, momentum, magnetic moment, and spin, respectively, of the $i^{th}$ particle.

In the special case of $kr<<1$, which holds for nuclear dimensions and with k corresponding to gamma rays of a few MeV energy, the Bessel functions can be approximated as

$$j_J(kr) = \frac{(kr)^J}{(2J+1)!!}$$

With this approximation and the application of vector identities, the expressions for $A^M_{\mu J}$ reduce the J- dependent coefficients and more managable vector operations on $[(kr)^J Y^M_J]$. The transition probability for the nucleus going from state $|i>$ to state $|f>$ via an electromagnetic transition can be expressed as

$$T_{if} = \frac{2\pi}{\hbar} \rho_E |<f|H_{int}|i>|^2$$

where $\rho_E = \frac{1}{\pi\hbar c}$ is the density of states available to the multipole waves. This leads to the expression already given in I.2,

$$T = \frac{8\pi(J+1)}{[J(2J+1)!!]^2} \frac{k^{2J+1}}{\hbar} |<f|H_{int}|i>|^2$$

Crude estimates of the transition probabilities, involving several approximations (4), show that the ratio of the matrix element for magnetic to that for electric transitions ranges between 0.2 and 0.03. Hence, the ratio of the corresponding

transition probabilities is between 0.04 and 0.001. This means that for a given J, an electric transition would be expected to be about two orders of magnitude faster than a magnetic transition between analagous states with the proper parities.

Furthermore, using the same approximation to the matrix element, the ratio of the transition probability of a given multipole of order J +1 to that of order J is approximately $(kR)^2/(2J+3)^2$. More accurate expressions, known as the Weisskopf estimates, have been derived for single particle transitions. These, and the numerical values are presented in many texts, such as Reference 1, 69, and 71.

As previously mentioned, kR<<1 in the nuclear case, hence only the lowest J multipole will contribute significantly to the transition probability. Therefore, although conservation laws permit

$$J = |J_f - J_i| \ldots\ldots (J_f + J_i)$$

as possible angular momentum values of the photon, only $J = |J_f - J_i|$ will be observed in practice if the parities specify an electric transition. But if the lowest J corresponds to a magnetic transition, then an electric transition of order J+1 may still have a significant relative transition probability. A special case exists if $J_f = J_i$. If there is no parity change, then the decay

may proceed via an E0 conversion electron emission in competition with the more favored M1 or E2 photon de-excitations. M0 transitions are forbidden since the expectation value of $Y_o^o$ vanishes between states of opposite parity.

# APPENDIX B

## APPENDIX B: MANUFACTURE OF Ge(Li) DETECTORS

The basic objective is to obtain a crystal which has a compensated layer sandwiched between a heavily lithium doped n-type region and an uncompensated p-type region. Since only this drifted, or intrinsic, layer serves as a gamma ray detector, for efficient counting it is desirable to have crystals with large drifted volumes. Hence, drifting lithium into the crystal from all sides except one has become a common practice. Because drift depth typically exhibits a logarithmic time dependence, the large volumes can be obtained much more easily from large surface areas than from deep drifts.

After the raw crystal has been cut and lapped into the desired shape, lithium is applied to one or more of the sides. This may be done by evaporation or by painting on a lithium suspension in mineral oil or toluene. The crystal is then heated in an inert atmosphere to a temperature of 350-400°C, and, after 10-15 minutes, allowed to cool slowly to room temperature, still in the inert atmosphere. The excess lithium may be removed from the surface by washing with methyl alcohol. A 15 minute diffusion of this nature gives the crystal a heavily doped n-type layer that is approximately 0.3 to 0.5 mm deep at the surface.

In order to obtain good diode characteristics, which are necessary for efficient drifting of lithium into the

crystal, all contaminations causing large surface currents, must be removed. These surface currents bypass the p-n junction. Etching the detector in approximately a 3:1 mixture of $HNO_3$:HF for one to two minutes, followed by a thorough rinse with deionized water, generally removes enough germanium from the crystal surfaces to leave the exposed junction clean. Unless cleaning of the lithium diffused surfaces is desired, they should be masked with wax or etch resistant tape.

Desirable diode characteristics are illustrated in Figure 34A. The critical point is that $\Delta I/I_o$ should be small. A somewhat arbitrary criterion used in this laboratory is that this ratio by $\leq 0.10$. If $\Delta I$ is too large, the etching process should be repeated.

The diode is drifted as is schematically shown in Figure 34B. The series resistor protects the diode, and together with the heat capacity of the sink, determines the amount of power that can be supplied to the diode for a given voltage. Denoting the diode resistance by r, the power supplied to the diode can be expressed by $P = \left(\frac{V}{r + R}\right)^2 r$. Hence, for a fixed voltage V, the power is maximum when r = R, and the voltage drop across the diode is V/2. It should be noted that when large surface currents are present, as is indicated by poor diode characteristics, a large fraction of the power is applied to the surfaces and, besides lowering the drift efficiency, may cause non-uniform

A. TYPICAL GE(LI) DIODE CHARACTERISTICS AT ROOM TEMPERATURE

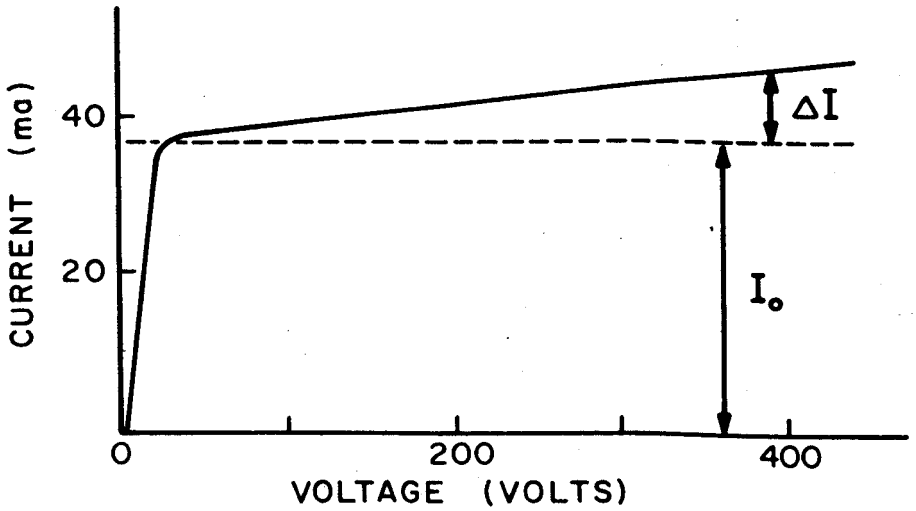


Fig. 34 A typical room temperature diode characteristics of a Ge(Li) detector.

B. DIAGRAM OF GE(LI) DRIFT APPARATUS

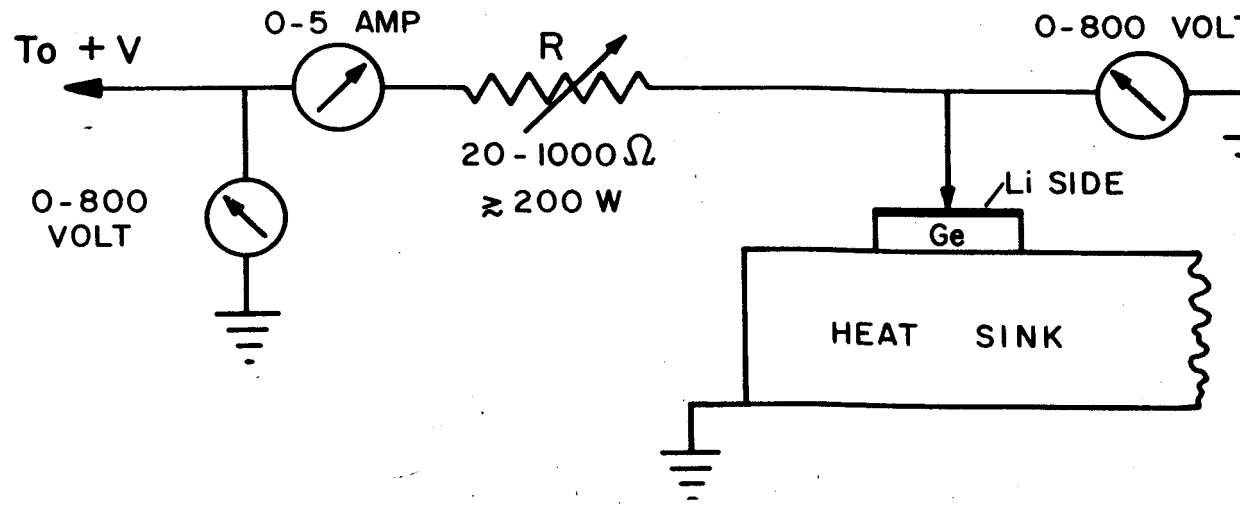


Fig. 34B A schematic illustration of a Ge(Li) drift apparatus.

drifting. Common heat sinks are cooled metal blocks. Or the diode may be immersed in a boiling liquid (such as freon) system.

The depth of drift can be checked periodically by immersing the exposed junction of the diode in a $CuSO_4$ solution, and applying a reverse bias of 10-100 volts for a few seconds. The copper will plate out on the p-type region of the crystal immediately beyond the depleted layer.

# APPENDIX C

## APPENDIX C: INTERPRETATION OF ANGULAR CORRELATION DATA

The angular distribution $W(\theta)$ of particles emitted in the deexcitation of nuclei in an oriented system can be described (72) by

$$W(\theta) = \sum_{\ell}^{\ell_{max}} A_\ell \, P_\ell \, (\cos \theta)$$

where the $A_\ell$ are weighting coefficients of the Legendre polynomials $P_\ell \, (\cos \theta)$. The $A_\ell$ are dependent upon the kind of particle which is emitted, upon the angular momentum of the emitted particle and of the initial and final states of the nucleus. The quantity $l_{max}$ is the smallest of the quantities $2J$, $2L$, or $2L_2$, where $J$, $L_\ell$, and $L_2$ are the spins of the intermediate state and the first and second particles, respectively. In the present discussion, only photons will be considered, although the description for other particles is very similar.

If two gamma rays are emitted in cascade, then the direction of the first photon can be taken as the axis, with the angle $\theta$ describing the angle between the directions of the two photons. The assumption is made that the lifetime of the intermediate state is short in comparison to any "nuclear relaxation periods." If this condition is not satisfied, then before the second gamma ray is emitted the nucleus can lose its orientation with respect to the direction of the

first gamma ray, and more complex treatments are necessary.

For a cascade meeting the above requirements, the coefficients $A_\ell$ are dependent upon the spins of the initial, intermediate, and final states and upon the multipolarities and angular momenta of both transitions, and can be written in product form as

$$A_\ell = A_{\ell 1}\,(J_i, J_1, L_1, \delta_1)\; A_{\ell 2}\,(J, J_f, L_2, \delta_2)$$

The quantum numbers $J_i$, $J$ and $J_f$ are the spins of the initial, intermediate and final states, respectively, and $L_1$ and $L_2$ are the angular momenta carried off by transitions 1 and 2, respectively. The parameter $\delta$ is defined as the ratio of the reduced matrix element for the transition carrying off angular momentum $(L + 1)$ to the reduced matrix element for the transition of order L. In practice, $\delta$ is seldom non-zero for any mixed transitions other than M1 + E2.

Parameters from which theoretical values of $A_\ell$ can be obtained are tabulated in several texts (71, 72). The numerical values for $A_\ell$ were computed in this investigation using the tables in Reference 72. The computations were performed on the CDC-3600 and the SDS SIGMA-7 computers.

In order to obtain the desired information from comparisons of measured and calculated $A_\ell$ values, two additional factors must be considered. The first of these is the attenuation of $A_\ell$ due to the finite solid angles subtended by the detectors. This was already in Chapter II.

A second correction arises if a multiple cascade is involved and one or more unobserved intermediate transitions occur between the two gamma rays of interest. In this case each $A_\ell$ is attenuated, with the attenuation factor $U_\ell$ (n) given for each intermediate transition by (73).

$$U_\ell = (-1)^{j_2-j_1-L} [(2j_2 + 1)\ (2j_1 + 1)]^{1/2}$$

$$W(j_1\ j_1\ j_2\ j_2;\ \ell L)$$

where L, $j_1$,and $j_2$ are the angular momenta of the unobserved intermediate transitions and of the initial and final states which it connects, respectively, and W ($j_1\ j_1\ j_2\ j_2$; $\ell$L) is a Racah coefficient.

Because the measurements are restricted to the directions of the gamma rays and do not depend upon the circul polarizations, the summation in W($\theta$) reduces to terms containi even order polynomials only (72). In general, terms of up to order $\ell = 4$ are sufficient to describe the angular distribution. Hence, the correlation function is usually written as

$$W(\theta) = 1 + A_2\ P_2\ (\cos\ \theta) + A_4\ P_4\ (\cos\ \theta)$$

By convention, the normalization $A_0 = 1$ is used.

The experiemntal $A_2$ and $A_4$ values were obtained from a least squares Legendre polynomial fit to the data points. The computations were done by the POLYFIT program which was writte specifically for this study.

## APPENDIX D: DESCRIPTION OF THE MIKIMAUS PROGRAM

A major difficulty involved in any kind of peak analysis is the subtraction of an appropriate background under a peak. In the case of Ge(Li) gamma ray detectors, this is complicated by electron escape from the sensitive volume of the detector and by long charge collection times which contribute a shelf and a decaying tail, respectively on the low energy side of the peak. Rather than attempt t rigorously strip out the effects on the peak of both these phenomena, one can make an approximation to the background under the peak. Although the error introduced by this approximation is energy dependent, it can be systematicall built into calibration curves to automatically correct for itself when applied to "unknown" peaks.

The background is calculated from a third order polynominal, which has been least squares fitted to severa points from both sides of the peak. The value of the back ground is thus, in a sense, dependent upon the judgement o the experimenter. However, in general, it is very insensi to the particular beginning and end points for the fit, provided that a large enough number ($\gtrsim$ 10) of points is us

After the background is subtracted from each point in the peak, the centroid is located using the formula

$$C = \frac{\Sigma_i N_i I}{\Sigma_i N_i}$$

where $N_i$ = number of counts in the $i^{th}$ channel.

In order to avoid effects of tailing near the bottom of the peaks, a first and last channel are found for each peak. These are the abscissa points for which the linearl interpolated ordinate has dropped to one third the peak height. The net number of counts in each of the channels from first to last, as specified by the experimenter, are summed for the peak area.

The program, in its present form, is designed to handle either internal or external calibrations. That is, the computer can be told whether certain peaks within a given spectrum are to be used to determine a calibration curve or whether the curve must be calculated from a separ spectrum. Once the calibration is obtained, it can be applied to any number of unknown peaks in the same spectru and/or in any number of subsequent spectra.

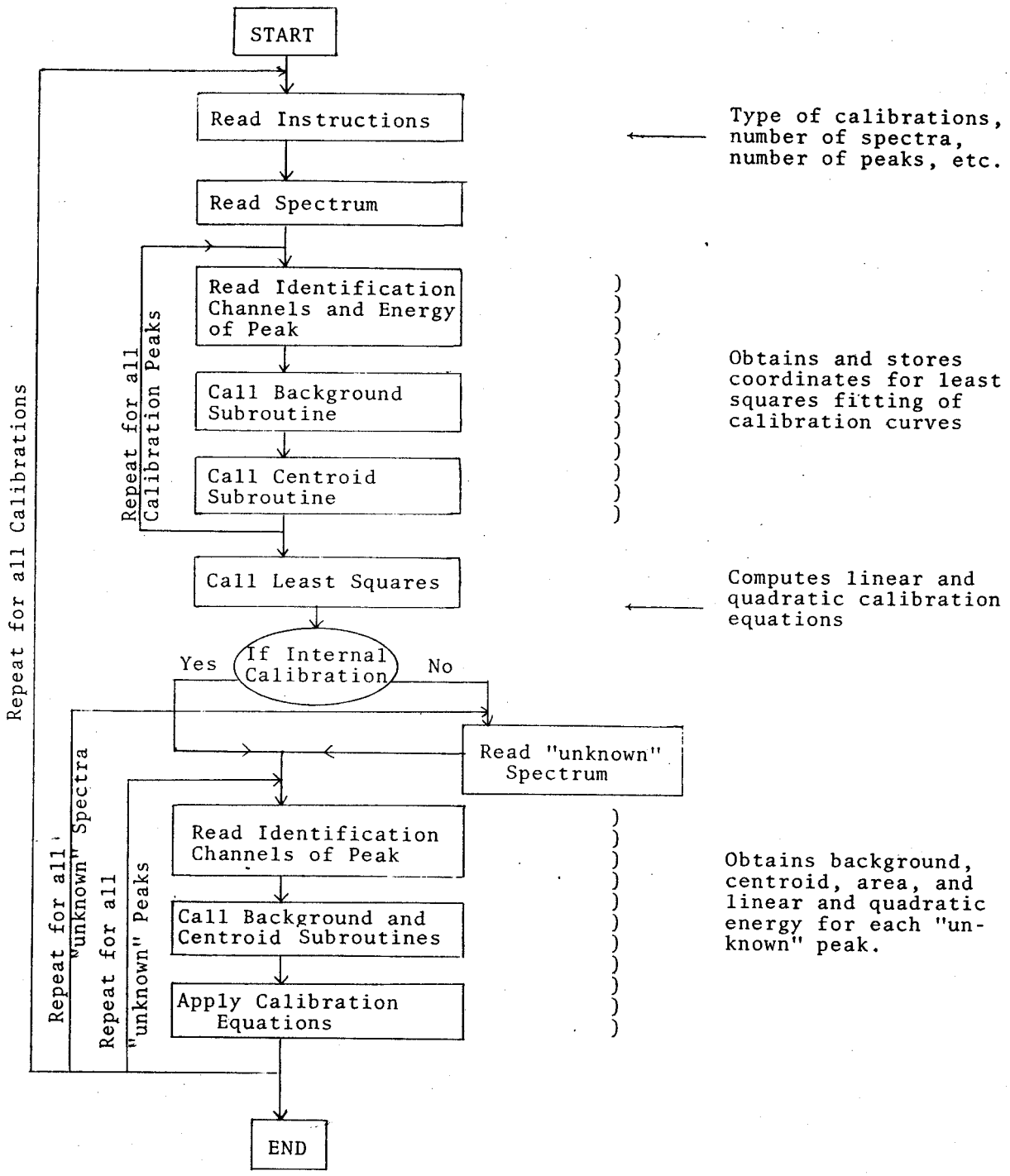


Fig. 35 A schematic flow chart of the MIKIMAUS program.